

# Higgs production at the IHC

---

**Julien Baglio**

*Laboratoire de Physique Théorique, U. Paris-Sud et CNRS, 91405 Orsay Cedex, France.*  
*E-mail: Julien.Baglio@th.u-psud.fr*

**Abdelhak Djouadi**

*Laboratoire de Physique Théorique, U. Paris-Sud et CNRS, 91405 Orsay Cedex, France.*  
*Theory Unit, CERN, 1211 Genève 23, Switzerland.*  
*E-mail: Abdelhak.Djouadi@cern.ch*

**ABSTRACT:** We analyze the production of Higgs particles at the early stage of the CERN large Hadron Collider with a 7 TeV center of mass energy (IHC). We first consider the case of the Standard Model Higgs boson that is mainly produced in the gluon–gluon fusion channel and to be detected in its decays into electroweak gauge bosons,  $gg \rightarrow H \rightarrow WW, ZZ, \gamma\gamma$ . The production cross sections at  $\sqrt{s} = 7$  TeV and the decay branching ratios, including all relevant higher order QCD and electroweak corrections, are evaluated. An emphasis is put on the various theoretical uncertainties that affect the production rates: the significant uncertainties from scale variation and from the parametrization of the parton distribution functions as well as the uncertainties which arise due to the use of an effective field theory in the calculation of the next–to–next–to–leading order corrections. The parametric uncertainties stemming from the values of the strong coupling constant and the heavy quark masses in the Higgs decay branching ratios, which turn out to be non-negligible, are also discussed. The implications for different center of mass energies of the proton collider,  $\sqrt{s} = 8\text{--}10$  TeV as well as for the design energy  $\sqrt{s} = 14$  TeV, are briefly summarized. We then discuss the production of the neutral Higgs particles of the Minimal Supersymmetric extension of the Standard Model in the two main channels: gluon–gluon and bottom quark fusion leading to Higgs bosons which subsequently decay into tau lepton or  $b$ -quark pairs,  $gg, b\bar{b} \rightarrow \text{Higgs} \rightarrow \tau^+\tau^-, b\bar{b}$ . The Higgs production cross sections at the IHC and the decay branching ratios are analyzed. The associated theoretical uncertainties are found to be rather large and will have a significant impact on the parameter space of the model that can be probed.

**KEYWORDS:** Higgs, SUSY, QCD, theoretical uncertainties, hadron collider.

---

## Contents

<b>1. Introduction</b>	<b>2</b>
<b>2. The SM Higgs boson at the LHC</b>	<b>6</b>
2.1 The Higgs production cross sections	6
2.2 The theoretical uncertainties	8
2.2.1 Higher order contributions and scale variation	8
2.2.2 The use of an effective theory approach	10
2.2.3 The PDFs and $\alpha_s$ uncertainties	12
2.3 The combined uncertainty	16
2.4 The cross sections at $\sqrt{s} = 8\text{--}10$ TeV and 14 TeV	19
<b>3. The Higgs decay branching fractions</b>	<b>23</b>
3.1 The parametric uncertainties	23
3.2 Uncertainties on the Higgs branching ratios	24
3.3 Combination with the cross section uncertainty	26
<b>4. The MSSM neutral Higgs particles</b>	<b>29</b>
4.1 The MSSM Higgs sector	29
4.2 The production cross sections at the LHC	31
4.3 The theoretical uncertainties	34
4.4 The Higgs decay branching fractions	38
4.5 Combined uncertainties	40
<b>5. Conclusions</b>	<b>44</b>

---

## 1. Introduction

The Standard Model (SM) of the electroweak and strong interactions crucially relies on the Higgs mechanism in order to spontaneously break the electroweak symmetry and generate in a gauge invariant way the elementary particle masses [1, 2]. In this minimal realization of electroweak symmetry breaking, one complex Higgs doublet field is introduced which implies the existence of a single neutral scalar particle, the Higgs boson  $H$ . In supersymmetric theories [3], that are widely considered as the most attractive extensions of the SM as they protect the Higgs boson mass against large radiative corrections and stabilize the hierarchy between the electroweak and Planck scales, the Higgs sector is extended to contain at least two Higgs doublet fields. The Minimal Supersymmetric Standard Model (MSSM) predicts the existence of five Higgs particles: two CP-even Higgs particles  $h$  and

$H$ , a CP-odd  $A$  boson and two charged  $H^\pm$  particles [4–7]. The search for these new scalar particles is the main goal of present high-energy colliders.

With its very successful operation in the last years, the Fermilab Tevatron  $p\bar{p}$  collider has now collected a substantial amount of integrated luminosity which allows the CDF and D0 experiments to be sensitive to Higgs particles. Exclusion limits beyond the well established LEP bounds [8] are now being set on Higgs masses both in the SM [9] and in the MSSM [10]. The CERN proton-proton collider successfully started operation but at a reduced center of mass energy of 7 TeV [11]. Not to confuse it with the LHC, which is expected to operate at the design energy close to 14 TeV, we will call this early stage machine the IHC for large (or littler) Hadron Collider. The IHC will also be sensitive to the SM Higgs particle and will start to be competitive with the Tevatron once it will accumulate the expected  $1 \text{ fb}^{-1}$  of data [11–14]. However, with the present expectations, the Tevatron and presumably also the IHC will only be able to exclude the existence of the SM Higgs particle in some given mass range. An undebatable discovery in the entire Higgs mass range favored by theoretical considerations,  $115 \text{ GeV} \lesssim M_H \lesssim \mathcal{O}(1 \text{ TeV})$ , has to await for the full-fledged LHC with a center of mass energy of 14 TeV and  $\mathcal{O}(10 \text{ fb}^{-1})$  of integrated luminosity. Observing the MSSM Higgs bosons at the Tevatron and the IHC will be more likely as, in some areas of the supersymmetric parameter space, the production cross sections are much higher than in the SM [5].

The exclusion of Higgs mass regions relies crucially on the theoretical predictions for the production cross sections for the Higgs signal as well as for the relevant SM backgrounds. At the Tevatron, the two main search channels for the SM Higgs boson are the top and bottom quark loops mediated gluon-gluon fusion mechanism  $gg \rightarrow H$  [15] with the Higgs decaying into  $WW$  pairs which lead to  $\ell\nu\ell\bar{\nu}$  (with  $\ell = e, \mu$ ) final states [16] and the Higgs-strahlung processes  $q\bar{q} \rightarrow VH$  (with  $V = W, Z$ ) [17] with the subsequent  $H \rightarrow b\bar{b}$  and  $V \rightarrow \ell + X$  decays of the Higgs and the associated gauge bosons. Analyses performed by the CDF and D0 experiments, under some assumptions for the production cross sections and their associated uncertainties, have recently excluded the Higgs mass range  $M_H = 158\text{--}175 \text{ GeV}$  at the 95% confidence level (CL) [9]. In this mass range, the Higgs signal is mainly due to the  $gg \rightarrow H \rightarrow WW \rightarrow \ell\nu\ell\bar{\nu}$  production and decay channels.

At the IHC, the Higgs-strahlung processes, as well as as other production channels such as weak vector-boson fusion and associated Higgs production with top quark pairs, have too small cross sections and/or are plagued with too large QCD backgrounds. Thus, in practice, only the gluon-gluon fusion process with the Higgs boson decaying into  $H \rightarrow WW \rightarrow \ell\nu\ell\bar{\nu}$ ,  $H \rightarrow ZZ \rightarrow 2\ell + X$ , where  $X$  stands for charged leptons, neutrinos and eventually also jets including  $b$ -quark jets, and to a lesser extent  $H \rightarrow \gamma\gamma$  final states will be mostly relevant. At a center of mass energy  $\sqrt{s} = 7 \text{ TeV}$  and with  $1 \text{ fb}^{-1}$  of data, recent studies by the ATLAS and CMS collaborations have shown that the mass range  $M_H \approx 150\text{--}190 \text{ GeV}$  can be excluded at 95% CL if no Higgs signal is observed [12, 13].

Nevertheless, it is well known that the production cross sections at hadron colliders as well as the associated kinematical distributions are generally affected by various and possibly large uncertainties. In a recent study of SM Higgs production at the Tevatron [18], it has been re-emphasized that while the signal production cross sections are well

under control in the Higgs-strahlung processes, the theoretical uncertainties are rather large in the case of the gluon-gluon fusion channel. These uncertainties are stemming mainly from the variation of the energy scale at which the process is evaluated (a variation that provides a hint of the not yet calculated perturbative higher order corrections) and the parametrization of the parton distribution functions or PDFs (in particular, the gluon density at moderate to high Bjorken- $x$  values). At the Tevatron, these uncertainties can shift the central values of the  $gg \rightarrow H$  cross section [19–22], by more than  $\approx 20\%$  in both the case of the scale and the PDF uncertainty. Arguing that these are two theoretical uncertainties that have in principle no statistical ground and should thus not be added in quadrature, we have proposed a more adequate procedure to combine them which led to a total theoretical uncertainty of about  $\pm 40\%$  on the  $gg \rightarrow H \rightarrow \ell\nu\ell\bar{\nu}$  signal. This overall uncertainty is much larger than the uncertainty assumed in the CDF and D0 combined analysis that excluded the SM Higgs boson at the 95% CL in the mass range  $M_H = 158\text{--}175$  GeV [9]. To our opinion, this exclusion limit should thus be reconsidered.

In the present paper we extend the analysis of Ref. [18] to the case of the LHC, i.e. for proton-proton collisions with a center of mass energy of 7 TeV. We first update the Higgs production cross sections in the  $gg \rightarrow H$  channel, including all the relevant higher order QCD and electroweak corrections and then analyze the various uncertainties that affect them. We show that the scale and PDF uncertainties, as well as the non-negligible uncertainty due to the use of an effective approach in the calculation of QCD and electroweak higher order corrections beyond next-to-leading order, add up to  $\approx 25\text{--}30\%$  depending on the considered Higgs mass range. The total uncertainty is significantly smaller than that obtained at the Tevatron, as a result of smaller QCD radiative corrections and a better knowledge of the gluon distribution function at the energies relevant at the LHC.

We then discuss an additional source of theoretical uncertainties that has not been considered neither in the experimental analyses [9, 12, 13] nor in Ref. [18]: the one affecting the Higgs decay branching ratios. Indeed, while the Higgs decays into lepton and gauge boson pairs are well under control (as mainly small electroweak effects are involved), the partial decays widths into quark pairs and gluons are plagued with uncertainties that are mainly due to the imperfect knowledge of the bottom and charm quark masses and the value of the strong coupling constant  $\alpha_s$ . Updating a previous analysis [23], we show that at least in the intermediate mass range,  $M_H \approx 120\text{--}150$  GeV, where the SM Higgs decay rates into  $b\bar{b}$  and  $W^+W^-$  final states have the same order of magnitude, the parametric uncertainties on these two main Higgs decay branching ratios are non-negligible, being of the order of 3 to 10% at the  $1\sigma$  level.

For completeness, we will extend our analysis and explore the implications for SM Higgs searches at center of mass energies beyond  $\sqrt{s} = 7$  TeV. Not only the full-fledged LHC with  $\sqrt{s} = 14$  TeV will be considered, but also intermediate energies between  $\sqrt{s} = 7$  and 10 TeV that are being currently considered for a very near future, with integrated luminosities significantly larger than  $1 \text{ fb}^{-1}$  [11]. The main result that we obtain is that while the production cross sections for the SM Higgs particle are higher at energies  $\sqrt{s} = 8\text{--}14$  TeV compared to  $\sqrt{s} = 7$  TeV, the overall theoretical uncertainties that affect them are approximately the same.

In the MSSM, the chances of observing at the LHC the neutral Higgs particles, that we will collectively denote by  $\Phi$ , are significantly higher than in the case of the SM Higgs boson. Indeed, for large values of the ratio of the vacuum expectation values of the two MSSM Higgs fields,  $\tan\beta = v_2/v_1$ , the couplings of some of the Higgs bosons to isospin down-type particles are strongly enhanced. For not too heavy Higgs particles, this leads to production cross sections that are possibly orders of magnitude larger than in the SM, in processes in which the MSSM Higgs particles couple to bottom-quarks [5, 6]. This is the case of the gluon-gluon fusion mechanism for neutral Higgs production  $gg \rightarrow \Phi$  which, in this context, dominantly proceeds through  $b$ -quark triangular loops [15, 20], as well as bottom-quark fusion, in which the bottom quarks are directly taken from the protons in a five active flavor scheme,  $b\bar{b} \rightarrow \Phi$  [24–26]. For the relevant high values of  $\tan\beta$ , the  $\Phi$  bosons decay almost exclusively into  $b\bar{b}$  and  $\tau^+\tau^-$  final states with, respectively,  $\approx 90\%$  and  $\approx 10\%$  branching ratios. This leads to the dominant production channels,  $gg, b\bar{b} \rightarrow \Phi \rightarrow \tau^+\tau^-, b\bar{b}$ . Again, besides the uncertainties due to scale variation and the parametrization of the PDFs, additional uncertainties originate from errors in the extraction of the bottom quark mass  $m_b$  and the strong coupling constant  $\alpha_s$ . These uncertainties affect both the production cross sections, as the amplitudes involve the Higgs- $b\bar{b}$  Yukawa coupling  $\propto m_b$ , and the  $\Phi \rightarrow \tau^+\tau^-, b\bar{b}$  decay branching fractions.

A second aim of this paper is to analyze in detail these two main MSSM Higgs production channels at the LHC: the production cross sections, including the relevant higher order radiative corrections are updated, the important QCD effects are summarized and the various theoretical uncertainties are evaluated. We show that the uncertainties from scale variation and the parametrization of the PDFs in the cross sections are at least as large as in the SM  $gg \rightarrow H$  case. Additional parametric uncertainties in both the production and the decay rates, as well as a freedom in the choice of the renormalization scheme that defines the  $b$ -quark mass, lead to a total theoretical uncertainty that is even larger, of the order of 40 to 50% depending on the Higgs masses. This uncertainty will thus have a significant impact on the MSSM parameter space that can be probed at the LHC.

The rest of the paper is organized as follows. In the next section we discuss the production of the SM Higgs boson at the LHC with  $\sqrt{s} = 7$  TeV, mainly concentrating on the dominant  $gg \rightarrow H$  production channel; the total inclusive cross section including the relevant higher order contributions is updated, the various theoretical uncertainties evaluated and combined, and the implications for higher center of mass energies summarized. In section 3, the parametric uncertainties in the SM Higgs decay branching ratios are summarized and combined with the uncertainties in the production cross sections. In section 4, we discuss the production of the MSSM neutral Higgs bosons: the cross sections in the two production channels,  $gg \rightarrow \Phi$  and  $b\bar{b} \rightarrow \Phi$  are analyzed and the associated uncertainties from scale and scheme dependence, the PDF uncertainties as well as the parametric uncertainties are discussed; the errors in the Higgs branching ratios in the main decay modes  $\Phi \rightarrow \tau^+\tau^-$  and  $\Phi \rightarrow b\bar{b}$  are addressed and the way to combine all these theoretical uncertainties in the production and in the decays is discussed. Here, we only discuss the case of the LHC with  $\sqrt{s} = 7$  TeV and simply summarize the implications at slightly higher energies,  $\sqrt{s} = 8$ –10 TeV. Finally, a conclusion is given in the last section.

## 2. The SM Higgs boson at the LHC

### 2.1 The Higgs production cross sections

The main production channel for the Higgs particles at hadron colliders is the gluon–gluon fusion channel,  $gg \rightarrow H$ , which proceeds through triangular heavy quark loops [15]. In the SM, it is dominantly mediated by the top quark loop contribution, with a bottom quark contribution that does not exceed the 10% level at leading order. This process is known to be subject to extremely large QCD radiative corrections [19–22, 27–29] that can be described by an associated  $K$ -factor defined as the ratio of the higher order (HO) to the lowest order (LO) cross sections, consistently evaluated with the value of the strong coupling  $\alpha_s$  and the parton distribution functions (PDF) taken at the considered order,

$$K_{\text{HO}} = \sigma^{\text{HO}}|_{(\alpha_s^{\text{HO}}, \text{PDF}^{\text{HO}})} / \sigma^{\text{LO}}|_{(\alpha_s^{\text{LO}}, \text{PDF}^{\text{LO}})} \quad (2.1)$$

The next-to-leading-order (NLO) corrections in QCD are known both for infinite [19] and finite [20] loop quark masses and, at  $\sqrt{s} = 7$  TeV, lead to a  $K$ -factor  $K_{\text{NLO}} \sim 1.8$  in the low Higgs mass range, if the central scale of the cross section is chosen to be the Higgs mass. It has been shown in Ref. [20] that working in an effective field theory (EFT) approach in which the top quark mass is assumed to be infinite is a very good approximation for Higgs mass values below the  $t\bar{t}$  threshold  $M_H \lesssim 2m_t$ , provided that the leading order cross section contains the full  $m_t$  and  $m_b$  dependence. The calculation of the next-to-next-to-leading-order (NNLO) contribution has been done [21] only in the EFT approach  $M_H \ll 2m_t$  and, at  $\sqrt{s} = 7$  TeV, it leads to a  $\approx 25\%$  increase of the cross section<sup>1</sup>,  $K_{\text{NNLO}} \sim 2.5$ . The resummation of soft gluons is known up to next-to-next-to-leading-logarithm (NNLL) and, again, increases the cross section by slightly less than 10% [22, 28]. The effects of soft–gluon resummation at NNLL can be accounted for in  $\sigma^{\text{NNLO}}(gg \rightarrow H)$  by lowering the central value of the renormalization and factorization scales<sup>2</sup>, from  $\mu_0 = M_H$  to  $\mu_0 = \frac{1}{2}M_H$ . We will thus choose for definiteness the value

$$\mu_0 = \mu_R = \mu_F = \frac{1}{2}M_H \quad (2.2)$$

for the central scale of the process which, in passing, also improves the convergence of the perturbative series and is more appropriate to describe the kinematics of the process [33]. The electroweak corrections are known exactly up to NLO [34, 35] and contribute at the

---

<sup>1</sup>The QCD corrections to  $gg \rightarrow H$  at  $\sqrt{s} = 7$  TeV are thus smaller than the corresponding ones at the Tevatron as the  $K$ -factors in this case are  $K_{\text{NLO}} \approx 2$  and  $K_{\text{NNLO}} \approx 3$  (with a central scale equal to  $M_H$ ). At the LHC with  $\sqrt{s} = 14$  TeV, the  $K$ -factors are even smaller,  $K_{\text{NLO}} \approx 1.7$  and  $K_{\text{NNLO}} \approx 2$ . The perturbative series shows thus a better (converging) behavior at LHC than at Tevatron energies.

<sup>2</sup>We will include the soft–gluon resummation contributions in this indirect way since, as discussed in Ref. [18], we would like to stick to the fixed order NNLO calculation for two main reasons: *i*) there are not yet parton distribution functions which include soft–gluon resummation and it appears inconsistent to fold a partonic cross section with PDFs that are not at the same order of perturbation theory (although the effects might be small in practice [30]) and *ii*) the soft–gluon resummation is not available for the Higgs+jet production cross sections and/or the Higgs cross sections including kinematical cuts (both are known only at NNLO [31, 32]) which, ultimately, are the basic experimental inputs.

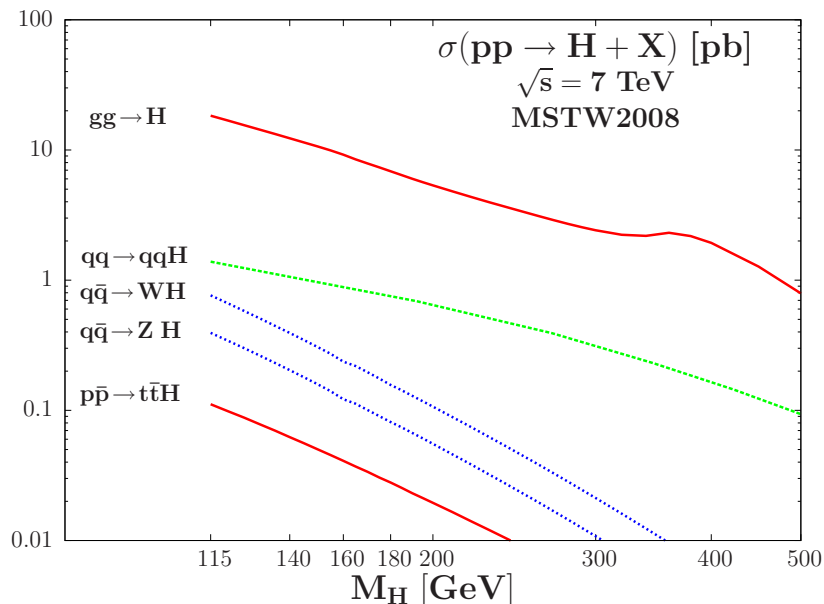


**Figure 1:** The total cross sections for Higgs production at the IHC with  $\sqrt{s} = 7$  TeV as a function of the Higgs mass. The MSTW set of PDFs has been used and the higher order corrections are included as discussed in the text.

level of a few percent; there are also small mixed NNLO QCD–electroweak effects which have been calculated [27] in an effective approach valid for  $M_H \ll M_W$ .

Our calculation<sup>3</sup> of the  $gg \rightarrow H$  production cross section at the IHC, including these higher order corrections strictly follows the one performed in Ref. [18] for the Tevatron: the starting point is the Fortran code `HIGLU` [37] which evaluates the  $gg \rightarrow H$  cross section at exact NLO in QCD (i.e. with the exact contributions of the top and bottom quark loops) to which we add the NNLO QCD contribution in the infinite top–quark mass limit, but with the LO normalisation containing the exact  $m_t$  and  $m_b$  dependence; grids for the exact NLO electroweak and the mixed QCD–electroweak corrections are then implemented within the code (they have been added in the partial factorization scheme [34], see section 2.2.2). The production cross sections are shown at the IHC with  $\sqrt{s} = 7$  TeV in Fig. 1 for an updated value of the top quark mass and when the partonic cross section is folded with the latest NNLO MSTW2008 public set of PDFs [38]. The renormalization and factorization scales are fixed to the central values  $\mu_F = \mu_R = \frac{1}{2}M_H$ . Our results agree with those given in Refs. [27, 28] and updated in Ref. [14] within a few percent.

For completeness, we also display in Fig. 1 the cross sections for the three other Higgs production channels at hadron colliders that we evaluate using the programs of Ref. [37]:

- i)* the Higgs–strahlung processes  $q\bar{q} \rightarrow HV$  with  $V = W, Z$  that are known exactly up to NNLO in QCD [6, 39, 40] and up to NLO for the electroweak corrections [41]; they are evaluated at  $\mu_0 = M_{HV}$  (the invariant mass of the  $HV$  system) for the central scale<sup>4</sup>;

<sup>3</sup>Other recent updates of the  $gg \rightarrow H$  cross section can be found in Ref. [27, 28, 36].

<sup>4</sup>Here, the QCD  $K$ -factors are moderate,  $K_{\text{NNLO}} \sim 1.5$  and the electroweak corrections reduce the cross section by an amount of  $\approx 3 - 8\%$ . For the evaluation of the cross section, we have used the NLO code `V2HV` [37] in which we implemented these higher order contributions. Our results agree with those of Ref. [14].

- ii) the weak vector boson fusion channel  $qq \rightarrow Hqq$  evaluated at the scale  $\mu_0 = Q_V$  (the momentum transfer at the gauge boson leg) in which only the NLO QCD corrections [6, 42] have been included; the NNLO corrections have been found to be very small [43] and we omit the electroweak corrections [44];
- iii) associated Higgs production with top quark pairs in which only the leading order contribution is implemented but at a central scale  $\mu_0 = \frac{1}{2}(M_H + 2m_t)$ , which is a good approximation at these energies as the NLO  $K$ -factor is very close to unity [45, 46].

As can be seen, the  $gg \rightarrow H$  process is by far dominating in the entire Higgs mass range, with a cross section that is one to two orders of magnitudes larger than in the other production channels. For low Higgs masses,  $M_H \lesssim 2M_W$ , it leads to more than 10.000 events for a luminosity of order  $1 \text{ fb}^{-1}$ . Table 1 displays the values of the cross sections for the five Higgs production processes for a selection of Higgs masses relevant at the LHC.

## 2.2 The theoretical uncertainties

### 2.2.1 Higher order contributions and scale variation

In the calculation of production cross sections and kinematical distributions at hadron colliders, as the perturbative series are truncated and the results are available only at a given perturbative order, there is a residual dependence of the observables on the renormalization scale  $\mu_R$  which defines the strong coupling constant  $\alpha_s$  and on the factorization scale  $\mu_F$  at which the matching between the perturbative matrix elements calculation and the non-perturbative parton distribution functions is performed. The uncertainty due to the variation of these two scales is viewed as an estimate of the unknown (not yet calculated) higher-order terms and is rather often the dominant source of theoretical uncertainties.

In general, starting with the median scale  $\mu_F = \mu_R = \mu_0$  for which the central value of the cross section is obtained, the two scales  $\mu_R$  and  $\mu_F$  are varied within the interval  $\mu_0/\kappa \leq \mu_R, \mu_F \leq \kappa \times \mu_0$  with the value of the constant  $\kappa = 2, 3, 4$ , etc... to be chosen. The additional restriction  $1/\kappa \leq \mu_F/\mu_R \leq \kappa$  is also often applied<sup>5</sup>. The choice of the scale variation domain and hence the constant factor  $\kappa$ , is rather subjective and a possibility would be to adopt the  $\kappa$  value which allows the uncertainty band due to the scale variation of the lower order cross section to incorporate the central value of the cross section (i.e. with  $\mu_R = \mu_F = \mu_0$ ) calculated at the highest available order.

In our analysis, we have adopted the central scale value  $\mu_R = \mu_F = \mu_0 = \frac{1}{2}M_H$  as discussed earlier. At  $\sqrt{s} = 7 \text{ TeV}$ , for the scale uncertainty band of  $\sigma^{\text{NLO}}(gg \rightarrow H)$  to catch the central value of  $\sigma^{\text{NNLO}}(gg \rightarrow H)$  for  $\mu_0 = \frac{1}{2}M_H$ , a value  $\kappa = 2$  is sufficient. Adopting the range  $\frac{1}{2}\mu_0 \leq \mu_R, \mu_F \leq 2\mu_0$  with  $\mu_0 = \frac{1}{2}M_H$  for the cross section  $\sigma^{\text{NNLO}}(gg \rightarrow H)$ , one obtains the scale variation displayed in Fig. 2 as a function of  $M_H$ ; it is compared to a variation with a factor  $\kappa = 3$ . In the insert, shown are the maximal and minimal variations of  $\sigma^{\text{NNLO}}(gg \rightarrow H)$  compared to the central value. One sees that for  $\kappa = 2$ , a scale uncertainty of  $\approx \pm 10\%$  is obtained in the low mass range,  $M_H \approx 120 \text{ GeV}$ , which

---

<sup>5</sup>In the case of the  $gg \rightarrow H$  process, the maximal (minimal) cross sections at a given fixed order in perturbation theory (in particular at NNLO) is obtained for the scale choices  $\mu_R = \mu_F = \mu_0/\kappa$  ( $\kappa\mu_0$ ) and, hence, this restriction is irrelevant in practice.



$M_H$	$\sigma_{gg \rightarrow H}^{\text{NNLO}}$	$\sigma_{qq \rightarrow Hqq}^{\text{NLO}}$	$\sigma_{q\bar{q} \rightarrow HW}^{\text{NNLO}}$	$\sigma_{q\bar{q} \rightarrow HZ}^{\text{NNLO}}$	$\sigma_{pp \rightarrow t\bar{t}H}^{\text{LO}}$
115	18347.4	1386.1	764.1	394.0	111.5
120	16844.6	1313.2	664.8	343.2	98.7
125	15509.2	1259.5	580.0	300.3	87.9
130	14322.6	1192.1	507.5	263.2	78.1
135	13260.6	1148.6	446.0	231.4	69.8
140	12305.6	1087.0	392.9	203.6	62.3
145	11446.4	1051.5	347.3	180.0	56.0
150	10665.9	1006.2	307.1	159.1	50.2
155	9936.4	964.6	272.0	140.4	45.3
160	9205.9	908.4	236.8	121.7	40.9
165	8470.8	875.3	218.9	112.3	37.0
170	7872.3	842.5	196.0	100.6	33.7
175	7345.3	796.6	175.6	90.2	30.5
180	6861.2	768.0	156.8	81.2	27.9
185	6416.3	732.8	142.7	74.0	25.4
190	6010.0	705.0	129.3	67.1	23.1
195	5654.8	683.8	117.5	60.9	21.2
200	5344.1	651.5	106.8	55.3	19.5
220	4357.0	556.7	74.4	38.4	14.0
240	3646.4	479.6	52.9	27.2	10.4
260	3110.7	411.6	38.4	19.7	7.8
280	2706.4	360.7	28.3	14.5	6.1
300	2415.4	312.6	21.2	10.8	4.8

**Table 1:** The total Higgs production cross sections (in fb) in the processes  $gg \rightarrow H$ , vector-boson fusion  $qq \rightarrow Hqq$ , Higgs-strahlung  $q\bar{q} \rightarrow HW.HZ$  and associated production  $pp \rightarrow t\bar{t}H$  at the LHC with  $\sqrt{s} = 7$  TeV for given Higgs mass values (in GeV) with the corresponding central scales described in the main text. The MSTW sets of PDFs have been used at the relevant order.

decreases to the level of  $\approx -8\%, +4\%$  at high masses,  $M_H \approx 500$  GeV. Note that if the domain for scale variation were extended to  $\kappa = 3$ , the uncertainty would have increased to  $\approx \pm 17\%$  in the low  $M_H$  range<sup>6</sup> as also shown in the figure.

---

<sup>6</sup>In the analysis of Ref. [18] for the case of the Tevatron, the value  $\kappa = 3$  was adopted instead of  $\kappa = 2$  and, hence, a larger domain for the scale variation was assumed as the higher order QCD corrections in  $\sigma(gg \rightarrow H)$  are larger at the Tevatron compared to the LHC.

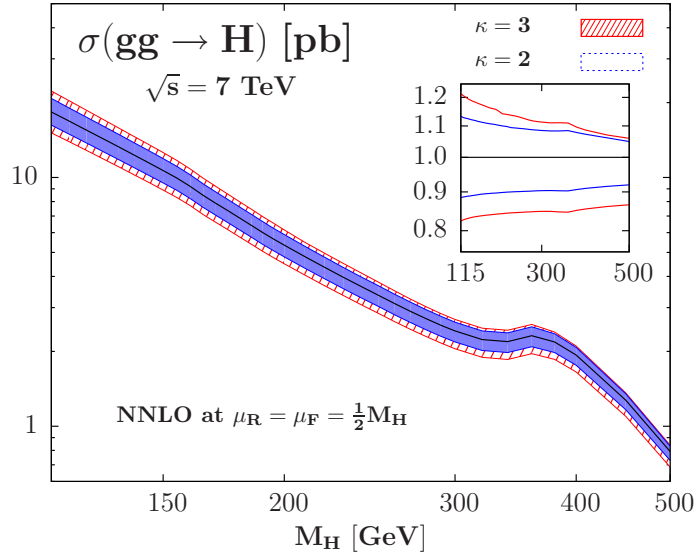


**Figure 2:** The scale uncertainty band of  $\sigma^{\text{NNLO}}(gg \rightarrow H)$  at the IHC as a function of  $M_H$  for a scale variation in the domain  $M_H/(2\kappa) \leq \mu_R, \mu_F \leq \kappa \times \frac{1}{2}M_H$  for  $\kappa = 2$  and  $3$ ; in the insert, shown are the relative deviations from the central value with a scale  $\mu_R = \mu_F = \frac{1}{2}M_H$ .

### 2.2.2 The use of an effective theory approach

Another source of theoretical uncertainties is specific to the gluon–gluon fusion mechanism in which the cross section beyond the NLO approximation is evaluated in an effective theory (EFT) approach where the particles that are running in the loops are assumed to be much heavier than the produced Higgs boson. At NLO, the approximation  $m_t \gg M_H$  for the contribution of the top quark in the loop is rather good for Higgs masses below the  $t\bar{t}$  threshold,  $M_H \lesssim 340$  GeV, in particular when the full quark mass dependence of the leading order cross section  $\sigma_{\text{exact}}^{\text{LO}}$  is taken into account [20]. At NNLO, this approximation for the top quark contribution seems also to be accurate as studies of the effect of a finite  $m_t$  value in expansions of  $M_H/(2m_t)$  have shown a difference below the percent level with respect to the EFT calculation for  $M_H \lesssim 300$  GeV [47].

Nevertheless, the EFT approach should definitely not be valid for Higgs masses beyond the  $t\bar{t}$  threshold, where the  $gg \rightarrow H$  amplitude develops imaginary parts. This can be seen at NLO where both the exact and the approximate results are known. We will thus include an uncertainty related to the use of the EFT approach for  $M_H \gtrsim 2m_t$  which is taken as the difference between  $\sigma_{\text{exact}}^{\text{NLO}}$  and  $\sigma_{m_t \rightarrow \infty}^{\text{NLO}}$  when the exact top quark mass dependence is included in the LO cross section and when one rescales this difference with the relative magnitudes of the NLO and NNLO  $K$ -factors, i.e.  $K_{m_t \rightarrow \infty}^{\text{NLO}}/K_{m_t \rightarrow \infty}^{\text{NNLO}}$ .

In the left–hand side of Fig. 3, shown is this difference in percent for  $\sqrt{s} = 7$  TeV. It is small for Higgs masses below  $M_H = 400$  GeV, at most 2%, it increases very rapidly with increasing  $M_H$  values and, for  $M_H \gtrsim 500$  GeV, it is larger than  $\approx 5\%$ . This uncertainty is thus not negligible and it should be accounted for (at the Tevatron, this uncertainty has not been discussed [18] as only Higgs masses below 200 GeV were considered).

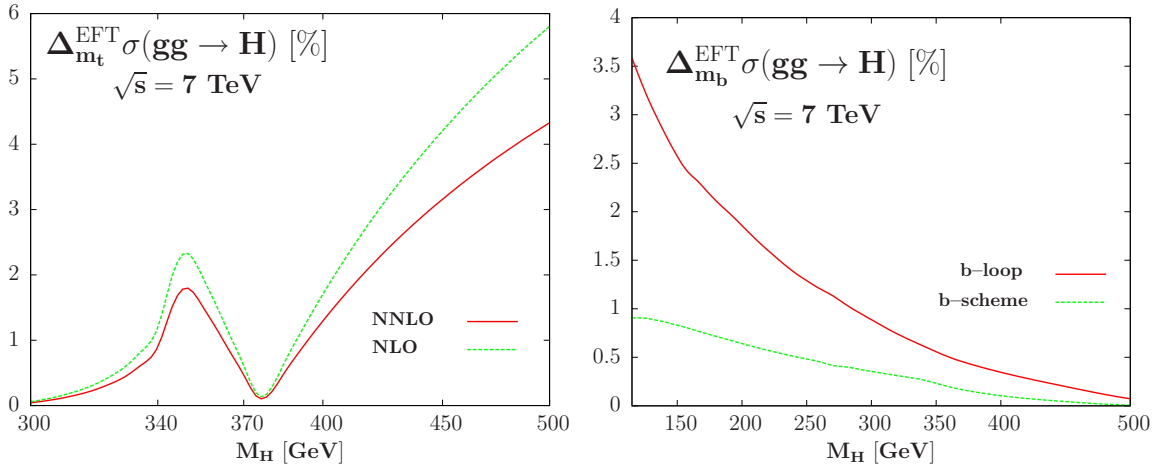


**Figure 3:** The estimated uncertainties (in %) due to the use of the EFT approach in the evaluation of  $\sigma(gg \rightarrow H)$  at NNLO for the top quark loop contribution for Higgs masses beyond  $2m_t$  (left) and for the bottom-quark loop contributions (right).

Furthermore, the EFT approach is certainly also not valid for the  $b$ -quark loop and, for instance, the omission of this contribution (at LO) leads to a  $\approx 10\%$  difference compared to the exact case. Furthermore, the NLO  $K$ -factor for the  $b$ -quark loop,  $K_{b\text{-loop}}^{\text{NNLO}} \approx 1.2\text{--}1.4$ , is much smaller than that for the top-quark loop. In fact, the problem arises mainly because of the significant negative interference between the top and bottom loop contributions (the bottom quark contribution itself is rather small) up to NLO and the fact that the bottom contribution has been factorized out in the LO cross section. Thus, including the top quark contribution only using the EFT approach might overestimate the NNLO correction as this interference component is missing (and, since it is resulting from an approximation it is not, in principle, accounted for by e.g. the scale variation that is performed at NNLO).

In order to estimate the uncertainty due the missing  $b$ -loop contribution at NNLO, we simply follow the previous procedure for the top quark: we assign an error on the NNLO QCD result which is approximately the difference between the exact result  $\sigma_{\text{exact}}^{\text{NLO}}$  and the approximate result  $\sigma_{m_t \rightarrow \infty}^{\text{NLO}}$  obtained at NLO but rescaled with the relative magnitude of the  $K$ -factors that one obtains at NLO and NNLO for the top-loop, i.e.  $K_{m_t \rightarrow \infty}^{\text{NLO}}/K_{m_t \rightarrow \infty}^{\text{NNLO}}$ . This leads to the uncertainty on the  $\sigma^{\text{NNLO}}(gg \rightarrow H)$  at  $\sqrt{s} = 7$  TeV that is shown in the right-hand side of Fig. 3. It ranges from  $\sim \pm 3\%$  for low Higgs values  $M_H \sim 120$  GeV where the  $b$ -loop is relatively important to less than  $\sim \pm 1\%$  for Higgs masses above  $M_H \sim 300$  GeV. Note that this correction is larger than that obtained at the Tevatron [18] where a different central scale,  $\mu_0 = M_H$ , has been adopted for its evaluation.

In addition, there is some freedom in the choice of the renormalization scheme for the  $b$ -quark mass in the  $gg \rightarrow H$  amplitude: for instance, one can use the on-shell scheme in which the pole mass is  $m_b \approx 4.7$  GeV or the  $\overline{\text{MS}}$  scheme in which the mass  $\overline{m}_b(\overline{m}_b) \approx 4.2$  GeV is adopted. This leads to a difference of  $\approx 1\%$  in the  $b$ -quark loop contribution at NLO that we will take as an additional uncertainty due to the scheme dependence (this scheme dependence will be discussed in more details in the MSSM case).

Finally, in the corrections to the  $gg \rightarrow H$  amplitude, the mixed QCD–electroweak corrections have been calculated at NNLO [27] in an EFT approach with  $M_{W/Z} \gg M_H$ , a limit that is obviously not valid in practice. We thus should be cautious when using this correction and assign an uncertainty which is of the same size as the contribution itself [18]. This uncertainty is comparable in size to the difference between the electroweak correction calculated exactly at NLO [34] evaluated in the partial factorization scheme (where the correction  $\sigma^{\text{LO}}\Delta_{\text{EW}}$  is simply added to the QCD corrected cross section) compared to the result in the complete factorization scheme (where the NNLO cross section is multiplied by  $1 + \Delta_{\text{EW}}$ ). This generates an additional uncertainty of  $\approx 3\%$  at most, which is not shown as it is the same as the one discussed in Ref. [18] for the Tevatron.

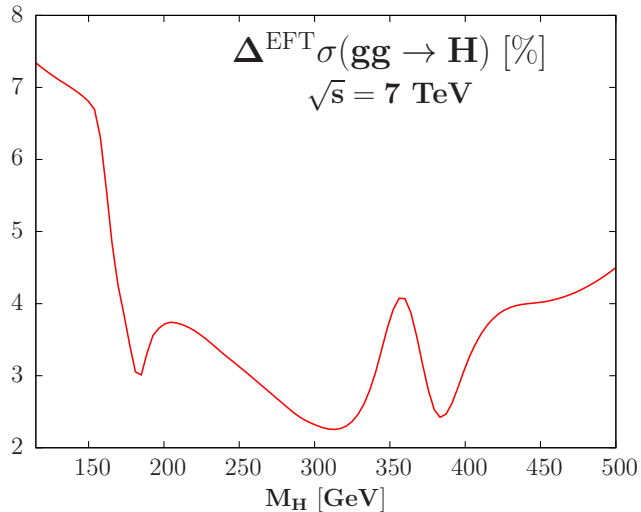


**Figure 4:** The estimated total uncertainty (in %) at LHC energies and as a function of  $M_H$  from the use of the EFT approach for the calculation of the  $gg \rightarrow H$  amplitude at NNLO and from the scheme dependence of the  $b$ -quark mass.

Adding the uncertainties from these three sources linearly, the resulting overall uncertainty is displayed in Fig. 4 as a function of  $M_H$ . It amounts to  $\approx 7\%$  in the low Higgs mass range, drops to the level of  $\approx 4\%$  in the mass range  $M_H \approx 200\text{--}400$  GeV, and then increases to reach the level of  $\approx 6\%$  at 600 GeV, as a result of the bad  $M_H \ll 2m_t$  approximation for the top loop contribution. Since this is a pure theoretical uncertainty, it should be added linearly to the uncertainty from scale variation.

### 2.2.3 The PDFs and $\alpha_s$ uncertainties

One of the most important sources of theoretical uncertainties in the  $gg \rightarrow H$  production cross section is the one stemming from the parametrization of the gluon densities. There are two quite different ways to estimate this uncertainty.

The first one is the so-called Hessian method where, besides the best fit PDF with which the central values of the cross sections are evaluated, a set of  $2N_{\text{PDF}}$  PDF parameterizations is provided that reflect the  $\pm 1\sigma$  variation of all ( $N_F$ ) parameters that enter into the global fit. These uncertainties are thus mostly due to the experimental errors in the various data that are used in the fits.

If one takes the latest NNLO public set provided by the MSTW collaboration [38, 48] for instance, the PDF uncertainty at the 90% CL that is obtained at the IHC for the NNLO  $gg \rightarrow H$  cross section is shown (by the red lines and red band) in Fig. 5 as a function of  $M_H$ . For low Higgs masses, the uncertainty is at the level of 5% but it increases to reach the level of  $\approx 8\%$  at high Higgs masses,  $M_H \approx 500$  GeV. If only the (more optimistic) 68%CL errors are to be considered, the previous numbers have to be divided by  $\approx 1.6$ .

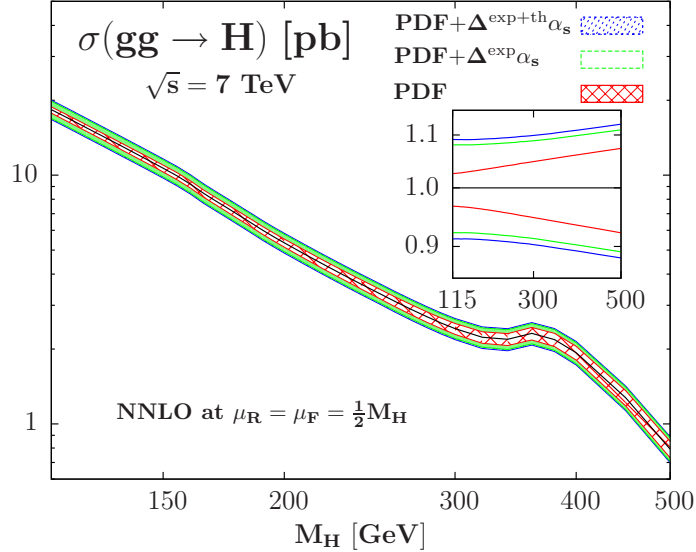


**Figure 5:** The central values and the 90% CL PDF, PDF+ $\Delta^{\text{exp}}\alpha_s$  and PDF+ $\Delta^{\text{exp}}\alpha_s + \Delta^{\text{th}}\alpha_s$  uncertainty bands in  $\sigma^{\text{NNLO}}(gg \rightarrow H+X)$  at the IHC when evaluated within the MSTW scheme. In the inserts, shown are the same but with the cross sections normalized to the central cross section.

The previous Hessian errors do not account for the theoretical assumptions that enter into the parametrization of the PDFs and which may come from many different sources. These assumptions lead to an uncertainty in the parametrization that is difficult to quantify in a given scheme, say the MSTW scheme. A way to access this theoretical uncertainty is to compare the results for the central values of the cross section (and hence, using the best fit PDFs) when using different sets of PDFs which involve, in principle, different assumptions. In Fig. 6, we display the values of  $\sigma^{\text{NNLO}}(gg \rightarrow H)$  that are obtained when folding the partonic cross section with the gluon densities that are predicted by the four PDF sets<sup>7</sup> that have parameterizations at NNLO: MSTW [38], JR [51], ABKM [52] and HERAPDF [53]. In the later case, two sets are provided: one with the value  $\alpha_s = 0.1176$  that is close to the world average value [54] and the MSTW best-fit  $\alpha_s = 0.1171$  [38], and one with the value  $\alpha_s = 0.1145$  used also in the ABKM set [52], that is close to the preferred values that one obtains using deep-inelastic scattering data alone.

As can be seen, while the differences in the cross sections are moderate in the low Higgs mass range, being of the order of 10% or less, there is a significant difference at

<sup>7</sup>As we make the choice of using parton cross sections and PDFs that are consistently taken at the same perturbative order, we will not consider two other parameterizations, CTEQ [49] and NNPDF [50], which provide PDF sets only at NLO.

higher Higgs masses,  $\mathcal{O}(25\%)$  for  $M_H \approx 500$  GeV. Even with the same  $\alpha_s$  input or best-fit values, HERAPDF with  $\alpha_s = 0.1176$  and MSTW results are strikingly different. For the large  $M_H$  values, this discrepancy is mainly due to the gluon densities at moderate to high Bjorken- $x$  values which are less constrained by the data (in particular if the Tevatron high  $E_T$  jet data are not included as is the case of the ABKM and HERAPDF sets).

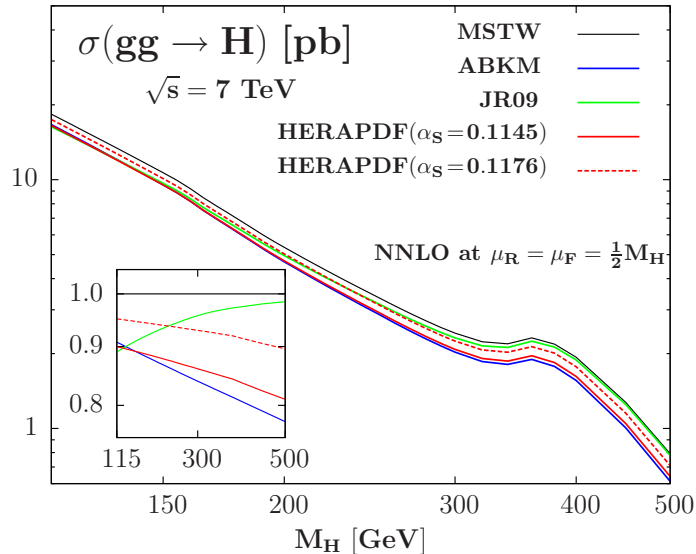


**Figure 6:** The central values of the NNLO cross section  $\sigma(gg \rightarrow H + X)$  at the LHC as a function of  $M_H$  when evaluated in the four schemes which provide NNLO PDFs. In the inserts, shown are the same but with the cross sections normalized to the MSTW central cross section.

We thus conclude when comparing Fig. 5 and Fig. 6 that, depending on how the uncertainties are estimated, through the  $2 \times 20$  grids given in the MSTW scheme (other PDF sets such as ABKM for instance give approximately the same error) or by comparing the cross sections evaluated using PDFs from different schemes, a rather different uncertainty is obtained. To partly reconcile these two different results, we will follow the analysis made in Ref. [18] and include the additional errors on the coupling  $\alpha_s$ .

As a matter of fact, in addition to the PDF uncertainties, one should also consider the ones coming from the uncertainties in the determination of the value of the strong coupling constant<sup>8</sup>  $\alpha_s$  which, in general, is fitted together with the PDFs and this point is now well taken by the experimental collaborations. Indeed, since already at leading order one has  $\sigma^{\text{LO}}(gg \rightarrow H) \propto \mathcal{O}(\alpha_s^2)$  and the  $K$ -factors are large, the uncertainty in the determination of  $\alpha_s$  may induce a non-negligible error on the final cross section. In the MSTW scheme, the value of  $\alpha_s$  together with its experimental accuracy, is [48]

$$\alpha_s(M_Z^2) = 0.1171^{+0.0014}_{-0.0014} \text{ (68\% CL) or } ^{+0.0032}_{-0.0032} \text{ (90\% CL) at NNLO} \quad (2.3)$$

<sup>8</sup>One can see that the input value of  $\alpha_s$  is very important by comparing the two HERAPDF results in Fig. 6. Nevertheless, the difference in  $\alpha_s$  is not sufficient to explain the behavior of the cross sections in the MSTW and HERAPDF cases for instance, and there is some part that is presumably also due to the different shapes of the gluon densities.

We have evaluated the 90% CL correlated PDF+ $\Delta^{\text{exp}}\alpha_s$  uncertainties using the new set-up provided by the MSTW collaboration [48] and the result is shown in Fig. 5 (green band and green lines) as a function of  $M_H$ . As one can see, the obtained uncertainties are much larger than the pure PDF uncertainties alone. This is particularly true at low Higgs masses where the uncertainty is doubled. Nevertheless, even with this additional uncertainty, one still cannot reconcile the MSTW and the ABKM/HERAPDF predictions for instance, in particular at high Higgs masses.

However, it has been argued in Ref. [18] that one also needs to consider the theoretical uncertainty on  $\alpha_s$  that is due to the truncation of the perturbative series, the different heavy flavor schemes, etc... This is particularly true as one has a significant difference between the  $\alpha_s$  world average value and the value obtained from deep-inelastic scattering data alone, a difference which could be reduced if this theory uncertainty is included. The MSTW collaboration estimates the theoretical uncertainty to be  $\Delta^{\text{th}}\alpha_s = 0.003$  at NLO [48], which gives  $\Delta^{\text{th}}\alpha_s = 0.002$  at most at NNLO. Using a fixed  $\alpha_s$  NNLO grid with central PDFs given by the MSTW collaboration, with  $\alpha_s$  values different from the best-fit value (in the range 0.107–0.127 with steps of 0.001 and which thus include the values  $\alpha_s(M_Z^2) = 0.1171 \pm 0.002$  at NNLO), we have evaluated this uncertainty. Adding it in quadrature to the PDF+ $\Delta^{\text{exp}}\alpha_s$  uncertainty, we obtain a total PDF+ $\Delta^{\text{exp}}\alpha_s + \Delta^{\text{th}}\alpha_s$  uncertainty of  $\approx 11\% - 15\%$  depending on the Higgs mass. At least for not too heavy Higgs bosons, this larger uncertainty reconciles the MSTW and ABKM/HERAPDF predictions<sup>9</sup>.

Note that for  $M_H \lesssim 200$  GeV, we obtain smaller uncertainties compared to the  $\approx \pm 15\% - 20\%$  uncertainty of  $\sigma^{\text{NNLO}}(gg \rightarrow H)$  at the Tevatron, a reflection of the better control on the behavior of the gluon density at moderate- $x$  values (relevant for the IHC) compared to high- $x$  values (relevant for the Tevatron).

We note also that the result that we obtain here for the PDF+ $\Delta^{\text{exp}}\alpha_s + \Delta^{\text{th}}\alpha_s$  uncertainty is larger than what one obtains using the recommendation of the PDF4LHC group [56], that is, to take the envelope of the PDF+ $\Delta^{\text{exp}}\alpha_s$  values provided by the MSTW, CTEQ and NNPDF sets or more simply (and more consistently at NNLO), take the 68%CL MSTW PDF+ $\Delta^{\text{exp}}\alpha_s$  error and multiply it by a factor of two. To our opinion, this estimate of the uncertainty is rather optimistic and, as can be seen from Fig. 6, cannot account for the difference between the predictions using the various NNLO parameterizations.

In the rest of our analysis, we will take the 90% CL PDF+ $\Delta^{\text{exp}}\alpha_s + \Delta^{\text{th}}\alpha_s$  uncertainty evaluated as above as the total PDF uncertainty in the determination of the  $gg \rightarrow H$  production cross section. However, we will view this uncertainty as a measure of the difference between the various possible parameterizations of the PDFs and, hence, consider it as a true theoretical uncertainty with no statistical ground as will be discussed shortly.

---

<sup>9</sup>Note that we could also take into account the effects due to the bottom and charm quark masses on the PDFs. Indeed, a change in the fitted masses for these quarks may affect the gluon splitting and hence alter the shape of the gluon-gluon luminosity in  $gg \rightarrow H$ . We have estimated quantitatively this effect by using the  $m_b$  and  $m_c$  dependent MSTW PDFs [55] with  $m_c = 1.40 \pm 0.15$  GeV and  $m_b = 4.75 \pm 0.05$  GeV. In the case of the charm quark, we obtain a  $\approx 0.2\%$  change at  $M_H = 115$  GeV and at most  $\approx 1.5\%$  change at  $M_H = 500$  GeV. In the case of the  $b$ -quark, the change is below the percent level (see also section 4.3). These uncertainties can be neglected as we adopted the attitude of adding them in quadrature with the ones due to the PDF and  $\alpha_s$  which are much larger.

### 2.3 The combined uncertainty

A very important issue that remains is the way to combine the various theoretical uncertainties on the cross section discussed in the previous subsection. Let us first reiterate an important comment: the uncertainties associated to the PDFs in a given scheme should be viewed as purely theoretical uncertainties despite of the fact that they are presented as the  $1\sigma$  or more departure from the central values of the data included in the PDF fits. Indeed, this uncertainty should be interpreted as being due to the parametrization of the quark and gluon densities and, hence, to the theoretical assumptions in determining these densities and equivalent to the spread that one observes when comparing different parameterizations. Thus, the PDF uncertainties should be considered as having no statistical ground<sup>10</sup> and they cannot be combined in quadrature with the two other purely theoretical errors, namely the scale and the scheme (EFT) uncertainties. This should be contrasted to what has been done, for instance, by the CDF and D0 collaborations in their combined Higgs analysis at the Tevatron [9], where the scale and PDF uncertainties have been added in quadrature.

Here, we discuss three possible ways to combine the various uncertainties.

- A) A reasonable procedure to combine the uncertainty from scale and scheme dependence with the PDF uncertainties has been presented in Ref. [18], which also takes into account the correlation between the scale and the PDFs (which are evaluated at a given factorization scale): one calculates the maximal/minimal cross sections with respect to the scale variation and apply on these cross sections the PDF+ $\Delta^{\text{exp}}\alpha_s+\Delta^{\text{th}}\alpha_s$  uncertainty. This procedure has been in fact already proposed, together with other possibilities which give similar results, in Ref. [57] where top quark pair production at hadron colliders was discussed. An argument for the approach put forward in Ref. [57] is that unknown high order effects also enter in the PDFs determination and one needs to use the full information on the PDF uncertainties in the determination of the scale dependence. To this combined scale+PDF uncertainty, one can linearly add the scheme/EFT uncertainty to obtain the overall theoretical error.
- B) In fact, a much simpler way to combine the scale, EFT/scheme and the PDF uncertainties which, as mentioned before, should all be considered as pure theoretical errors, is to add them linearly. Doing so, one in general obtains uncertainties that are slightly larger than with the procedure A described above.
- C) A third possibility is to take the different predictions of the cross sections when evaluated with the various sets of NNLO PDF sets as a measure of the PDF uncertainty. Since the maximal cross section for  $gg \rightarrow H$  is obtained with the MSTW parametrization and the minimal one with the ABKM set (see Fig. 6), the total uncertainty on the production cross section will be simply the sum of the scale and scheme/EFT uncertainties when evaluated with the MSTW PDF set (for the + uncertainty) and when evaluated with the ABKM PDF set (for the - uncertainty) which maximizes/minimizes the cross section.

---

<sup>10</sup>In statistical language, the PDF uncertainties should be considered as having a flat prior, exactly like the scale uncertainty. A more elaborated discussion can be found in [14] where the recommended combination is that of the linear type.



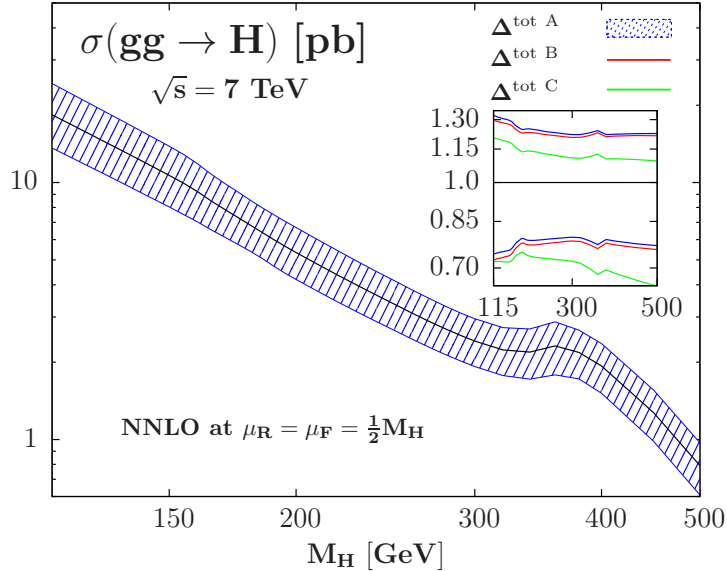


**Figure 7:** The production cross section  $\sigma(gg \rightarrow H)$  at NNLO at the IHC with  $\sqrt{s} = 7$  TeV, including the total theoretical uncertainty band when all the individual uncertainties are combined using the three procedures A, B and C described in the text. In the inserts, the relative deviations from the central cross section value are shown.

Using the three procedures A, B, C described above, one obtains the overall theoretical uncertainties on  $\sigma^{\text{NNLO}}(gg \rightarrow H)$  at the 7 TeV IHC that are shown in Fig. 7 as a function of the Higgs mass. With the procedure A, the uncertainty amounts<sup>11</sup> to  $\approx -23\%$ ,  $+25\%$  for  $M_H \lesssim 160$  GeV, reduces to  $\approx -21\%$ ,  $+22\%$  for  $M_H \gtrsim 200$  GeV to reach the value  $\approx \pm 22\%$  at  $M_H \approx 500$  GeV. With the procedure B, i.e. when the various sources of uncertainties are added linearly, one obtains approximately the same total uncertainty as above; they are a few percent (2 to 3%) smaller for the + uncertainty and higher for the - uncertainty. In the case of procedure C, as we use for the central prediction of  $\sigma^{\text{NNLO}}(gg \rightarrow H)$  the MSTW PDF set, the + uncertainty is simply the sum of the scale and scheme uncertainties which add to less than 20% in the entire Higgs mass and are thus much smaller (in particular in the low Higgs mass range) than in procedures A and B, while for the - uncertainty, one has to add the difference between the MSTW and ABKM predictions. In this case, the overall uncertainty is comparable to what is obtained using the procedures A and B in the low Higgs mass range where the difference between MSTW and ABKM is of the order of 10% and, hence, the Hessian MSTW PDF+ $\alpha_s$  uncertainty. It becomes much larger at higher  $M_H$  values where the difference between the MSTW and ABKM predictions becomes significant: at  $M_H = 500$  GeV, one obtains an uncertainty of  $\approx -35\%$ , compared to  $\approx -23\%$  using procedures A and B.

<sup>11</sup>Note that the overall uncertainty on  $\sigma^{\text{NNLO}}(gg \rightarrow H)$  at the IHC is significantly smaller than what has been obtained at the Tevatron using the procedure A for the combination,  $\approx -35\%$ ,  $+40\%$ , as a result of the reduction of both the scale and the PDF uncertainties at  $\sqrt{s} = 7$  TeV compared to  $\sqrt{s} = 1.96$  TeV. The main reasons are that, at the IHC, the QCD  $K$ -factors are smaller and the gluon density has a less uncertain behavior for not too heavy Higgs bosons.

$M_H$	$\sigma_{gg \rightarrow H}$	$\pm\Delta_\mu \pm\Delta^{\text{PDF}} \pm\Delta^{\text{EFT}}$	A	B	C
115	18.35	+9.1%+9.1%+7.3% -10.2%-8.8%-7.3%	+27.8% -24.6%	+25.6% -26.3%	+16.4% -26.8%
120	16.84	+8.9%+9.1%+7.3% -10.2%-8.8%-7.3%	+27.5% -24.5%	+25.3% -26.2%	+16.2% -26.8%
125	15.51	+8.8%+9.1%+7.2% -9.9%-8.8%-7.2%	+27.1% -24.1%	+25.1% -25.8%	+16.0% -26.7%
130	14.32	+8.5%+9.1%+7.1% -9.8%-8.8%-7.1%	+26.7% -24.0%	+24.7% -25.6%	+15.6% -26.7%
135	13.26	+8.4%+9.1%+7.0% -9.6%-8.8%-7.0%	+26.4% -23.7%	+24.5% -25.4%	+15.4% -26.6%
140	12.31	+8.3%+9.1%+7.0% -9.5%-8.8%-7.0%	+26.2% -23.6%	+24.3% -25.2%	+15.3% -26.7%
145	11.45	+8.2%+9.1%+6.9% -9.5%-8.8%-6.9%	+26.0% -23.6%	+24.2% -25.2%	+15.1% -26.8%
150	10.67	+8.1%+9.1%+6.8% -9.5%-8.8%-6.8%	+25.8% -23.5%	+24% -25.1%	+14.9% -26.9%
155	9.94	+7.9%+9.1%+6.6% -9.4%-8.8%-6.6%	+25.4% -23.2%	+23.6% -24.8%	+14.5% -26.8%
160	9.21	+7.8%+9.1%+5.9% -9.4%-8.8%-5.9%	+24.4% -22.7%	+22.8% -24.2%	+13.7% -26.4%
165	8.47	+7.7%+9.1%+4.9% -9.4%-8.8%-4.9%	+23.4% -21.7%	+21.7% -23.1%	+12.6% -25.5%
170	7.87	+7.7%+9.1%+4.2% -9.4%-8.8%-4.2%	+22.7% -21.0%	+21.1% -22.5%	+11.9% -25.0%
175	7.35	+7.6%+9.1%+3.7% -9.4%-8.9%-3.7%	+22.0% -20.5%	+20.4% -21.9%	+11.3% -24.6%
180	6.86	+7.5%+9.2%+3.1% -9.3%-8.9%-3.1%	+21.4% -19.9%	+19.8% -21.3%	+10.6% -24.2%
185	6.42	+7.4%+9.2%+3.0% -9.3%-8.9%-3.0%	+21.1% -19.8%	+19.6% -21.2%	+10.4% -24.2%
190	6.01	+7.4%+9.2%+3.4% -9.3%-8.9%-3.4%	+21.5% -20.3%	+20.0% -21.7%	+10.8% -24.9%
195	5.65	+7.4%+9.2%+3.6% -9.3%-8.9%-3.6%	+21.8% -20.5%	+20.3% -21.9%	+11.0% -25.2%
200	5.34	+7.3%+9.3%+3.7% -9.3%-9.0%-3.7%	+21.8% -20.6%	+20.3% -21.9%	+11.0% -25.4%
210	4.81	+7.2%+9.3%+3.7% -9.3%-9.0%-3.7%	+21.7% -20.6%	+20.2% -22.0%	+10.9% -25.8%
220	4.36	+7.2%+9.3%+3.6% -9.2%-9.1%-3.6%	+21.6% -20.6%	+20.2% -21.9%	+10.9% -26.0%
230	3.97	+7.0%+9.4%+3.5% -9.2%-9.2%-3.5%	+21.4% -20.5%	+19.9% -21.8%	+10.5% -26.2%
240	3.65	+7.0%+9.5%+3.3% -9.2%-9.2%-3.3%	+21.1% -20.5%	+19.8% -21.8%	+10.3% -26.5%
250	3.37	+6.9%+9.5%+3.1% -9.2%-9.3%-3.1%	+20.9% -20.4%	+19.5% -21.6%	+10.0% -26.6%
260	3.11	+6.8%+9.6%+3.0% -9.2%-9.4%-3.0%	+20.6% -20.3%	+19.3% -21.6%	+9.7% -26.8%
270	2.89	+6.7%+9.7%+2.8% -9.2%-9.5%-2.8%	+20.5% -20.2%	+19.1% -21.4%	+9.4% -27.0%
280	2.71	+6.8%+9.8%+2.6% -9.2%-9.5%-2.6%	+20.5% -20.1%	+19.2% -21.4%	+9.4% -27.2%
290	2.55	+6.8%+9.8%+2.4% -9.1%-9.6%-2.4%	+20.3% -20.0%	+19.1% -21.1%	+9.2% -27.2%
300	2.42	+6.7%+9.9%+2.3% -9.1%-9.7%-2.3%	+20.2% -19.9%	+18.9% -21.1%	+9.0% -27.4%
320	2.23	+6.7%+10.1%+2.3% -9.2%-9.9%-2.3%	+20.2% -20.1%	+19.0% -21.4%	+9.0% -28.2%
340	2.19	+6.9%+10.3%+3.0% -9.2%-10.1%-3.0%	+21.4% -21.1%	+20.2% -22.3%	+10.0% -29.6%
360	2.31	+7.0%+10.5%+4.1% -9.2%-10.3%-4.1%	+22.5% -22.3%	+21.6% -23.6%	+11.0% -31.3%
380	2.18	+6.3%+10.7%+2.5% -9.1%-10.5%-2.5%	+20.4% -20.9%	+19.6% -22.2%	+8.8% -30.3%
400	1.93	+5.9%+11.0%+3.1% -8.8%-10.7%-3.1%	+20.7% -21.5%	+20.0% -22.7%	+9.0% -31.3%
450	1.27	+5.0%+11.6%+4.0% -8.4%-11.3%-4.0%	+21.4% -22.6%	+20.5% -23.8%	+9.0% -33.4%
500	0.79	+4.4%+12.2%+4.5% -8.1%-11.9%-4.5%	+22.1% -23.3%	+21.1% -24.5%	+8.9% -35.2%
600	0.31	+3.7%+13.3%+6.6% -7.7%-13.0%-6.6%	+24.5% -26.1%	+23.7% -27.3%	+10.4% -40.0%

**Table 2:** The NNLO total Higgs production cross sections in the  $gg \rightarrow H$  process at the LHC with  $\sqrt{s} = 7$  TeV (in pb) for given Higgs mass values (in GeV) at a central scale  $\mu_F = \mu_R = \frac{1}{2}M_H$ . Shown also are the corresponding shifts due to the theoretical uncertainties from the various sources discussed (first from scale, then from PDF+ $\Delta^{\text{exp+th}}\alpha_s$  at 90%CL and from EFT), as well as the total uncertainty when all errors are added using the procedures A, B and C described in the text.

In Table 2, we summarize the results obtained in this section<sup>12</sup>. The  $gg \rightarrow H$  production cross section for values of the Higgs mass relevant at the IHC with  $\sqrt{s} = 7$  TeV are given together with the uncertainties from scale variations, the PDF+ $\Delta^{\text{exp}}\alpha_s+\Delta^{\text{th}}\alpha_s$  uncertainty in the MSTW scheme and the uncertainty due the use of the EFT approach beyond the NLO approximation. The combined uncertainties obtained using the three procedures A, B and C proposed above are also given.

## 2.4 The cross sections at $\sqrt{s} = 8\text{--}10$ TeV and 14 TeV

As already stated, intermediate center of mass energies between  $\sqrt{s} = 7$  and 10 TeV are being currently considered for the IHC in a very near future, with the possibility of collecting integrated luminosities that are significantly larger than  $1 \text{ fb}^{-1}$  [11]. We therefore also display the theoretical predictions for the Higgs production rates in the  $gg \rightarrow H$  channel at these energies, following exactly the same steps as the ones discussed in section 2.1. The results for  $\sigma^{\text{NNLO}}(gg \rightarrow H)$ , again for a central scale  $\mu_R = \mu_F = \frac{1}{2}M_H$  and using the MSTW2008 set of NNLO PDFs, are displayed for  $\sqrt{s} = 8, 9$  and 10 TeV in Fig. 8 as a function of  $M_H$  and in Table 3 for the relevant Higgs mass values .

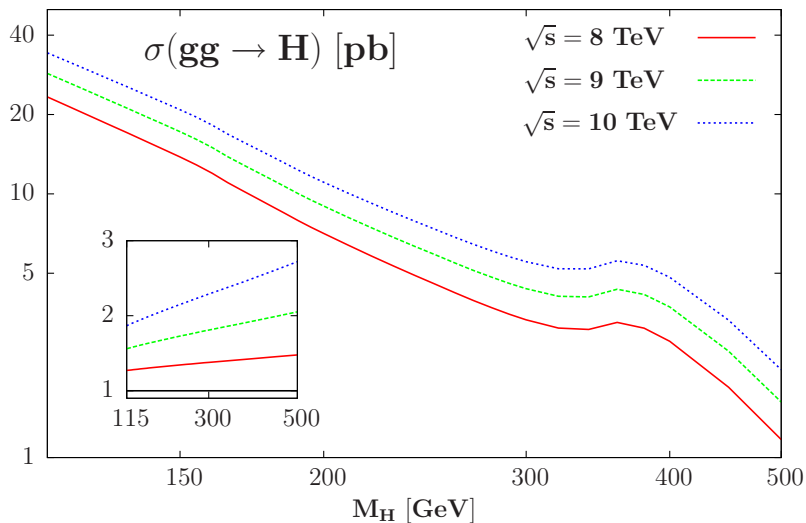


**Figure 8:** The production cross section  $\sigma(gg \rightarrow H)$  at NNLO as a function of  $M_H$  at the IHC with center of mass energies of  $\sqrt{s} = 8, 9$  and 10 TeV. In the inserts, the relative increase compared to the cross section at  $\sqrt{s} = 7$  TeV are shown.

We see that in the low Higgs mass range,  $M_H \approx 120$  GeV, the cross section  $\sigma(gg \rightarrow H)$  is  $\approx 20\%$ ,  $40\%$  and  $\approx 100\%$  higher at, respectively,  $\sqrt{s} = 8, 9$  and 10 TeV, compared to  $\sqrt{s} = 7$  TeV. At higher Higgs masses,  $M_H \gtrsim 300$  GeV, the increase of the cross section is slightly larger as a result of the reduction of the phase space at lower energies.

As far as the theoretical uncertainties are concerned, we have verified that they differ only by a small amount, less than one to two percent, when increasing the center of mass energy from  $\sqrt{s} = 7$  to  $\sqrt{s} = 10$  TeV. To a good approximation, one can therefore use the

<sup>12</sup>An extended table for Higgs masses up to 1 TeV can be found in the  $gg$ -fusion section of Ref. [14].

$M_H$	$\sigma_{gg \rightarrow H}^{8 \text{ TeV}}$	$\sigma_{gg \rightarrow H}^{9 \text{ TeV}}$	$\sigma_{gg \rightarrow H}^{10 \text{ TeV}}$	$M_H$	$\sigma_{gg \rightarrow H}^{8 \text{ TeV}}$	$\sigma_{gg \rightarrow H}^{9 \text{ TeV}}$	$\sigma_{gg \rightarrow H}^{10 \text{ TeV}}$
115	23.31	28.63	34.26	210	6.39	8.15	10.07
120	21.46	26.42	31.68	220	5.82	7.44	9.22
125	19.81	24.44	29.37	230	5.33	6.84	8.50
130	18.34	22.68	27.30	240	4.91	6.32	7.88
135	17.03	21.10	25.44	250	4.55	5.88	7.34
140	15.84	19.67	23.76	260	4.22	5.47	6.85
145	14.77	18.38	22.24	270	3.94	5.13	6.44
150	13.80	17.21	20.86	280	3.70	4.83	6.08
155	12.89	16.10	19.55	290	3.50	4.58	5.78
160	11.97	14.98	18.22	300	3.33	4.37	5.53
165	11.04	13.85	16.87	320	3.10	4.09	5.20
170	10.28	12.92	15.77	340	3.06	4.07	5.19
175	9.62	12.11	14.80	360	3.26	4.35	5.58
180	9.00	11.36	13.90	380	3.09	4.15	5.36
185	8.44	10.66	13.08	400	2.76	3.73	4.83
190	7.92	10.03	12.32	450	1.85	2.53	3.32
195	7.47	9.47	11.65	500	1.17	1.62	2.15
200	7.07	8.99	11.07	600	0.47	0.68	0.92

**Table 3:** The cross sections in the  $\sigma^{\text{NNLO}}(gg \rightarrow H)$  at the LHC with  $\sqrt{s} = 8, 9, 10$  TeV (in pb) for given Higgs mass values (in GeV) at a central scale  $\mu_F = \mu_R = \frac{1}{2}M_H$  using the MSTW PDF set.

values of the scale, scheme/EFT and PDF+ $\Delta^{\text{exp}}\alpha_s + \Delta^{\text{th}}\alpha_s$  uncertainties, as well as the combined uncertainties, that are given in Table 2 for the  $\sqrt{s} = 7$  TeV case.

Finally, let us briefly summarize the expectations for the LHC with the design center of mass energy of  $\sqrt{s} = 14$  TeV, which is expected to collect at least  $\sim 30 \text{ fb}^{-1}$  of data that should allow to discover the Higgs boson in its entire mass range  $115 \text{ GeV} \leq M_H \lesssim 1 \text{ TeV}$ . The results for the  $gg \rightarrow H$  cross section at  $\sqrt{s} = 14$  TeV are summarized in Figs. 9, 10, 11 and in Table 4, following exactly the same lines and procedure as at  $\sqrt{s} = 7$  TeV.

We will simply make a few comments to highlight the main differences:

- The scale uncertainty, estimated by varying  $\mu_R$  and  $\mu_F$  again in the domain  $\frac{1}{4}M_H \leq \mu_R = \mu_F \leq M_H$ , does not significantly change when comparing to the LHC case: one obtains a variation of  $\approx \pm 10\%$  at low and  $\approx \pm 5\%$  at high Higgs masses; see Fig. 9 (left).

- The EFT/scheme uncertainty is almost exactly the same than at  $\sqrt{s} = 7$  TeV, as its most important component enters as a multiplicative factor in the  $gg \rightarrow H$  amplitude but is larger starting from  $M_H \gtrsim 500$  GeV; Fig. 9 (right).

- For the PDF uncertainties, one can see in Fig. 10 (left) that one still has significant differences when folding the partonic  $gg \rightarrow H$  cross section with the gluon luminosities given by the four NNLO PDFs sets. Fig. 10 (right) displays the PDF, PDF+ $\Delta^{\text{exp}}\alpha_s$  and the combined PDF+ $\Delta^{\text{exp}}\alpha_s + \Delta^{\text{th}}\alpha_s$  uncertainties at the LHC. One obtains a slightly smaller PDF+ $\alpha_s$  uncertainty than at the LHC, 1 to 2% , since lower  $x$  values are probed.

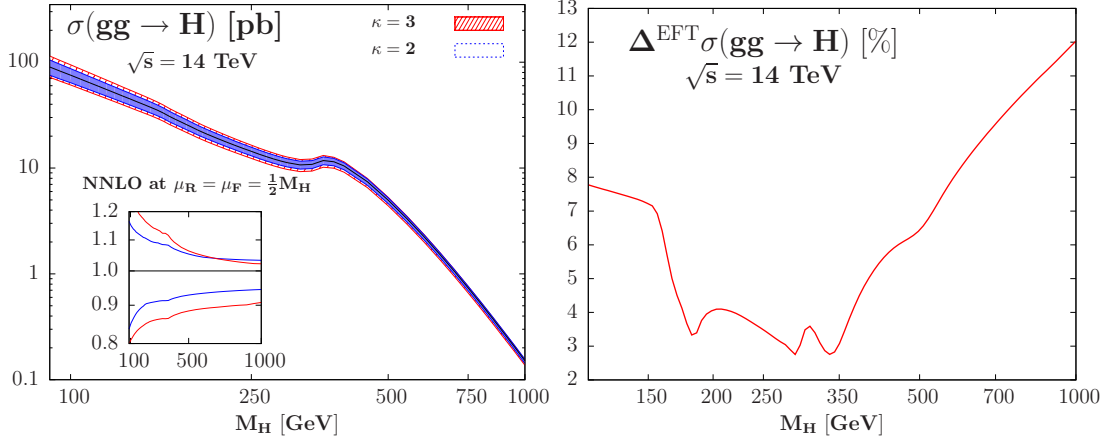


**Figure 9:** The uncertainty bands of  $\sigma_{gg \rightarrow H}^{\text{NNLO}}$  from scale variation with  $\kappa = 2$  (left) and the total EFT uncertainty (right) at  $\sqrt{s} = 14$  TeV as a function of  $M_H$ .

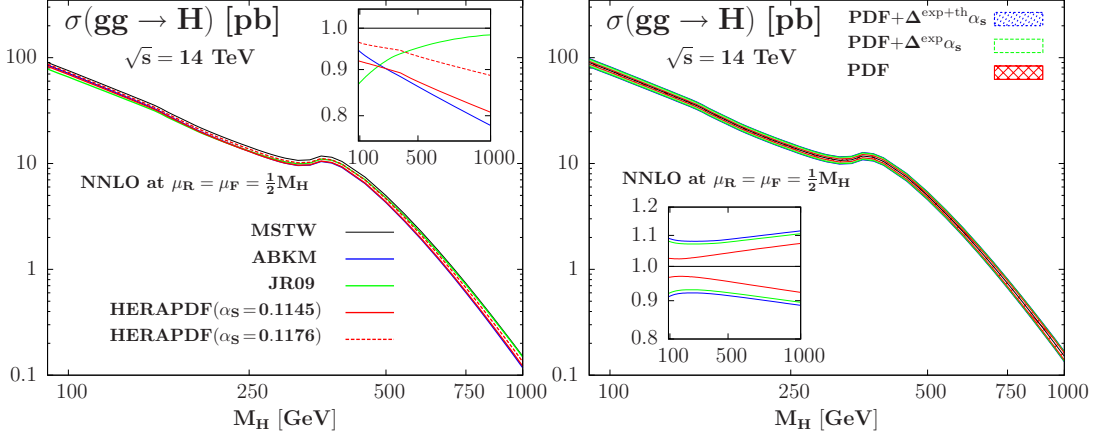


**Figure 10:** The PDF uncertainties in  $\sigma^{\text{NNLO}}(gg \rightarrow H)$  at the LHC with  $\sqrt{s} = 14$  TeV as a function of  $M_H$ . Left: the central values when using the four NNLO PDFs and right: the 90% CL PDF, PDF+ $\Delta^{\text{exp}}\alpha_s$  and PDF+ $\Delta^{\text{exp}}\alpha_s + \Delta^{\text{th}}\alpha_s$  uncertainties in the MSTW scheme.

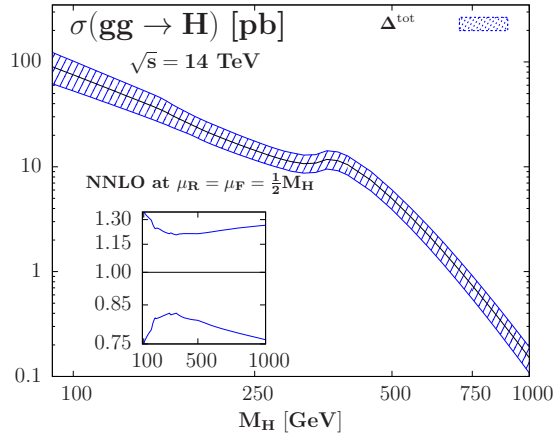


**Figure 11:** The cross section  $\sigma^{\text{NNLO}}(gg \rightarrow H)$  at the LHC with the uncertainty band when all theoretical uncertainties are added using our procedure A described in the text.

– For the overall uncertainty on  $\sigma^{\text{NNLO}}(gg \rightarrow H)$  shown in Fig. 11, where we have restricted ourselves to procedure A only, it is more or less the same at 14 TeV than at 7 TeV in the low Higgs mass range, but is slightly smaller for heavier Higgs bosons. As an example, we obtain for  $M_H = 500$  GeV a total  $\approx \pm 21\%$  uncertainty at 14 TeV compared to  $\approx \pm 23\%$  at 7 TeV.

Table 4 which displays the cross sections together with the individual and overall theoretical uncertainties for the Higgs masses relevant at the LHC, summarizes our results.

$M_H$	$\sigma_{gg \rightarrow H}^{\pm \Delta_\mu \pm \Delta_{\text{PDF}} \pm \Delta_{\text{EFT}}}$	A	B	$M_H$	$\sigma_{gg \rightarrow H}^{\pm \Delta_\mu \pm \Delta_{\text{PDF}} \pm \Delta_{\text{EFT}}}$	A	B
115	$59.37^{+9.4\%+8.7\%+7.8\%}_{-12.2\%-8.5\%-7.8\%}$	+28.1% -26.6%	+25.8% -28.5%	240	$15.30^{+7.0\%+8.0\%+3.7\%}_{-8.2\%-7.8\%-3.7\%}$	+20.0% -18.6%	+18.7% -19.6%
120	$55.20^{+9.2\%+8.6\%+7.7\%}_{-11.9\%-8.4\%-7.7\%}$	+27.8% -26.1%	+25.5% -28.0%	250	$14.38^{+6.9\%+8.0\%+3.5\%}_{-8.2\%-7.8\%-3.5\%}$	+19.7% -18.4%	+18.4% -19.5%
125	$51.45^{+9.0\%+8.5\%+7.6\%}_{-11.6\%-8.4\%-7.6\%}$	+27.4% -25.7%	+25.1% -27.5%	260	$13.52^{+6.8\%+8.0\%+3.3\%}_{-8.1\%-7.8\%-3.3\%}$	+19.4% -18.2%	+18.1% -19.2%
130	$48.09^{+8.9\%+8.5\%+7.5\%}_{-11.4\%-8.3\%-7.5\%}$	+27.2% -25.5%	+25.0% -27.3%	270	$12.79^{+6.7\%+8.0\%+3.1\%}_{-8.1\%-7.8\%-3.1\%}$	+19.1% -18.1%	+17.9% -19.1%
135	$45.06^{+8.7\%+8.4\%+7.5\%}_{-11.1\%-8.2\%-7.5\%}$	+26.8% -25.1%	+24.6% -26.8%	280	$12.17^{+6.7\%+8.0\%+2.9\%}_{-8.1\%-7.8\%-2.9\%}$	+18.9% -17.8%	+17.7% -18.8%
140	$42.30^{+8.5\%+8.4\%+7.4\%}_{-10.8\%-8.2\%-7.4\%}$	+26.4% -24.7%	+24.3% -26.4%	290	$11.65^{+6.6\%+8.0\%+2.8\%}_{-8.0\%-7.8\%-2.8\%}$	+18.6% -17.6%	+17.4% -18.6%
145	$39.80^{+8.4\%+8.3\%+7.3\%}_{-10.6\%-8.1\%-7.3\%}$	+26.0% -24.4%	+24.0% -26.1%	300	$11.22^{+6.5\%+8.0\%+3.4\%}_{-8.0\%-7.8\%-3.4\%}$	+19.2% -18.4%	+18.0% -19.3%
150	$37.50^{+8.3\%+8.3\%+7.2\%}_{-10.4\%-8.1\%-7.2\%}$	+25.8% -24.1%	+23.8% -25.7%	320	$10.70^{+6.5\%+8.1\%+3.1\%}_{-8.0\%-7.9\%-3.1\%}$	+18.8% -18.1%	+17.8% -19.1%
155	$35.32^{+8.1\%+8.3\%+7.0\%}_{-10.2\%-8.1\%-7.0\%}$	+25.3% -23.7%	+23.4% -25.3%	340	$10.83^{+6.5\%+8.1\%+2.8\%}_{-8.0\%-7.9\%-2.8\%}$	+18.4% -17.8%	+17.4% -18.7%
160	$33.08^{+8.0\%+8.2\%+6.3\%}_{-10.0\%-8.0\%-6.3\%}$	+24.4% -22.9%	+22.6% -24.4%	360	$11.77^{+6.4\%+8.1\%+3.5\%}_{-8.0\%-8.0\%-3.5\%}$	+19.0% -18.6%	+18.1% -19.5%
165	$30.77^{+7.9\%+8.2\%+5.3\%}_{-9.8\%-8.0\%-5.3\%}$	+23.1% -21.8%	+21.4% -23.1%	380	$11.46^{+6.0\%+8.2\%+4.4\%}_{-7.7\%-8.1\%-4.4\%}$	+19.5% -19.2%	+18.6% -20.2%
170	$28.89^{+7.8\%+8.2\%+4.5\%}_{-9.7\%-8.0\%-4.5\%}$	+22.3% -21.0%	+20.6% -22.3%	400	$10.46^{+5.6\%+8.2\%+5.0\%}_{-7.4\%-8.1\%-5.0\%}$	+19.7% -19.7%	+18.9% -20.6%
175	$27.24^{+7.8\%+8.2\%+4.0\%}_{-9.5\%-7.9\%-4.0\%}$	+21.6% -20.2%	+20.0% -21.4%	450	$7.42^{+5.0\%+8.4\%+6.0\%}_{-7.0\%-8.3\%-6.0\%}$	+20.0% -20.4%	+19.3% -21.3%
180	$25.71^{+7.7\%+8.2\%+3.5\%}_{-9.4\%-7.9\%-3.5\%}$	+20.9% -19.6%	+19.3% -20.8%	500	$4.97^{+4.6\%+8.6\%+6.4\%}_{-6.7\%-8.6\%-6.4\%}$	+20.4% -20.9%	+19.7% -21.7%
185	$24.28^{+7.6\%+8.1\%+3.3\%}_{-9.1\%-7.9\%-3.3\%}$	+20.6% -19.2%	+19.0% -20.4%	550	$3.32^{+4.3\%+8.9\%+7.4\%}_{-6.5\%-8.8\%-7.4\%}$	+21.3% -21.9%	+20.7% -22.7%
190	$22.97^{+7.6\%+8.1\%+3.8\%}_{-9.1\%-7.9\%-3.8\%}$	+21.0% -19.6%	+19.5% -20.7%	600	$2.24^{+4.1\%+9.2\%+8.3\%}_{-6.3\%-9.1\%-8.3\%}$	+22.1% -22.9%	+21.6% -23.7%
195	$21.83^{+7.5\%+8.1\%+4.0\%}_{-9.0\%-7.9\%-4.0\%}$	+21.1% -19.7%	+19.6% -20.8%	650	$1.53^{+3.9\%+9.5\%+9.0\%}_{-6.2\%-9.4\%-9.0\%}$	+22.7% -23.9%	+22.4% -24.6%
200	$20.83^{+7.4\%+8.1\%+4.1\%}_{-8.8\%-7.9\%-4.1\%}$	+21.0% -19.6%	+19.5% -20.7%	700	$1.05^{+3.8\%+9.8\%+9.6\%}_{-6.1\%-9.6\%-9.6\%}$	+23.4% -24.6%	+23.2% -25.3%
210	$19.10^{+7.3\%+8.1\%+4.1\%}_{-8.6\%-7.8\%-4.1\%}$	+20.9% -19.4%	+19.5% -20.5%	800	$0.52^{+3.5\%+10.4\%+10.5\%}_{-6.0\%-10.2\%-10.5\%}$	+24.6% -26.1%	+24.4% -26.7%
220	$17.64^{+7.2\%+8.1\%+4.0\%}_{-8.4\%-7.8\%-4.0\%}$	+20.6% -19.2%	+19.3% -20.3%	900	$0.27^{+3.4\%+11.0\%+11.3\%}_{-5.9\%-10.7\%-11.3\%}$	+25.6% -27.5%	+25.7% -28.0%
230	$16.38^{+7.1\%+8.0\%+3.8\%}_{-8.3\%-7.8\%-3.8\%}$	+20.4% -18.9%	+19.0% -20.0%	1000	$0.15^{+3.3\%+11.5\%+12.0\%}_{-5.8\%-11.3\%-12.0\%}$	+26.4% -28.8%	+26.9% -29.1%

**Table 4:** The NNLO total Higgs production cross sections in the  $gg \rightarrow H$  process at the LHC with  $\sqrt{s} = 14$  TeV (in pb) for given Higgs mass values (in GeV) at a central scale  $\mu_F = \mu_R = \frac{1}{2}M_H$ . Shown also are the corresponding shifts due to the theoretical uncertainties from the various sources discussed (first from scale, then from PDF+ $\Delta^{\text{exp+th}}\alpha_s$  at 90%CL and from EFT), as well as the total uncertainty when all errors are added using the procedures A and B described in the text.

### 3. The Higgs decay branching fractions

#### 3.1 The parametric uncertainties

There is an additional source of theoretical errors which has not been considered in Ref. [18] and not included in the Tevatron and LHC experimental analyses [9, 12, 13]: the one due to the branching ratios in the Higgs boson decays<sup>13</sup>. Indeed, contrary to the partial widths of Higgs decays into leptons and gauge bosons where only electroweak corrections appear at the lowest orders and are thus known precisely, the partial decay widths into quark pairs and gluons are plagued with various uncertainties due to strong interactions [23].

As it is well known, the QCD corrections to the  $H \rightarrow Q\bar{Q}$  partial widths, with  $Q = b$  and  $c$ , are extremely large; for reviews, see Refs. [2, 6]. The bulk of these corrections can be absorbed into running quark masses by defining an effective  $HQ\bar{Q}$  Yukawa interaction in which the pole quark masses  $M_Q(M_Q)$  are replaced by running quark masses in the  $\overline{\text{MS}}$  scheme,  $\overline{m}_Q$ , with  $\alpha_s$  evaluated at the scale of the pole mass  $\mu = M_Q$  [58]. One then evolves  $\overline{m}_Q$  from  $M_Q$  upward to a renormalization scale  $\mu$ , which should be chosen to be close to the Higgs mass,  $\mu \approx M_H$ . Using as starting points the pole masses  $M_Q$ , the values of the running  $b, c$  masses at the scale  $\mu \sim 100$  GeV are, respectively,  $\approx 1.5$  and  $\approx 2$  times smaller than the pole masses. The partial widths,  $\Gamma(H \rightarrow Q\bar{Q}) \propto \overline{m}_Q^2$  (but where additional QCD corrections that are known up to three-loops need to be implemented [6, 59]), are thus reduced by factors of  $\approx 2$  and  $\approx 4$  for Higgs decays into  $b\bar{b}$  and  $c\bar{c}$ , respectively.

Nevertheless, residual uncertainties in the  $H \rightarrow Q\bar{Q}$  partial decay widths will remain. These uncertainties are mainly due to three sources: *i*) the imperfect knowledge of the input bottom and charm quark masses, *ii*) the error on  $\alpha_s$  which migrates into uncertainties on the running quark masses at the scale  $\mu$  and on the residual QCD corrections to the partial widths and, finally, *iii*) the variation of the scale  $\mu$  which enters as an argument in  $\alpha_s$ , in the running quark masses  $\overline{m}_Q$  and in the residual QCD corrections. This last uncertainty, which is expected to account for the missing (not yet calculated) higher order contributions to the partial widths, turns out to be very small (as both the quark mass evolution and the residual corrections are known up to three loops) and can be safely neglected [60].

In the case of the decay  $H \rightarrow gg$ , the leading order partial width, that is proportional to  $\alpha_s^2$ , has to be corrected by large QCD corrections which nearly double the width [20, 61]. It is affected by uncertainties due to the error on  $\alpha_s$  and to the residual scale dependence which is about  $\approx 10\%$  at NNLO [61]. However, as the branching ratio of this decay is of order a few percent at most in the entire Higgs mass range, these uncertainties do not affect the total Higgs width and thus, the dominant branching ratios, in a substantial way.

We will assume that the uncertainties in the decays widths  $H \rightarrow \tau^+\tau^-$  and  $H \rightarrow VV^*$  are negligible<sup>14</sup> as QCD effects will enter the partial widths only at higher orders,  $\geq \mathcal{O}(\alpha_s^2)$ .

<sup>13</sup>A discussion of QCD uncertainties in Higgs decays has also been made recently in Ref. [14].

<sup>14</sup>This might not be entirely true in the case of the  $H \rightarrow WW$  and  $H \rightarrow ZZ$  decay channels near the  $2M_W$  and  $2M_Z$  thresholds where the regularization of the spurious spikes that appear when including one-loop electroweak corrections [62], might introduce some ambiguities. Furthermore, for heavy Higgs bosons  $M_H \gtrsim 500$  GeV, additional corrections to the partial  $H \rightarrow WW, ZZ$  widths from the Higgs self-coupling,  $\lambda_{HHH} \propto M_H^2$  become very large [63]; these uncertainties mostly cancel in the branching ratios, though (but

In the case of  $H \rightarrow \gamma\gamma$ , the decay is mediated mainly by a  $W$  loop and to a lesser extent by a top–quark loop; in the low to moderate  $M_H$  range where the decay is important, the uncertainty due to the latter contribution is small, less than 1%, as the QCD corrections are tiny and the large  $m_t$  limit a good approximation [64].

### 3.2 Uncertainties on the Higgs branching ratios

An analysis of the uncertainties affecting the Higgs branching ratios has been performed long ago in Ref. [23]. Here, we update this analysis in the following way:

- i)* For the strong coupling constant  $\alpha_s$ , we adopt for consistency reasons the same value that we use for determining the central predictions for the production cross section, that is, the MSTW value with its associated  $1\sigma$  error,  $\alpha_s(M_Z^2) = 0.1171 \pm 0.0014$  at NNLO.
- ii)* As starting points for the  $b, c$  masses we use the  $\overline{\text{MS}}$  masses  $\overline{m}_Q$  evaluated at the mass itself with values<sup>15</sup>  $\overline{m}_b(\overline{m}_b) = 4.19_{-0.06}^{+0.18}$  GeV and  $\overline{m}_c(\overline{m}_c) = 1.27_{-0.09}^{+0.07}$  GeV [54]. When we will quote separately the impact of these uncertainties on the Higgs branching ratio, we will assume the central value  $\alpha_s(M_Z^2) = 0.1171$  at NNLO for the strong coupling constant.
- iii)* For the  $H \rightarrow gg$  channel we will consider only the parametric uncertainties that is, the error on  $\alpha_s$  and quark masses (the latter being negligible). At NNLO, the scale uncertainty is of the order 10% but since the branching ratio is small it migrates into an error of less than 1%. In addition, the N<sup>3</sup>LO contribution would reduce this scale variation to the level of a few percent at most and this uncertainty can be safely neglected.

Using an adapted version of the program HDECAY [66] which calculates the partial and total Higgs decay widths including the relevant QCD and electroweak higher order corrections, we have evaluated<sup>16</sup> the uncertainties discussed above and added in quadrature the errors due the input masses  $\overline{m}_b, \overline{m}_c$  and the coupling  $\alpha_s(M_Z^2)$ . We obtain the branching ratios (BR) shown in Fig. 12 as a function of the Higgs mass, including the total uncertainty bands. In Table 5, the branching ratios for the main decay modes  $H \rightarrow b\bar{b}$  and  $H \rightarrow WW$  are given for three selected values of the Higgs mass,  $M_H = 120, 135$  and  $150$  GeV, together with the individual and total uncertainties. The uncertainties (in percentage)

---

they will substantially affect the cross sections for Higgs production in the vector boson fusion processes which are related to the  $H \rightarrow WW/ZZ$  partial decay widths).

<sup>15</sup>While the central values of these masses are close to those obtained in Ref. [65] directly from QCD sum rules in a consistent  $\mathcal{O}(\alpha_s)$  expansion, the corresponding uncertainties are larger. We thus conservatively adopt the PDG values [54], which could also account for possible theory errors; in any case the total uncertainties obtained when using the errors of Ref. [65] would nearly be equal to the uncertainty due to  $\alpha_s$  error alone. Note that with these starting inputs and the value of  $\alpha_s(M_Z^2)$  given above, the central values of the  $b, c$  pole masses are  $m_b = 4.71$  GeV and  $m_c = 1.54$  GeV with variation ranges of, respectively, 4.64–4.90 GeV and 1.42–1.63 GeV. For the pole bottom–quark mass, the central value is rather close to the one adopted in the MSTW scheme for parameterizing the parton densities [38],  $m_b = 4.75$  GeV, and we expect that this difference will have no practical impact.

<sup>16</sup>We thank M. Spira and collaborators for pointing to us a numerical problem in the evaluation of  $H \rightarrow gg$  with HDECAY in an earlier version of the paper.



on the branching ratios for the  $H \rightarrow \tau^+\tau^-$  and  $H \rightarrow ZZ, \gamma\gamma$  channels are the same as those affecting the  $H \rightarrow WW$  mode. In Table 6, displayed are the branching ratios for the various decays as well as their corresponding total uncertainties for a selection of Higgs masses that are relevant for the IHC (and the Tevatron as well).

The largest total errors are by far the ones that affect  $\text{BR}(H \rightarrow c\bar{c})$  which are of the order of 20%, while the errors on  $\text{BR}(H \rightarrow gg)$  are at the level of a few to 10% at most. In the case of the  $H \rightarrow c\bar{c}$  channel, it is mainly due to the uncertainty on the input charm–quark mass  $\bar{m}_c$  and, to a lesser extent, to the uncertainty on  $\alpha_s$ ; their combination leads to a very strong variation of the charm–quark mass at the high scale  $\mu$ ,  $\bar{m}_c(\mu) \propto [\alpha_s(\mu)]^{12/13}$ . For the  $H \rightarrow gg$  channel the uncertainty is mainly due to the uncertainty on  $\alpha_s$ , and in both cases, the error on the input  $b$ –quark mass leads to a 2 to 5% uncertainty. Nevertheless, since the branching ratios for these two decays are small, at most a few percent in the Higgs mass range of interest, the associated uncertainties will affect the Higgs total width, and hence the branching ratios for the other decay channels, in a less significant way.

channel	$M_H$	BR(%)	$\Delta m_c$	$\Delta m_b$	$\Delta\alpha_s$	$\Delta\text{BR}$
$H \rightarrow b\bar{b}$	120	65.40	+0.7% −0.6%	+3.4% −1.2%	+0.7% −0.8%	+3.6% −1.6%
	135	41.01	+0.4% −0.4%	+6.0% −2.1%	+1.3% −1.3%	+6.2% −2.5%
	150	16.07	+0.2% −0.1%	+8.7% −3.0%	+1.9% −1.9%	+8.9% −3.6%
$H \rightarrow WW$	120	14.06	+0.7% −0.6%	+2.3% −6.3%	+1.4% −1.4%	+2.8% −6.5%
	135	39.86	+0.4% −0.4%	+1.4% −4.0%	+0.9% −0.9%	+1.7% −4.1%
	150	69.45	+0.2% −0.1%	+0.5% −1.6%	+0.3% −0.3%	+0.7% −1.6%

**Table 5:** The Higgs decay branching ratio  $\text{BR}(H \rightarrow b\bar{b})$  and  $\text{BR}(H \rightarrow WW)$  (in %) for given Higgs mass values (in GeV) with the corresponding uncertainties from the various sources discussed in the text; the total uncertainties (adding the individual ones in quadrature) are also shown.

The uncertainty on the  $H \rightarrow b\bar{b}$  decay channel (which is important at the Tevatron) depends strongly on the considered Higgs mass range. For  $M_H \lesssim 120$  GeV where the branching ratio is by far the dominant one,  $\text{BR}(H \rightarrow b\bar{b}) \gtrsim 65\%$ , the uncertainty is less than a few percent ( $\approx -1\%$ ,  $+2\%$  at  $M_H = 100$  GeV and  $\approx -2\%$ ,  $+4\%$  at  $M_H = 120$  GeV). This is mainly due to the fact that as the channel is dominant, the  $b\bar{b}$  partial width is the major component of the total width and the errors partly cancel in the branching ratio. There is, however, a residual error stemming mainly from the input bottom mass and to a lesser extent,  $\alpha_s$  and the charm mass.

In the mass range  $M_H \approx 120$ – $150$  GeV, the partial widths for  $H \rightarrow b\bar{b}$  and  $WW$  decays have the same magnitude and the two branching ratios have larger uncertainties. The uncertainty on  $\text{BR}(H \rightarrow b\bar{b})$  increases from a few percent at  $M_H \approx 120$  GeV to  $\approx -4\%$ ,  $+9\%$  at  $M_H \approx 150$  GeV. At the same time, the uncertainty on  $\text{BR}(H \rightarrow WW)$ , which is the same as the one on  $\text{BR}(H \rightarrow ZZ^*)$  and  $\text{BR}(H \rightarrow \gamma\gamma)$ , drops from  $\approx -7\%$ ,  $+3\%$  at  $M_H \approx 120$  GeV to  $\approx -2\%$ ,  $+1\%$  at  $M_H \approx 150$  GeV. Here,  $\bar{m}_c$  has little impact as  $\text{BR}(H \rightarrow c\bar{c})$  is small.

For higher Higgs masses,  $M_H \gtrsim 160$  GeV, the Higgs width is mainly controlled by the  $H \rightarrow WW$  decay (and  $H \rightarrow ZZ$  for  $M_H \gtrsim 2M_Z$ ) and the uncertainty on the branching

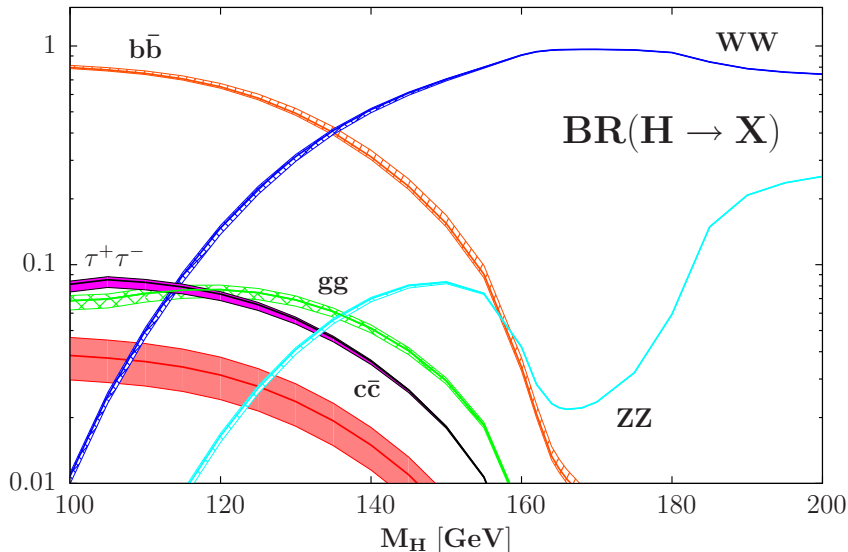


**Figure 12:** The Higgs decay branching ratios as a function of  $M_H$  including the total uncertainty bands from the  $1\sigma$  errors on the input quark masses and the coupling  $\alpha_s$  (the individual errors have been added in quadrature).

ratio  $\text{BR}(H \rightarrow WW)$  drops to a level below 1%. The uncertainty on  $\text{BR}(H \rightarrow b\bar{b})$  stays relatively large,  $\approx -4\%, +11\%$ , but the branching ratio itself is too small to be relevant.

For Higgs masses beyond  $M_H \gtrsim 350$  GeV, the decay channel  $H \rightarrow t\bar{t}$  opens up and has a branching ratio of  $\approx 20\%$  at  $M_H \approx 500$  GeV dropping to less than 10% for  $M_H \lesssim 400$  GeV or  $M_H \gtrsim 700$  GeV. It will be affected by the uncertainties on  $m_t, \alpha_s$  as well as by some electroweak contributions from the Higgs self-couplings. This leads to a total uncertainty that is estimated to be below the 5% level [14], which translates to an uncertainty of less than 1% in the branching ratios for the important decays  $H \rightarrow WW, ZZ$ .

Thus, the uncertainties on the important Higgs branching ratios  $\text{BR}(H \rightarrow WW, ZZ, \gamma\gamma)$  as well as  $\text{BR}(H \rightarrow b\bar{b})$  can be significant in the intermediate mass range  $M_H \approx 120\text{--}150$  GeV where the  $b\bar{b}$  and  $WW$  decays are competing with each other. These uncertainties should therefore be included in the experimental analyses.

### 3.3 Combination with the cross section uncertainty

In the previous section we have discussed the overall uncertainty on the Higgs production cross section. To this overall uncertainty, one has to add the uncertainty on the Higgs branching ratios obtained when considering a specific Higgs decay channel. This combination<sup>17</sup> is in general rather complicated to perform when several production and decay channels are involved as is the case for the Tevatron where both  $q\bar{q} \rightarrow HV$  and  $gg \rightarrow H$  production and  $H \rightarrow b\bar{b}$  and  $H \rightarrow WW$  decays channel have to be considered, the main reason being that the rates for the  $H \rightarrow b\bar{b}$  and  $H \rightarrow WW$  decays are anti-correlated, the sum of all branching ratios being equal to unity. At the LHC, the situation is much simpler

<sup>17</sup>Here, we will not address two (connected) issues which become important for heavy Higgs bosons: *i*) the effect of the total Higgs decay width which becomes large and *ii*) the interference between the  $gg \rightarrow H \rightarrow VV$  signal and the  $gg \rightarrow VV$  background. A study of these two effects is in progress [67].

$M_H$	$b\bar{b}$	$\Delta^{\text{tot}}$	$c\bar{c}$	$\Delta^{\text{tot}}$	gg	$\Delta^{\text{tot}}$	WW	ZZ	$\tau\tau$	$\gamma\gamma$	$\Delta^{\text{tot}}$
100	79.48	+2.2% -1.1%	3.90	+20.9% -22.7%	6.94	+5.6% -9.2%	1.09	0.11	8.22	0.16	+3.4% -7.8%
105	77.69	+2.4% -1.1%	3.81	+20.9% -22.7%	7.50	+5.4% -8.9%	2.39	0.21	8.11	0.18	+3.3% -7.8%
110	74.96	+2.6% -1.2%	3.68	+20.8% -22.7%	7.97	+5.3% -8.7%	4.75	0.43	7.89	0.19	+3.2% -7.5%
115	70.95	+3.1% -1.4%	3.48	+20.8% -22.7%	8.27	+5.1% -8.3%	8.54	0.86	7.53	0.21	+3.0% -7.1%
120	65.40	+3.6% -1.6%	3.21	+20.7% -22.8%	8.34	+4.9% -7.8%	14.06	1.57	7.00	0.22	+2.7% -6.6%
125	58.32	+4.4% -1.8%	2.86	+20.7% -22.8%	8.11	+4.6% -7.1%	21.35	2.62	6.29	0.23	+2.4% -5.9%
130	50.00	+5.3% -2.1%	2.45	+20.6% -22.9%	7.56	+4.2% -6.4%	30.13	3.95	5.43	0.22	+2.1% -5.0%
135	41.01	+6.2% -2.5%	2.01	+20.5% -23.0%	6.72	+3.9% -5.5%	39.86	5.42	4.49	0.21	+1.7% -4.1%
140	32.02	+7.2% -2.8%	1.57	+20.5% -23.1%	5.68	+3.6% -4.7%	49.92	6.82	3.53	0.19	+1.3% -3.2%
145	23.60	+8.1% -3.2%	1.16	+20.6% -23.1%	4.51	+3.2% -4.0%	59.82	7.86	2.62	0.17	+1.0% -2.4%
150	16.07	+8.9% -3.5%	0.79	+20.6% -23.2%	3.31	+3.0% -3.4%	69.45	8.21	1.79	0.14	+0.6% -1.6%
155	9.47	+9.7% -3.7%	0.46	+20.7% -23.3%	2.09	+2.8% -3.0%	79.28	7.33	1.06	0.10	+0.4% -1.0%
160	3.58	+10.4% -3.9%	0.18	+20.7% -23.4%	0.84	+2.7% -2.7%	90.63	4.19	0.40	0.05	+0.1% -0.4%
165	1.23	+10.7% -4.0%	0.06	+20.8% -23.4%	0.30	+2.6% -2.6%	95.97	2.22	0.14	0.02	+0.0% -0.1%
170	0.82	+10.7% -4.0%	0.04	+20.8% -23.4%	0.21	+2.6% -2.5%	96.43	2.35	0.09	0.02	+0.0% -0.1%
175	0.63	+10.7% -4.1%	0.03	+20.8% -23.5%	0.17	+2.5% -2.6%	95.84	3.21	0.07	0.01	+0.0% -0.1%
180	0.51	+10.7% -4.1%	0.02	+20.8% -23.5%	0.15	+2.5% -2.5%	93.28	5.94	0.06	0.01	+0.0% -0.0%
185	0.40	+10.7% -4.0%	0.02	+20.8% -23.4%	0.12	+2.6% -2.4%	84.52	14.86	0.05	0.01	+0.0% -0.0%
190	0.32	+10.7% -4.1%	0.02	+20.8% -23.4%	0.10	+2.5% -2.5%	78.72	20.77	0.04	0.01	+0.0% -0.0%
195	0.28	+10.8% -4.1%	0.01	+20.8% -23.4%	0.10	+2.5% -2.5%	75.89	23.66	0.03	0.01	+0.0% -0.0%
200	0.25	+10.8% -4.1%	0.01	+20.8% -23.5%	0.09	+2.5% -2.5%	74.26	25.34	0.03	0.01	+0.0% -0.0%

**Table 6:** The Higgs decay branching ratios (in %) for given Higgs mass values (in GeV) with the corresponding total uncertainties from the various sources discussed in the text.

as, in practice, only the  $gg \rightarrow H$  production channel is to be considered and only the decays  $H \rightarrow WW, ZZ$  and to a lesser extent  $H \rightarrow \gamma\gamma$  are relevant. Since we have considered only the dominant QCD uncertainties, these decays are affected by the same uncertainties as discussed previously (see the last column of Table 6).

Nevertheless, combining the uncertainty in the production cross section and the uncertainty in the Higgs decay branching ratios is still not obvious. Indeed, while the uncertainties on the Higgs production cross section are purely theoretical, one should in principle consider the uncertainties on the Higgs branching ratios as experimental errors, since they are mainly due to the “experimental” determination of the quark masses and  $\alpha_s$  (and we have not included the corresponding theoretical errors). In addition, there is one parameter which is common in the calculation of the branching ratios and the production cross sections: the coupling  $\alpha_s$ . The uncertainty on  $\alpha_s$  will affect at the same time  $\sigma(gg \rightarrow H)$  and  $\text{BR}(H \rightarrow VV)$  and it occurs that, in both the Higgs production and in Higgs decays,

the minimal (maximal) values are obtained with the minimal (maximal) value of  $\alpha_s$  when the error  $\Delta^{\text{exp}}\alpha_s$  is included (we have assumed that no theoretical uncertainty on  $\alpha_s$  is present in the decays).

Here, we will thus adopt the simple attitude of adding linearly the errors on the Higgs branching ratios to the theoretical uncertainty on the production cross section. In the case of the procedure A for the combination of the cross sections uncertainties, for consistency reasons, one should also use the 90% CL error on the branching ratios due to  $\Delta^{\text{exp}}\alpha_s$  together with the 90% CL PDF+ $\Delta^{\text{exp}}\alpha_s$  uncertainties in the cross section. In this case, one obtains the combined uncertainty of  $\sigma^{\text{NNLO}}(gg \rightarrow H) \times \text{BR}(H \rightarrow VV^*)$  at the IHC that is displayed in Fig. 13 in the case of the  $H \rightarrow WW$  decay as a function of  $M_H$ . Besides the uncertainty on the cross section which is shown by the dashed lines, we display the effect of adding the error on the  $H \rightarrow WW$  branching ratio as shown by the full lines which slightly increase the overall uncertainty. This is only visible in the region  $M_H \approx 100\text{--}150$  GeV where the errors on  $\text{BR}(H \rightarrow WW)$ , dominated in practice by the errors in the decay channel  $H \rightarrow b\bar{b}$ , is significant. Above the  $M_H \gtrsim 2M_W$  threshold, the branching ratio uncertainty is small, below  $\approx 1\%$ , and can be safely neglected<sup>18</sup>. Note, however, that for large  $M_H$  values, the total Higgs width becomes significant and should be taken into account in both the production and in the decay [14].

In the case of the  $H \rightarrow ZZ, \gamma\gamma$  (and  $\tau\tau$ ) decays, since the errors on the branching ratios are the same as those affecting  $\text{BR}(H \rightarrow WW)$ , the overall uncertainties in  $\sigma \times \text{BR}$  can also be seen from Fig. 13: only the normalization of the branching ratio is different and can be obtained for a specific decay mode from Table 6.

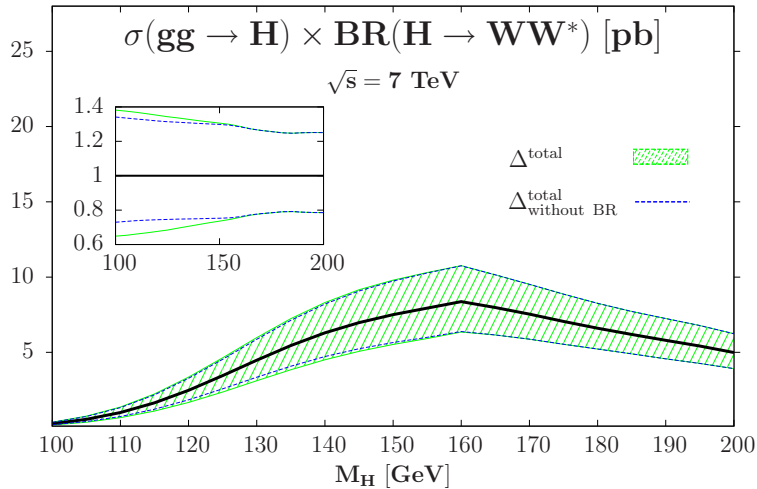


**Figure 13:** The production cross section times branching ratio for the process  $gg \rightarrow H \rightarrow WW$  at the IHC with  $\sqrt{s} = 7$  TeV, including the total theoretical uncertainty band when the errors in the decay branching ratios are taken into account. In the inserts the relative deviations are shown.

<sup>18</sup>For instance, the branching ratio uncertainties have no effect in the Higgs mass range  $M_H \approx 150\text{--}180$  GeV to which both the Tevatron and the IHC are most sensitive. However, at the Tevatron these errors should be taken into account for  $M_H \lesssim 150$  GeV in both the  $H \rightarrow b\bar{b}$  and  $WW$  channels.

## 4. The MSSM neutral Higgs particles

### 4.1 The MSSM Higgs sector

In supersymmetric extensions of the SM, at least two Higgs doublet fields are required for a consistent electroweak symmetry breaking and in the minimal model, the MSSM, the Higgs sector is extended to contain five Higgs bosons: two CP-even  $h$  and  $H$ , a CP-odd  $A$  and two charged Higgs  $H^\pm$  particles [4–7]. Besides the four masses, the properties of the MSSM Higgs sector are in principle determined by two more parameters: a mixing angle  $\alpha$  in the neutral CP-even sector and the ratio of the vacuum expectation values of the two Higgs fields  $\tan\beta$ ; the value of the latter is expected to lie in the range  $1 \lesssim \tan\beta \lesssim m_t/m_b$ . In fact, in the MSSM, the scalar potential does not involve arbitrary self couplings as in the case with the SM, but involves only the gauge couplings and, as a result, only two free parameters are needed at tree-level to describe the Higgs sector; these are usually taken to be the mass  $M_A$  of the pseudoscalar  $A$  boson and  $\tan\beta$ . In addition, while the masses of the heavy neutral and charged  $H, A, H^\pm$  particles are expected to range from  $M_Z$  to the SUSY breaking scale  $M_S = \mathcal{O}(1 \text{ TeV})$ , the mass of the lightest Higgs boson  $h$  is bounded from above,  $M_h \leq M_Z$  at the tree level.

It is well known that this relation is altered by the large radiative corrections which enter in the Higgs sector, the leading part of which grow as the fourth power of  $m_t$  and logarithmically with the SUSY scale or common squark mass  $M_S$ ; the mixing (or trilinear coupling) in the stop sector  $A_t$  and, to a lesser extent a Higgs mass parameter  $\mu$ , play an important role. When higher order corrections are included, the upper bound on the mass of the lightest  $h$  boson is shifted from the tree level value  $M_Z$  to the value  $M_h^{\max} \sim 110\text{--}135 \text{ GeV}$  [7] in the maximal mixing scenario where  $X_t = A_t - \mu/\tan\beta \sim \sqrt{6}M_S$ . The maximal mixing scenario, together with the no-mixing scenario with  $X_t \approx 0$  which leads to a lower  $M_h^{\max}$  value, are often used as benchmarks to describe MSSM Higgs phenomenology [68].

For a heavy enough  $A$  boson,  $M_A \gg M_Z$ , the  $h$  boson reaches its maximal mass value  $M_h \simeq M_h^{\max}$  and has SM-like couplings to fermions and gauge bosons. In this decoupling regime which, for large  $\tan\beta$  values occurs already for  $M_A \gtrsim M_h^{\max}$ , the three other Higgs particles are almost degenerate in mass,  $M_H \approx M_A \approx M_{H^\pm}$ . The couplings of the CP-even  $H$  boson (as well as those of the charged  $H^\pm$  bosons) become similar to that of the pseudoscalar  $A$  boson: no tree-level couplings to the gauge bosons and couplings to isospin down (up) type fermions that are (inversely) proportional to  $\tan\beta$ . In particular, for high  $\tan\beta$  values,  $\tan\beta \gtrsim 10$ , the  $H, A$  Yukawa couplings to bottom quarks and tau leptons are strongly enhanced, while those to top quarks are strongly suppressed.

For a light pseudoscalar boson,  $M_A \lesssim M_h^{\max}$  at high  $\tan\beta$ , the roles of the CP-even  $h$  and  $H$  states are reversed: it is the  $H$  boson which has a mass  $M_H \simeq M_h^{\max}$  and SM-like couplings, while the  $h$  particle behaves exactly like the pseudoscalar  $A$  state, i.e.  $M_h \simeq M_A$ , no couplings to gauge bosons and enhanced (suppressed) couplings to  $b, \tau$  ( $t$ ) states. We are thus always in a scenario where one has a SM-like Higgs boson  $H_{\text{SM}} = h$  ( $H$ ) and two CP-odd like Higgs particles  $\Phi = A$  or  $H$  ( $h$ ) when we are in the decoupling (anti-decoupling) regime<sup>19</sup> which, for values  $\tan\beta \gtrsim 10$ , occurs already for  $M_A \gtrsim M_h^{\max}$  ( $M_A \lesssim M_h^{\max}$ ).

<sup>19</sup>Note that there is an intermediate scenario for  $\tan\beta \gtrsim 10$ : the intense coupling regime [69] in which

Let us now discuss the Higgs Yukawa couplings to bottom quarks, which play a major role in the analysis that will be presented in this section. As mentioned earlier, in almost the entire parameter space for large enough  $\tan\beta$  values, the couplings of one of the CP-even Higgs particles are SM-like, thus leading to the phenomenology described in the previous sections for the SM Higgs boson, while the couplings of the other CP-even particle are the same as those of the pseudoscalar  $A$  boson, on which we will focus in the rest of our discussion. At the tree level, this coupling is given in terms of the  $b$ -quark mass, the SM vacuum expectation value  $v$  and  $\tan\beta$ , by

$$\lambda_{\Phi bb} = \frac{\sqrt{2}m_b}{v \cos\beta} \xrightarrow{\tan\beta \gg 1} \frac{\sqrt{2}m_b}{v} \tan\beta, \quad \Phi = A, H (h) \quad (4.1)$$

First of all, in the MSSM, one usually uses the modified dimensional reduction  $\overline{\text{DR}}$  scheme which, contrary to the  $\overline{\text{MS}}$  scheme, preserves Supersymmetry. In the case of the  $b$ -quark mass, the relation between the  $\overline{\text{DR}}$  and  $\overline{\text{MS}}$  running masses at a given scale  $\mu$  reads [70]

$$\overline{m}_b^{\overline{\text{DR}}}(\mu) = \overline{m}_b^{\overline{\text{MS}}}(\mu) \left[ 1 - \frac{1}{3} \frac{\alpha_s(\mu^2)}{\pi} - \frac{\alpha_s^2(\mu^2)}{\pi^2} + \dots \right] \quad (4.2)$$

where the strong coupling constant  $\alpha_s$  is also evaluated at the scale  $\mu$  and additional but small electroweak contributions are present. Since the difference between the quark masses in the two schemes is not very large,  $\Delta m_b/m_b \sim 1\%$ , to be compared with an “experimental” error on  $\overline{m}_b(\overline{m}_b)$  of the order of a few percent, it is common practice to neglect this difference, at least in unconstrained SUSY models where one does not have to evolve the parameters up to very high scales. We will thus adopt this approximation at least when we quote the central values of the cross sections (see later however, when the theoretical uncertainties will be considered).

A second important fact is that the Yukawa coupling eq. (4.1), besides the standard QCD corrections, receives additional one-loop vertex corrections which involve squarks and gluinos in the loops and which can be very large as they grow with  $\tan\beta$  [71],

$$\Delta_b \approx \frac{2\alpha_s}{3\pi} \mu m_{\tilde{g}} \tan\beta / \max(m_{\tilde{g}}^2, m_{\tilde{b}_1}^2, m_{\tilde{b}_2}^2) \quad (4.3)$$

with  $m_{\tilde{b}_{1,2}}$  and  $m_{\tilde{g}}$  the sbottom and gluino masses; large corrections, proportional to  $\mu A_t$  also appear when the electroweak stop and chargino loops are included. This correction is very important for large values of  $\tan\beta$  and  $\mu$  and significantly increase or decrease (depending on the sign of  $\mu$ ) the Yukawa coupling. It can be properly taken into account using a resummation procedure where one writes the modified Yukawa coupling, normalized to the coupling of the SM Higgs boson, as [70]

$$\lambda_{\Phi bb} / \lambda_{H_{\text{SM}} bb} = \frac{\tan\beta}{1 + \Delta_b} \left[ 1 - \frac{\Delta_b}{\tan^2\beta} \right] \xrightarrow{\tan\beta \gg 1} \frac{\tan\beta}{1 + \Delta_b} \quad (4.4)$$

the three neutral Higgs bosons have comparable masses,  $M_h \approx M_H \approx M_A \approx M_h^{\text{max}}$ . The couplings of the three states to isospin down type fermions are enhanced and the squares of the CP-even Higgs couplings approximately add to the square of the CP-odd Higgs coupling. This property, together with the fact that  $M_H \approx M_h$ , makes that for our main purpose in this paper, one has the same phenomenology as in the decoupling or anti-decoupling regimes.

It has been shown that in this case all terms of  $\mathcal{O}(\alpha_s \tan \beta)$  in perturbation theory are resummed [70]. The inclusion of the NNLO corrections in  $\Delta_b$  allows, in addition, to have a very precise description of the coupling, with a scale variation at the percent level [72].

The resummation procedure which allows to include properly the SUSY radiative corrections in the  $\Phi b\bar{b}$  Yukawa couplings is implemented in the major codes which calculate the MSSM Higgs spectra such as `HDECAY` [66], `FeynHiggs` [73] or the RGE codes that calculate the MSSM particle spectrum such as `SuSpect` [74]. Since in our analysis we will be mainly concerned with the standard QCD effects and we would like to have a model independent approach (see next subsection), we will assume that these SUSY QCD and electroweak corrections are handled by the previously mentioned programs that provide the radiatively corrected Higgs couplings. Nevertheless, we will see later that in the main channels discussed in this paper, the major part of these corrections cancels out.

Before closing this survey of the MSSM Higgs sector, we note that there are experimental constraints on the Higgs masses, which mainly come from the negative LEP2 searches [8]. In the decoupling limit where the  $h$  boson is SM-like, the constraint  $M_h \gtrsim 114$  GeV holds and rules out  $\tan \beta$  values smaller than  $\sim 3$ . Outside this regime, the most conservative and model independent limits on the Higgs masses from LEP2 searches are  $M_h, M_A \gtrsim M_Z$  [8]. Some exclusion limits in the  $[M_A, \tan \beta]$  parameter space are also available from Tevatron searches [10] and rule out extremely large  $\tan \beta$  and low  $M_A$  values.

## 4.2 The production cross sections at the IHC

In the MSSM, the dominant production processes for the CP-even neutral  $h$  and  $H$  bosons are essentially the same as those for the SM Higgs particle discussed in section 2.1. In fact, for the lighter  $h$  boson in the decoupling and the heavier  $H$  boson in the anti-decoupling regimes, the cross sections are almost exactly the same as for the SM Higgs particle with a mass  $\approx M_h^{\text{max}}$  shown in Fig. 1 with the numerical values of Table 1. The only difference is that some SUSY particles might contribute to the  $gg$  fusion processes and, eventually, to the SUSY radiative corrections in the other processes. However, for heavy enough squarks and gluinos, as is the case for the benchmark scenarios that are in general discussed and which have  $M_S \gg M_h^{\text{max}}$ , these contributions are rather small as the SUSY states decouple from the amplitudes (their couplings to the Higgs bosons are not proportional to their masses). These SUSY contributions, including even the known QCD corrections [75], can be nevertheless evaluated exactly using the program `HIGLU` for instance.

In the case of the CP-odd like particles, the situation is completely different. Because of CP invariance which forbids  $A$  couplings to gauge bosons at tree-level, the pseudoscalar  $A$  boson cannot be produced in the Higgs-strahlung and vector boson fusion processes; only the  $gg \rightarrow A$  fusion as well as associated production with heavy quark pairs,  $q\bar{q}, gg \rightarrow Q\bar{Q}A$ , will be in practice relevant (additional processes, such as associated production of CP-even and CP-odd Higgs particles, have too small cross sections). This will therefore be also the case of the CP-even  $H$  and  $h$  particles in, respectively, the decoupling and anti-decoupling scenario. In addition, if one concentrates on the high  $\tan \beta$  regime (that is the only relevant one in this context, both at the Tevatron and the IHC), the  $b$ -quark will play the major role as its couplings to the CP-odd like bosons are enhanced.

Therefore, for  $\Phi = A$  or  $H(h)$ , one first has to take into account in the  $gg \rightarrow \Phi$  processes the  $b$ -quark loop which provides the dominant contribution in the MSSM, as the one of the top-quark loop is suppressed,  $\lambda_{\Phi tt} \propto 1/\tan\beta$ . Moreover, in associated Higgs production with heavy quarks, the rates for the  $pp \rightarrow t\bar{t}\Phi$  processes are also suppressed and, instead, associated Higgs production with  $b\bar{b}$  final states must be considered. In fact, the  $pp \rightarrow b\bar{b}\Phi$  production processes become the dominant ones in the MSSM.

In the  $gg \rightarrow \Phi$  processes with only the  $b$ -quark loop included, as the  $b$ -quark mass is very small compared to the Higgs masses, chiral symmetry approximately holds and the cross sections are approximately the same for the CP-even  $H$  ( $h$ ) and CP-odd  $A$  bosons<sup>20</sup>. The QCD corrections are known only to NLO for which the exact calculation with finite loop quark masses is available [20]. Contrary to the SM case, they increase only moderately the production cross sections. The calculation of the higher order corrections that have been made available for the SM Higgs boson, the NNLO QCD corrections (performed in the infinite quark mass limit) and the NLO electroweak corrections (the dominant part of which arises because of the large Higgs- $t\bar{t}$  Yukawa coupling) do not apply here and will be thus ignored. However, in the case of  $h$  and  $H$  production, to approach properly the decoupling and anti-decoupling limits and to reproduce the SM Higgs results discussed in section 2 when these higher order corrections are included, we will adopt the central value  $\mu_0 = \frac{1}{2}M_\Phi$  for the renormalization and factorization scales, i.e. as in the SM case.

In the case of the  $pp \rightarrow b\bar{b}\Phi$  processes, the NLO QCD corrections have been calculated in Ref. [76] and turn out to be rather large, in contrast to  $pp \rightarrow t\bar{t}$ +Higgs production. Because of the small  $m_b$  value, the cross sections develop large logarithms  $\log(Q^2/m_b^2)$  with the scale  $Q$  being typically of the order of the factorization scale,  $\mu_F \sim M_\Phi \gg m_b$ . These logarithms can be resummed via the Altarelli-Parisi equations by considering the  $b$ -quark as a massless parton and using heavy quark distribution functions at a scale  $\mu_F \sim Q$  in a five active flavor scheme. In this scheme, the inclusive process where one does not require to observe the  $b$  quarks is simply the  $2 \rightarrow 1$  process  $b\bar{b} \rightarrow \Phi$  at leading order [24]. If one requires the observation of a high- $p_T$  final  $b$ -quark, one has to consider its NLO corrections [25] and in particular the  $2 \rightarrow 2$  process  $gb \rightarrow \Phi b$ , which indeed generates the  $p_T$  of the  $b$ -quark. Requiring the observation of two  $b$  quarks in the final state, one has to consider the  $2 \rightarrow 3$  process  $gg \rightarrow b\bar{b}\Phi$  discussed above, which is the leading mechanism at NNLO [26]. Thus, instead of  $q\bar{q}, gg \rightarrow b\bar{b}\Phi$ , we will consider the process  $b\bar{b} \rightarrow \Phi$  for which the cross section is known up to NNLO in QCD [25, 26], with corrections that are of moderate size if *i*) the bottom quark mass in the Yukawa coupling is defined at the scale  $M_\Phi$  to absorb large logarithms  $\log(\mu_R^2/m_b^2)$  and *ii*) if the factorization scale, that we will set here equal to the renormalization scale, is chosen to be small,  $\mu_F = \mu_R = \mu_0 = \frac{1}{4}M_\Phi$ .

In order to evaluate the Higgs production cross sections at IHC energies in these two main processes,  $gg \rightarrow \Phi$  and  $b\bar{b} \rightarrow \Phi$ , we will proceed as follows. We only evaluate the cross sections for the pseudoscalar  $A$  boson: in the  $gg \rightarrow A$  process at NLO using the program HIGLU [37] with a central scale  $\mu_R = \mu_F = \mu_0 = \frac{1}{2}M_A$  (and where only the bottom quark

---

<sup>20</sup>This is only true if the SUSY particle loop contributions are not included. In the case of the CP-even particles, their relative contribution are suppressed at high enough  $\tan\beta$  and we will ignore them here. In the case of the  $A$  boson, the SUSY contributions appear only at two-loops and they can be safely neglected.



loop contribution is included by setting  $\lambda_{Att} = 0$ ), and in the  $b\bar{b} \rightarrow A$  process up to NNLO using the program `bbh@nnlo` [26, 77] with a central scale  $\mu_R = \mu_F = \mu_0 = \frac{1}{4}M_\Phi$ . In both cases, we work in the  $\overline{\text{MS}}$  scheme for the renormalization of the bottom–quark mass. However, while  $\overline{m}_b(\overline{m}_b)$  is used in the  $gg$  fusion process,  $\overline{m}_b(\mu_R)$  is adopted in the  $b\bar{b}$  fusion channel. In both processes, we assume the  $Ab\bar{b}$  coupling to be SM–like, that is, we will not include the  $\tan\beta$  term and the SUSY corrections to  $\Delta m_b$ . To obtain the true cross sections for  $A$  production, one will have therefore to rescale the numbers that we provide by the factor of eq. (4.4) squared. Furthermore, to obtain the cross section for both CP–even and CP–odd Higgs production, an additional factor of two has to be included. As a consequence of chiral symmetry for  $M_\Phi \gg \overline{m}_b$  and since the  $H$  ( $h$ ) masses and couplings are very close to those of  $A$ , this turns out to be an excellent approximation.

Within this set–up, the best values of the cross sections for  $gg \rightarrow \Phi$  and  $b\bar{b} \rightarrow \Phi$  are shown in Fig. 14 as a function of the Higgs mass  $M_\Phi$  when the MSTW sets of (NLO for the former and NNLO for the latter process) PDFs are used to parametrize the gluon and bottom–quark densities. Center of mass energies in a range between  $\sqrt{s} = 7$  TeV and 14 TeV relevant for the LHC are considered. One can first notice that the cross sections for  $gg \rightarrow \Phi$  and  $b\bar{b} \rightarrow \Phi$  are comparable at a given energy and they significantly increase with increasing center of mass energies or decreasing Higgs mass. If, for example, the value  $\tan\beta = 10$  is adopted, the numbers in Fig. 14 have to be multiplied by a factor  $\simeq 200$  to obtain the true cross section for both  $A$  and  $H(h)$  production. For low to moderate  $M_\Phi$  values, the expected event rates are thus simply huge at the LHC, despite of the relatively low luminosities that are expected. This explains why the chances for observing a Higgs boson at the LHC are much higher in the MSSM than in the SM, as in the former case the production rates can be two to three orders of magnitude larger.

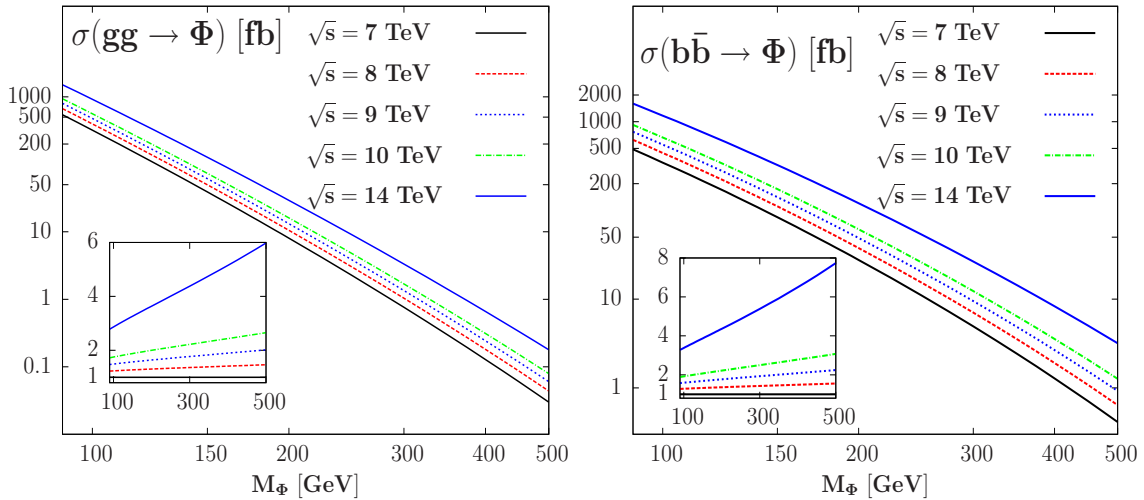


**Figure 14:** The production cross sections in the processes  $gg \rightarrow \Phi$  (left) at a central scale  $\mu_R = \mu_F = \mu_0 = \frac{1}{2}M_\Phi$  and  $b\bar{b} \rightarrow \Phi$  (right) at a central scale  $\mu_R = \mu_F = \mu_0 = \frac{1}{4}M_\Phi$  as a function of  $M_\Phi$  for several center of mass energies relevant for the LHC. The MSTW sets of PDFs at the required perturbative order have been used. Only the cross section in the pseudoscalar  $A$  case but with a SM-like Yukawa coupling is included.

### 4.3 The theoretical uncertainties

Left to evaluate are then the theoretical uncertainties on the production cross sections and, for this purpose, we will follow very closely the procedure (A) discussed in section 2.2 for the SM Higgs boson, at least for the scale and PDF+ $\alpha_s$  uncertainties. For the numerical analysis, we will only consider the case of the IHC at  $\sqrt{s} = 7$  TeV: the uncertainties at center of mass energies slightly above this value,  $\sqrt{s} = 8$ –10 TeV, and even for the LHC energy  $\sqrt{s} = 14$  TeV are expected to be comparable. The procedure and the main results that we obtain are briefly summarized in the following<sup>21</sup>.

In the case of the  $gg \rightarrow \Phi$  process, as for the SM Higgs boson, the scale uncertainty is evaluated by allowing for a variation of the renormalization and factorization scales within a factor of two around the central scale,  $\frac{1}{2}\mu_0 \leq \mu_R, \mu_F \leq 2\mu_0$  with  $\mu_0 = \frac{1}{2}M_\Phi$ . For the  $b\bar{b} \rightarrow \Phi$  case, we will extend the domain of scale variation to a factor of three around the central scale  $\mu_0 = \frac{1}{4}M_\Phi$ ,  $\frac{1}{3}\mu_0 \leq \mu_R, \mu_F \leq 3\mu_0$ . The reason for this non democratic treatment is that, first, in the  $gg \rightarrow \Phi$  process, there is another uncertainty due to the scheme dependence in the renormalization of the bottom–quark which will add to the scale uncertainty, as will be discussed later. A second reason is that it is well known that when the same final states are considered, the cross sections in the  $b\bar{b} \rightarrow \Phi$  process in the five–flavor scheme and in the  $q\bar{q}, gg \rightarrow b\bar{b}\Phi$  channel in the four–flavor scheme differ significantly [78] and only by allowing a wider domain for scale variation and, hence, a larger scale uncertainty that the two results become consistent with each other. In our final numbers for the uncertainties, we will assume a variation of  $\mu_R$  and  $\mu_F$  that is taken to be independent but with the additional restriction  $1/\kappa \leq \mu_R/\mu_F \leq \kappa$  imposed. However, to illustrate the much larger scale uncertainty that is possible in the  $b\bar{b} \rightarrow \Phi$  case, we will also show results when this constraint is relaxed, in much the same way as in Ref. [14].

The results for  $\sigma(gg \rightarrow \Phi)$  and  $\sigma(b\bar{b} \rightarrow \Phi)$  at the IHC, for scale variations in the domains  $\mu_0/\kappa \leq \mu_R, \mu_F \leq \kappa\mu_0$  with  $\kappa = 2$  and 3 are shown in Fig. 15 as a function of  $M_\Phi$ . One can see that the scale variation is moderate for  $gg \rightarrow \Phi$  with  $\kappa = 2$ , despite of the fact that the process is known only at NLO, leading to an uncertainty of order  $\pm 10\%$  in the entire Higgs mass range. Extending the variation domain to  $\kappa = 3$  will increase the uncertainty by another  $\approx 10\%$ . As in the SM Higgs case, the maximal and minimal values of the cross sections are approximately obtained for  $\mu_R \approx \mu_F$  and thus, varying independently the two scale does not affect the uncertainty. For  $\kappa = 2$  when the restriction  $\frac{1}{2} \leq \mu_R/\mu_F \leq 2$  is imposed, the uncertainty is also small in the case of  $b\bar{b} \rightarrow \Phi$ ,  $\approx \pm 10\%$  at low Higgs masses and less for higher masses; this was to be expected as the process is evaluated at NNLO. However, the extension to  $\kappa = 3$ , while keeping the restriction  $\frac{1}{3} \leq \mu_R/\mu_F \leq 3$ , will significantly increase the uncertainty: one would have  $-18\%, +24\%$  at  $M_\Phi = 100$  GeV and  $-13\%, +6\%$  at  $M_\Phi = 200$  GeV. If the restriction on  $\mu_R/\mu_F$  is ignored the uncertainty blows up, especially for very low Higgs masses: one would have a variation of  $-45\%, +25\%$  at  $M_\Phi = 100$  GeV, as also noticed in Ref. [14].

<sup>21</sup>Note that since in our analysis we are not considering the SUSY particle contributions and focus only on the standard QCD effects, additional uncertainties from the SUSY sector should, in principle, also be present. Nevertheless, at high  $\tan\beta$ , the genuine SUSY contributions should not be significant and can be ignored, while the corrections entering in  $\Delta_b$  will almost cancel out when the  $\tau^+\tau^-$  decays are considered.

Hence, the cross section for  $b\bar{b} \rightarrow \Phi$  is rather unstable against scale variation and this justifies, a posteriori, the choice of a larger domain of variation with  $\kappa = 3$  in this case, a choice that does not appear to be a too extreme one when looking at Fig. 15.

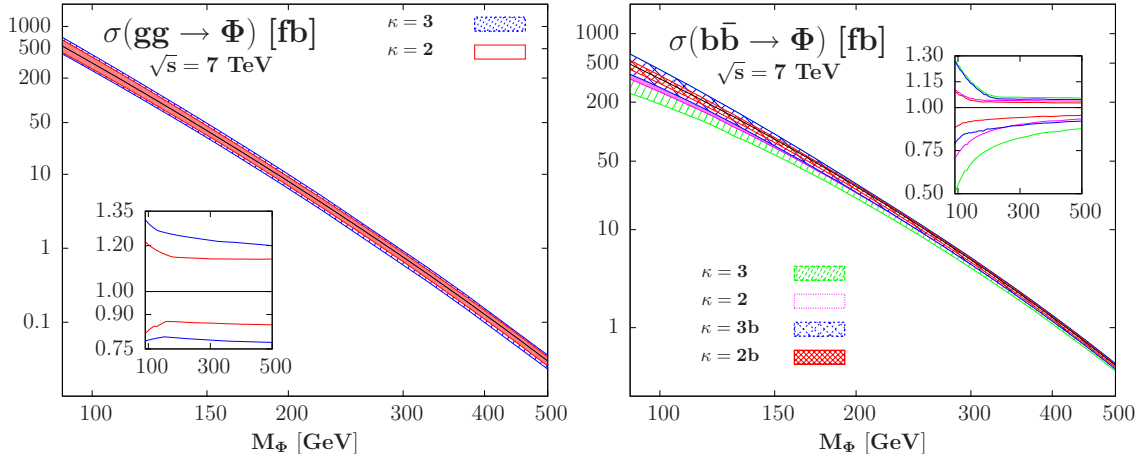


**Figure 15:** The scale uncertainty bands of the NLO  $gg \rightarrow \Phi$  (left) and the NNLO  $b\bar{b} \rightarrow \Phi$  (right) cross sections at the LHC at 7 TeV as a function of  $M_\Phi$ ; different values  $\kappa = 2, 3$  are used and the results are shown when the additional constraint  $1/\kappa \leq \mu_R/\mu_F \leq \kappa$  is imposed or not (marked as  $\kappa b$ ). In the inserts, the relative deviations (compared to the central cross section values) are shown.

Let us now turn to the estimation of the uncertainties from the parton densities and  $\alpha_s$ . The 90% CL PDF+ $\Delta^{\text{exp}}\alpha_s$  uncertainty, with  $\alpha_s(M_Z^2) = 0.120 \pm 0.002$  at NLO for  $gg \rightarrow \Phi$  and  $\alpha_s(M_Z^2) = 0.1171 \pm 0.0014$  at NNLO for  $b\bar{b} \rightarrow \Phi$ , is evaluated within the MSTW parametrization when including the experimental error on  $\alpha_s$ . To that, we add in quadrature the effect of the theoretical error on  $\alpha_s$ , estimated by the MSTW collaboration to be  $\Delta^{\text{th}}\alpha_s \approx 0.003$  at NLO and  $\Delta^{\text{th}} \approx 0.002$  at NNLO, using the MSTW fixed  $\alpha_s$  grid with central PDF sets. The 90%CL PDF, PDF+ $\Delta^{\text{exp}}\alpha_s$  and the PDF+ $\Delta^{\text{exp+th}}\alpha_s$  uncertainties at the LHC are shown in Fig. 16 as a function of  $M_\Phi$ . In both the  $gg \rightarrow \Phi$  and  $b\bar{b} \rightarrow \Phi$  processes, the total uncertainty is below  $\pm 10\%$  for  $M_\Phi \lesssim 200$  GeV but increases at higher masses, in particular in the  $b\bar{b} \rightarrow \Phi$  case.

For completeness, we also display the two cross sections when one adopts two other PDF sets, ABKM and (G)JR, and compare the results with that of MSTW. As can be seen in Fig. 17, the deviations from the MSTW values are moderate in the case of  $b\bar{b} \rightarrow \Phi$  for the JR scheme: a few percent at  $M_\Phi = 100$  GeV, increasing to  $\approx 10\%$  at  $M_\Phi = 500$  GeV. The ABKM scheme leads to substantial deviations at high masses,  $\approx 30\%$  at  $M_\Phi = 500$  GeV. In the  $gg$  fusion process, the prediction with the GJR PDF set at  $M_\Phi = 100$  GeV is  $\approx 20\%$  lower than in the MSTW and ABKM cases which give comparable results. The GJR and ABKM parameterizations cross at  $\approx 200$  GeV and at higher masses, the  $gg$  cross sections with the ABKM parametrization are  $\approx 20\%$  lower than for MSTW results while the predictions with the GJR set are  $\approx 10\%$  higher than for MSTW.

Finally, there is the effect of the uncertainty on the  $b$ -quark mass that had only a marginal impact in the SM Higgs case but which will be rather important here. In fact, there are three sources of uncertainties which can be attributed to the  $b$ -quark mass.

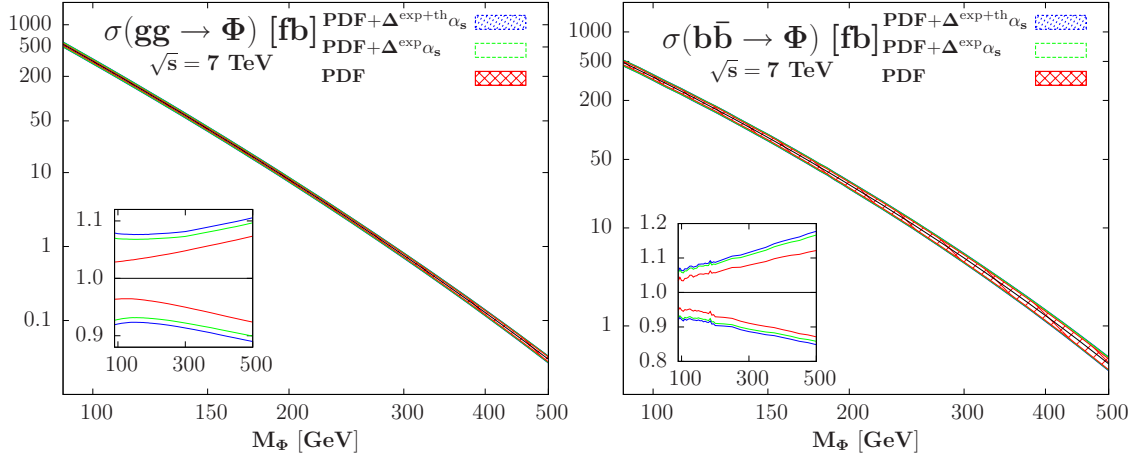


**Figure 16:** The PDF 90% CL PDF, PDF+ $\Delta^{\text{exp}}\alpha_s$  and PDF+ $\Delta^{\text{exp}}\alpha_s + \Delta^{\text{th}}\alpha_s$  uncertainties in the MSTW scheme in the  $gg \rightarrow \Phi$  (left) and  $b\bar{b} \rightarrow \Phi$  (right) cross sections at the IHC at 7 TeV as a function of  $M_\Phi$ . In the inserts, the relative deviations are shown.

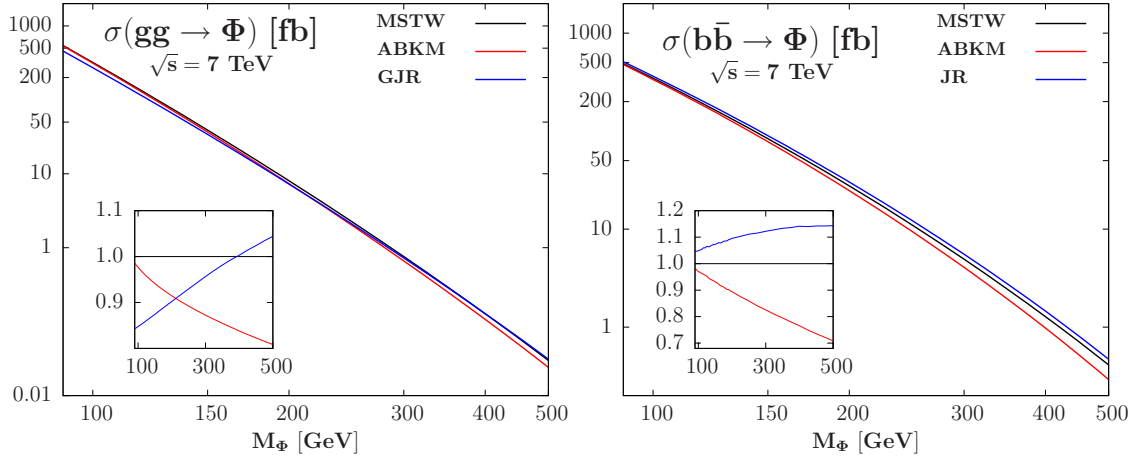


**Figure 17:** The cross sections in the  $gg \rightarrow \Phi$  (left) and  $b\bar{b} \rightarrow \Phi$  (right) at the IHC at 7 TeV as a function of  $M_\Phi$  evaluated when using the ABKM and (G)JR PDF sets. In the inserts, the relative deviations from the value in the MSTW scheme are shown.

The first one is of purely theoretical nature and is due to the choice of the renormalization scheme for the  $b$ -quark mass. In our analysis, we have adopted the  $\overline{\text{MS}}$  renormalization scheme mainly because of the fact that the calculation of the  $b\bar{b} \rightarrow \Phi$  process is available only in this scheme and we to have chosen to treat the same way both the  $b\bar{b} \rightarrow \Phi$  and  $gg \rightarrow \Phi$  channels. Nevertheless, one could choose another renormalization scheme such as the on-shell scheme as it was discussed in the case of the  $b$ -loop contribution in the  $gg$  fusion process for SM Higgs production. In the MSSM case, one could also adopt the  $\overline{\text{DR}}$  scheme which appears to be more consistent theoretically. To estimate this scheme dependence, one can evaluate the difference of the  $gg \rightarrow \Phi$  cross section in the cases where the  $b$ -quark mass is defined in the on-shell and in the  $\overline{\text{MS}}$  schemes. Using the program `HIGLU`, one obtains a  $\approx +15\%$  difference. Bearing in mind the fact that the corrections could have been negative if we had adopted another scheme (as would have been the case if we have

used the  $\overline{\text{DR}}$  scheme for instance, although the difference from the  $\overline{\text{MS}}$  result would have been at the level of a few percent only), one could assign an error  $\Delta_{m_b}^{\text{scheme}} \approx \pm 15\%$  to the  $gg \rightarrow \Phi$  cross section. This is the procedure that we will adopt here.

Another way to estimate the renormalization scheme dependence of the  $b$ -quark mass, would be to look at the differences that one obtains by using  $\overline{m}_b(\frac{1}{2}\overline{m}_b)$  and  $\overline{m}_b(2\overline{m}_b)$  as inputs in the  $gg \rightarrow \Phi$  cross section<sup>22</sup> [60]. In this case, one obtains an uncertainty that is in fact much larger than the difference between the on-shell and  $\overline{\text{MS}}$  schemes and which goes both ways,  $\Delta_{m_b}^{\text{scheme}} \approx -20\%, +40\%$  for  $M_\Phi = 90$  GeV for instance.

In the  $b\bar{b} \rightarrow \Phi$  process, we cannot perform this exercise as the cross section, using the program `bbh@nnlo` of Ref. [77], can only be evaluated in the  $\overline{\text{MS}}$  scheme with the Yukawa couplings evaluated at the scale  $\mu_R$ . This is the reason why we extended the domain of scale variation in this case to  $\frac{1}{3}\mu_0 \leq \mu_R, \mu_F \leq 3\mu_0$ . The larger scale uncertainty obtained this way could be seen as indirectly taking care of the scheme dependence.

The second source of uncertainty is of parametric nature and is the same as the one affecting the  $H \rightarrow b\bar{b}$  partial decay width of the Higgs boson discussed in section 3. It is estimated as previously, i.e. by evaluating the maximal values of the cross sections when one includes the error on the input  $b$ -quark mass at the scale  $\overline{m}_b$ ,  $\overline{m}_b(\overline{m}_b) = 4.19_{-0.06}^{+0.18}$  GeV, and in the case of the  $b\bar{b} \rightarrow \Phi$  process where the Yukawa coupling is defined at the high scale, the strong coupling constant,  $\alpha_s(M_Z^2) = 0.1171 \pm 0.0014$  at NNLO, used to run the mass  $\overline{m}_b(\overline{m}_b)$  upwards to  $\overline{m}_b(\mu_R)$ . In the considered Higgs mass range, one obtains an uncertainty of  $\Delta_{m_b}^{\text{input}} \approx -4\%, +14\%$  and  $\approx -3\%, +10\%$  in the case of, respectively, the  $gg \rightarrow \Phi$  and  $b\bar{b} \rightarrow \Phi$  processes (using the central MSTW PDF set). The difference is mainly due to the fact that the bottom quark masses in the two processes are not defined at the same scale and, also, in the case of the  $gg \rightarrow \Phi$  process, additional corrections which involve the  $b$ -quark mass,  $\propto \log(\overline{m}_b^2/M_\Phi^2)$ , occur at leading order.

Finally, a third source of uncertainty originates from the choice of the  $b$ -mass value in the  $b$ -quark densities. The MSTW collaboration has recently released a set of PDFs with different bottom quark masses [55]: it involves six different central PDFs with a range of on-shell  $m_b$  values between 4.00 GeV and 5.50 GeV in 0.25 GeV steps, in addition to the central best-fit with  $m_b = 4.75$  GeV. In order to distinguish between the parametric uncertainty in  $m_b$  and the one due to the correlated PDF- $\Delta m_b$  uncertainty, we have chosen to calculate the latter uncertainty by taking the minimal and maximal values of the production cross sections when using the central value  $m_b = 4.75$  GeV and the two closest ones upwards and downwards, i.e.  $m_b = 4.5$  GeV and  $m_b = 5$  GeV in the MSTW PDF set<sup>23</sup>. However, we kept in the partonic calculation the central value of  $\overline{m}_b(\overline{m}_b) = 4.19$  GeV which, approximately corresponds to the pole mass  $m_b = 4.75$  GeV. One obtains a  $\approx 3\text{--}5\%$

---

<sup>22</sup>We should note that the scheme dependence actually appears also as a result of the truncation of the perturbative series which, in principle, should already be accounted for by the scale variation. However, the scales which enter in the  $b$ -quark mass, that is defined at  $m_b$  itself, and in the rest of the  $gg \rightarrow \Phi$  matrix element, which is the Higgs mass or the scale  $\mu_R$ , are different. We have checked explicitly that the scale uncertainties due to the variation of  $\mu_R$  (and  $\mu_F$ ) in both schemes are comparable. Adding this scheme dependence to the scale variation, as we will do here, is similar in practice to increase the domain of scale variation from the central scale while sticking to a given mass renormalization scheme.

<sup>23</sup>Note that when including the  $1\sigma$  errors on  $\overline{m}_b(\overline{m}_b)$ , while the upper value corresponds to the pole mass

uncertainty depending on the considered Higgs mass range. Note that this uncertainty will not only affect the cross section in the  $b\bar{b} \rightarrow \Phi$  process in which the  $b$ -densities play the major role, but also the one of the  $g\bar{g} \rightarrow \Phi$  channel; however, in this case, the change is below the percent level and can be safely neglected.

The effect of these three sources of uncertainties is displayed in Fig. 18 for  $g\bar{g} \rightarrow \Phi$  and  $b\bar{b} \rightarrow \Phi$  as a function of  $M_\Phi$ . As can be seen, large uncertainties occur, in particular in  $g\bar{g} \rightarrow \Phi$  where the  $\approx 15\%$  scheme uncertainty that is absent in  $b\bar{b} \rightarrow \Phi$  dominates.

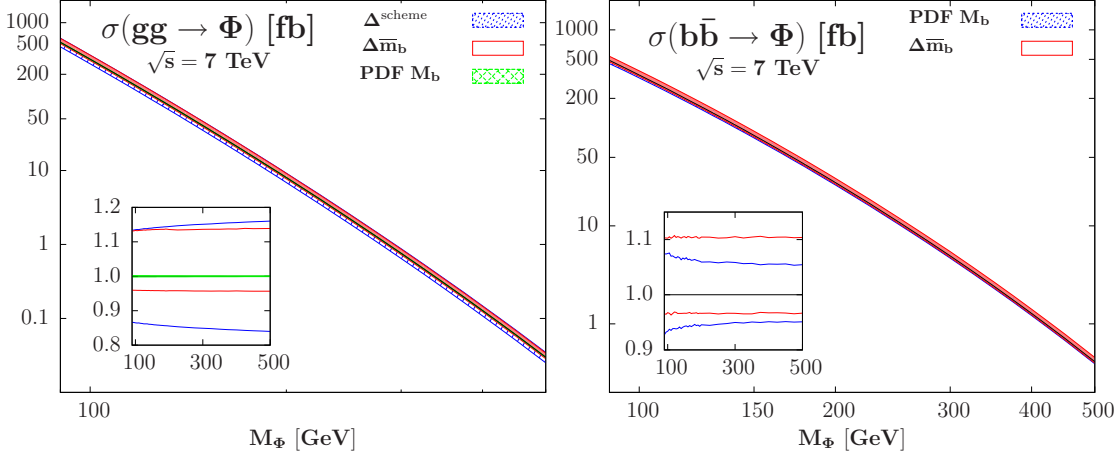


**Figure 18:** The scheme, parametric and PDF uncertainties due to the  $b$ -quark mass in the  $g\bar{g} \rightarrow \Phi$  (left) and  $b\bar{b} \rightarrow \Phi$  (right) cross sections at the LHC at 7 TeV as a function of  $M_\Phi$ . In the inserts, the relative deviations are shown.

#### 4.4 The Higgs decay branching fractions

In the most general case, the decay pattern of the MSSM Higgs particles can be rather complicated, in particular for the heavy states. Indeed, besides the standard decays into pairs of fermions and gauge bosons, the latter can have mixed decays into gauge and Higgs bosons (and the  $H$  bosons can decay into  $hh$  states) and, if some superparticles are light, SUSY decays would also occur. However, for the large values of  $\tan\beta \gtrsim 10$ , the couplings of the non-SM like Higgs particles to bottom quarks and  $\tau$  leptons are so strongly enhanced and those to top quarks and gauge bosons suppressed, that the pattern becomes very simple. To a very good approximation, the  $\Phi = A$  or  $H(h)$  bosons will decay almost exclusively into  $b\bar{b}$  and  $\tau^+\tau^-$  pairs with branching ratios of, respectively,  $\approx 90\%$  and  $\approx 10\%$ , with the  $t\bar{t}$  decay channel and the decay involving gauge or Higgs bosons suppressed to a level where the branching ratios are less than 1%. The CP-even  $h$  or  $H$  boson, depending on whether we are in the decoupling or anti-decoupling regime, will have the same decays as the SM Higgs boson in the mass range below  $M_h^{\text{max}} \lesssim 135$  GeV, decays that have been discussed in section 3 (note that for  $M_h^{\text{max}} \sim 135$  GeV, we are in the regime where the decays into  $b\bar{b}$  and  $WW$  are comparable and, thus, the uncertainties in the Higgs branching ratios are the largest).

---

$m_b \approx 5$  GeV, the lower value does not correspond to  $m_b = 4.5$  GeV; we will however adopt this smaller value to estimate the uncertainty as no other choice is possible within the MSTW set.

$M_\Phi$	$b\bar{b}$	$\Delta m_b$	$\Delta\alpha_s$	tot	$\tau\tau$	$\Delta m_b$	$\Delta\alpha_s$	tot
90	90.40	+0.9% -0.3%	+0.2% -0.2%	+0.9% -0.4%	9.60	+3.2% -8.6%	+1.9% -1.8%	+3.8% -8.8%
100	90.21	+0.9% -0.4%	+0.2% -0.2%	+1.0% -0.4%	9.79	+3.3% -8.6%	+1.9% -1.8%	+3.8% -8.8%
110	90.04	+0.9% -0.4%	+0.2% -0.2%	+1.0% -0.4%	9.96	+3.2% -8.6%	+2.0% -1.9%	+3.8% -8.8%
120	89.88	+1.0% -0.4%	+0.2% -0.2%	+1.0% -0.4%	10.12	+3.3% -8.6%	+2.0% -1.9%	+3.8% -8.8%
130	89.74	+1.0% -0.4%	+0.2% -0.2%	+1.0% -0.4%	10.26	+3.2% -8.5%	+2.0% -1.9%	+3.8% -8.7%
140	89.61	+1.0% -0.4%	+0.2% -0.2%	+1.0% -0.4%	10.39	+3.3% -8.5%	+2.0% -1.9%	+3.8% -8.7%
150	89.48	+1.0% -0.4%	+0.2% -0.2%	+1.0% -0.4%	10.52	+3.1% -8.6%	+2.0% -2.0%	+3.7% -8.8%
160	89.37	+1.0% -0.4%	+0.2% -0.2%	+1.0% -0.5%	10.63	+3.2% -8.5%	+2.1% -2.0%	+3.8% -8.7%
170	89.26	+1.0% -0.4%	+0.2% -0.2%	+1.1% -0.5%	10.74	+3.2% -8.5%	+2.0% -2.0%	+3.8% -8.8%
180	89.16	+1.0% -0.4%	+0.2% -0.3%	+1.1% -0.5%	10.84	+3.2% -8.5%	+2.1% -1.9%	+3.9% -8.7%
190	89.05	+1.0% -0.4%	+0.2% -0.2%	+1.1% -0.5%	10.95	+3.2% -8.5%	+2.0% -2.0%	+3.8% -8.7%
200	88.96	+1.0% -0.4%	+0.2% -0.3%	+1.1% -0.5%	11.04	+3.3% -8.4%	+2.2% -2.0%	+3.9% -8.7%
250	88.53	+1.1% -0.4%	+0.3% -0.3%	+1.1% -0.5%	11.47	+3.1% -8.5%	+2.1% -2.1%	+3.8% -8.7%
300	88.19	+1.1% -0.4%	+0.3% -0.3%	+1.2% -0.5%	11.81	+3.1% -8.5%	+2.1% -2.1%	+3.8% -8.7%
350	87.90	+1.2% -0.4%	+0.3% -0.3%	+1.2% -0.5%	12.10	+3.1% -8.4%	+2.1% -2.1%	+3.8% -8.7%
400	87.66	+1.2% -0.4%	+0.3% -0.3%	+1.2% -0.5%	12.34	+3.2% -8.3%	+2.2% -2.1%	+3.8% -8.6%
450	87.44	+1.2% -0.4%	+0.3% -0.3%	+1.2% -0.5%	12.56	+3.1% -8.4%	+2.2% -2.1%	+3.8% -8.6%
500	87.25	+1.2% -0.5%	+0.3% -0.3%	+1.3% -0.6%	12.75	+3.1% -8.3%	+2.3% -2.1%	+3.9% -8.6%

**Table 7:** The Higgs decay branching ratio into  $b\bar{b}$  and  $\tau^+\tau^-$  final states (in %) for given Higgs mass values (in GeV) with the corresponding individual uncertainties as well as the global uncertainties assuming  $1\sigma$  uncertainties on the inputs  $\bar{m}_b(\bar{m}_b)$  and  $\alpha_s(M_Z^2)$ .

For the evaluation of the theoretical uncertainties in the  $b\bar{b}$  and  $\tau^+\tau^-$  decay branching ratios of the  $\Phi$  states, the analysis of section 3 for the SM Higgs boson can be straightforwardly extended to the MSSM case. Here, one can ignore the error on the input mass of the charm quark (as the decays into  $c\bar{c}$  pairs are strongly suppressed) and consider only the uncertainties coming from the two other sources: the inputs  $\bar{m}_b(\bar{m}_b)$  and  $\alpha_s(M_Z^2)$ . Again, the impact of a scale variation in the range  $\frac{1}{2}M_\Phi \leq \mu \leq 2M_\Phi$  is negligibly small. The uncertainties on the two branching ratios are displayed in Table 7 for some values of the Higgs boson mass, together with the total uncertainties when the individual uncertainties resulting from the “ $1\sigma$ ” errors on the inputs  $\bar{m}_b(\bar{m}_b)$  and  $\alpha_s(M_Z^2)$  are added in quadrature.

The  $b\bar{b}$  branching ratios of the  $\Phi$  states,  $\text{BR}(\Phi \rightarrow b\bar{b}) \approx 3\bar{m}_b^2(M_\Phi)/[3\bar{m}_b^2(M_\Phi) + m_\tau^2]$ , slightly decrease with increasing  $M_\Phi$  as a result of the higher scale which reduces the  $b$ -quark mass  $\bar{m}_b(M_\Phi)$ , but the total uncertainty is practically constant and amounts to less than  $\approx 3\%$  as a consequence of the almost complete cancellation of the uncertainties in the numerator and denominator. In contrast, there is no such a cancellation in the branching fraction for Higgs decays into  $\tau^+\tau^-$  pairs,  $\text{BR}(\Phi \rightarrow \tau^+\tau^-) \approx m_\tau^2/[3\bar{m}_b^2(M_\Phi) + m_\tau^2]$ , and the total uncertainty, that is dominated by the error on the  $b$ -quark mass, reaches the level

of 10% for all Higgs masses<sup>24</sup>. If the error on the input  $b$ -quark mass is ignored, the total uncertainty in the  $\tau^+\tau^-$  branching ratio will reduce to  $\approx 3\%$ .

Finally, let us note that in the MSSM at high  $\tan\beta$ , the total decay widths of the  $\Phi$  particles should be taken into account. Indeed, they rise as  $\Gamma(\Phi) \propto M_\Phi \tan^2\beta$  and thus, reach the level of  $\mathcal{O}(10 \text{ GeV})$  for say,  $M_\Phi \approx 200 \text{ GeV}$  and  $\tan\beta \approx 50$ . The total Higgs width can thus possibly be larger than the experimental resolution on the  $\tau^+\tau^-$  and  $b\bar{b}$  invariant masses when decays into these final states are analyzed. If the total width has to be taken into account in the experimental analyses, the uncertainties that affect it should also be considered. These uncertainties are in fact simply those affecting the  $\Phi \rightarrow b\bar{b}$  partial widths and thus, to a good approximation, the  $\Phi \rightarrow \tau^+\tau^-$  branching ratio. The numbers given in Table 7 for the uncertainties of  $\text{BR}(\Phi \rightarrow \tau^+\tau^-)$  thus correspond (when multiplied by a factor  $\approx 1.1$ ) to the uncertainties on the total width  $\Gamma(\Phi)$  with a good accuracy.

#### 4.5 Combined uncertainties

Let us come to the delicate issue of combining all the uncertainties which come from the various sources. Here, we will adopt the procedure A of section 2.3 also used in Ref. [18], in which the overall uncertainty on the production cross section is obtained by applying the  $\text{PDF} + \Delta^{\text{exp}}\alpha_s + \Delta^{\text{th}}\alpha_s$  uncertainty on the maximal and minimal cross sections from the scale variation, adding linearly the scheme/EFT uncertainty.

As the difference from the SM case is simply the presence of the additional sources of uncertainties due to the  $b$ -quark mass, the combination problem reduces in fact to answering the question of how one should add these three  $m_b$  uncertainties in the production cross sections. The uncertainty from the scheme dependence in the  $gg \rightarrow \Phi$  process should be simply, i.e. linearly, added to the scale uncertainty as both emerge as a result of the truncation of the perturbative series and are thus of pure theoretical nature. The uncertainties of the input  $b$ -quark mass which appears in the parton densities should be added to the other  $\text{PDF} + \alpha_s$  uncertainties. As this uncertainty is of experimental origin, it should be combined in quadrature with the  $\text{PDF} + \Delta^{\text{exp}}\alpha_s + \Delta^{\text{th}}\alpha_s$  uncertainty and since it is much smaller than the latter, it will have practically no impact on the total  $\text{PDF} + \alpha_s$  error<sup>25</sup>. Finally, the parametric uncertainty, which has a special status as it appears also in the Higgs branching ratios, can be simply added linearly to the combined scale+scheme+PDF uncertainty; we will see below that it will have no impact in practice.

---

<sup>24</sup>We should note for completeness, that the same results are obtained in the case of the charged Higgs particles, where for  $M_{H^\pm} \geq m_t + m_b \approx 175 \text{ GeV}$  and  $\tan\beta \gg 1$ , one has to consider only the two decay modes,  $H^+ \rightarrow t\bar{b}$  and  $H^+ \rightarrow \tau^+\bar{\nu}$  with again,  $\text{BR}(H^+ \rightarrow t\bar{b}) \approx 3\overline{m}_b^2(M_{H^\pm})/[3\overline{m}_b^2(M_{H^\pm}) + m_\tau^2]$  and  $\text{BR}(H^+ \rightarrow \tau\nu) \approx m_\tau^2/[3\overline{m}_b^2(M_{H^\pm}) + m_\tau^2]$ . The values of the branching ratios, together with the associated uncertainties, are thus also those given in Table 7 when  $M_\Phi$  is replaced by  $M_{H^\pm}$ .

<sup>25</sup>However, one can also view this uncertainty as being due to the parametrization of the bottom-quark PDF which is a theoretical problem, and thus add it linearly to the  $\text{PDF} + \alpha_s$  so that it increases slightly to the total PDF uncertainty. We will refrain from doing so, though. Note that one may also consider an uncertainty related to the charm-quark mass dependence of the PDFs. This can be estimated again as in footnote 9 and we find at most  $\simeq \pm 2.6\%$  at  $M_\Phi = 500 \text{ GeV}$  in both channels. We then neglect this uncertainty added in quadrature to that of the other PDF-related.



Applying the procedure above for combining the uncertainties, the results for the processes  $gg \rightarrow \Phi$  and  $b\bar{b} \rightarrow \Phi$  at the IHC with  $\sqrt{s} = 7$  TeV are displayed in Fig. 19 as a function of  $M_\Phi$ ; the numerical values can also be found in the relevant columns of tables 8 and 9 where the individual and total uncertainties are given. One finds a total uncertainty of  $\approx +60\%$ ,  $-40\%$  for  $\sigma(gg \rightarrow \Phi)$  and  $\approx +50\%$ ,  $-35\%$  for  $\sigma(b\bar{b} \rightarrow \Phi)$ , in the low Higgs mass range and slightly less at higher masses. As mentioned previously, we expect that these numbers approximately hold at least for slightly higher energies,  $\sqrt{s} = 8\text{--}10$  TeV, and probably also at the full fledged LHC with  $\sqrt{s} = 14$  TeV.

Finally, the total uncertainty on the cross section times branching ratio,  $\Delta(\sigma \times \text{BR})$  is obtained by adding the total uncertainties on the production cross sections and the uncertainties on the branching fraction in Higgs decays into  $\tau^+\tau^-$  pairs, which is the most relevant detection channel. In this addition, at least in the  $b\bar{b} \rightarrow \Phi$  process where one defines the  $\Phi b\bar{b}$  coupling at the scale  $\mu_R$ , the uncertainty on the input  $b$ -mass, which is common to  $\sigma$  and to BR, almost cancels out; only  $\approx 10\%$  of the error is left out<sup>26</sup>. In the case of  $gg \rightarrow \Phi$  where the Yukawa coupling is defined at the scale  $m_b$  in contrast to the Higgs decay widths, the errors on  $\alpha_s$  used for the running from  $m_b$  to  $M_\Phi$  will induce a remaining uncertainty. This  $\alpha_s$  uncertainty is correlated in  $\sigma(gg \rightarrow \Phi)$  and  $\text{BR}(\Phi \rightarrow \tau^+\tau^-)$ : smaller  $\alpha_s$  values lower  $\sigma(gg \rightarrow \Phi) \propto \alpha_s^2$  at LO, and also  $\text{BR}(\Phi \rightarrow \tau^+\tau^-)$  as the resulting  $\bar{m}_b(M_\Phi)$  is higher, thus enhancing/reducing the  $\Phi \rightarrow b\bar{b}/\tau^+\tau^-$  rates. This uncertainty should thus be added linearly to the overall scale+scheme+PDF uncertainty of the cross section.

The impact of this additional uncertainty is shown by the dotted lines of Fig. 19 where the uncertainty  $\Delta(\sigma \times \text{BR})$  for tau decays is displayed for the two production processes. The impact is negligible in the case of  $b\bar{b}$  fusion and very modest in  $gg$  fusion.

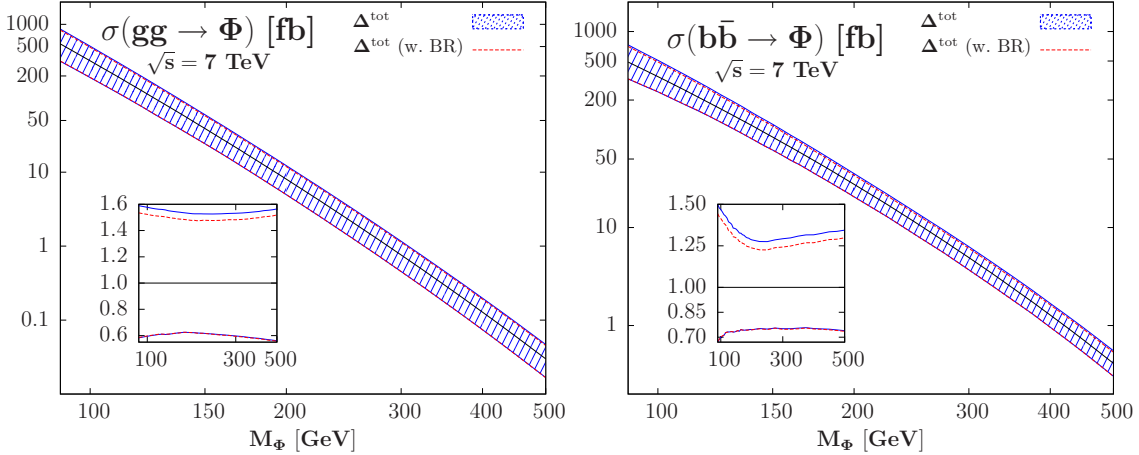


**Figure 19:** The total uncertainties due to the scale, PDF and  $b$ -quark mass in the  $gg \rightarrow \Phi$  (left) and  $b\bar{b} \rightarrow \Phi$  (right) cross sections at the IHC with 7 TeV as a function of  $M_\Phi$ . The dotted lines show the uncertainties when those on the branching ratios for Higgs decays into  $\tau^+\tau^-$  final states are added. In the inserts, the relative deviations are shown.

<sup>26</sup>This is also the case of the  $\Delta_b$  SUSY correction which enters both  $\sigma(gg, b\bar{b} \rightarrow \Phi)$  and  $\text{BR}(\Phi \rightarrow \tau^+\tau^-)$  and which thus cancels in the product. This justifies, a posteriori, why we ignored this correction.

$M_\Phi$	$\sigma_{gg \rightarrow \Phi}^{\pm \Delta_\mu \pm \Delta^{\text{PDF}} \pm \Delta^{\overline{m}_b}}$	$\Delta^{\text{tot}}$	$\times \text{BR}$
90	542.28 <sup>+21.7%</sup> <sub>-18.3%</sub> <sup>+7.9%</sup> <sub>-8.1%</sub> <sup>+26.7%</sup> <sub>-17.6%</sub>	+58.9% -41.7%	+53.5% -41.5%
95	414.48 <sup>+21.1%</sup> <sub>-17.6%</sub> <sup>+7.8%</sup> <sub>-8.0%</sub> <sup>+26.8%</sup> <sub>-17.7%</sub>	+58.3% -41.1%	+52.8% -40.9%
100	320.31 <sup>+20.4%</sup> <sub>-16.9%</sub> <sup>+7.8%</sup> <sub>-7.9%</sub> <sup>+27.0%</sup> <sub>-17.8%</sub>	+57.7% -40.5%	+52.3% -40.3%
105	250.43 <sup>+19.9%</sup> <sub>-16.3%</sub> <sup>+7.8%</sup> <sub>-7.9%</sub> <sup>+27.0%</sup> <sub>-17.9%</sub>	+57.1% -40.0%	+51.7% -39.8%
110	197.61 <sup>+19.4%</sup> <sub>-15.9%</sub> <sup>+7.7%</sup> <sub>-7.8%</sub> <sup>+27.1%</sup> <sub>-17.9%</sub>	+56.6% -39.6%	+51.3% -39.4%
115	157.34 <sup>+18.9%</sup> <sub>-15.4%</sub> <sup>+7.7%</sup> <sub>-7.8%</sub> <sup>+27.2%</sup> <sub>-18.0%</sub>	+56.2% -39.2%	+51.0% -39.0%
120	126.32 <sup>+18.5%</sup> <sub>-15.1%</sub> <sup>+7.7%</sup> <sub>-7.8%</sub> <sup>+27.3%</sup> <sub>-18.0%</sub>	+56.1% -39.0%	+50.7% -38.9%
125	102.14 <sup>+18.1%</sup> <sub>-15.3%</sub> <sup>+7.7%</sup> <sub>-7.7%</sub> <sup>+27.4%</sup> <sub>-18.1%</sub>	+55.8% -39.2%	+50.4% -39.1%
130	83.24 <sup>+17.7%</sup> <sub>-15.1%</sub> <sup>+7.7%</sup> <sub>-7.7%</sub> <sup>+27.4%</sup> <sub>-18.1%</sub>	+55.1% -39.0%	+50.0% -38.9%
135	68.25 <sup>+17.4%</sup> <sub>-14.7%</sub> <sup>+7.7%</sup> <sub>-7.7%</sub> <sup>+27.5%</sup> <sub>-18.2%</sub>	+54.8% -38.7%	+49.6% -38.7%
140	56.31 <sup>+17.1%</sup> <sub>-14.2%</sub> <sup>+7.7%</sup> <sub>-7.7%</sub> <sup>+27.6%</sup> <sub>-18.2%</sub>	+54.5% -38.4%	+49.3% -38.3%
145	46.73 <sup>+16.7%</sup> <sub>-13.8%</sub> <sup>+7.6%</sup> <sub>-7.7%</sub> <sup>+27.6%</sup> <sub>-18.3%</sub>	+54.1% -38.1%	+48.9% -38.2%
150	38.98 <sup>+16.4%</sup> <sub>-13.5%</sub> <sup>+7.6%</sup> <sub>-7.7%</sub> <sup>+27.7%</sup> <sub>-18.4%</sub>	+54.0% -37.8%	+48.7% -37.9%
155	32.68 <sup>+16.1%</sup> <sub>-13.1%</sub> <sup>+7.6%</sup> <sub>-7.7%</sub> <sup>+27.8%</sup> <sub>-18.4%</sub>	+53.7% -37.6%	+48.6% -37.5%
160	27.52 <sup>+15.9%</sup> <sub>-13.0%</sub> <sup>+7.6%</sup> <sub>-7.7%</sub> <sup>+27.9%</sup> <sub>-18.5%</sub>	+53.5% -37.5%	+48.3% -37.5%
165	23.29 <sup>+15.7%</sup> <sub>-13.0%</sub> <sup>+7.6%</sup> <sub>-7.7%</sub> <sup>+27.9%</sup> <sub>-18.5%</sub>	+53.3% -37.6%	+48.2% -37.5%
170	19.79 <sup>+15.4%</sup> <sub>-13.0%</sub> <sup>+7.6%</sup> <sub>-7.7%</sub> <sup>+28.0%</sup> <sub>-18.6%</sub>	+53.0% -37.7%	+47.9% -37.7%
175	16.88 <sup>+15.2%</sup> <sub>-13.1%</sub> <sup>+7.6%</sup> <sub>-7.7%</sub> <sup>+28.0%</sup> <sub>-18.6%</sub>	+52.8% -37.8%	+47.7% -37.7%
180	14.45 <sup>+15.0%</sup> <sub>-13.1%</sub> <sup>+7.7%</sup> <sub>-7.7%</sub> <sup>+28.1%</sup> <sub>-18.6%</sub>	+52.7% -37.8%	+47.7% -37.8%
185	12.42 <sup>+15.0%</sup> <sub>-13.1%</sub> <sup>+7.7%</sup> <sub>-7.7%</sub> <sup>+28.1%</sup> <sub>-18.7%</sub>	+52.7% -38.0%	+47.5% -38.2%
190	10.71 <sup>+14.9%</sup> <sub>-13.2%</sub> <sup>+7.6%</sup> <sub>-7.8%</sub> <sup>+28.2%</sup> <sub>-18.8%</sub>	+52.8% -38.1%	+47.6% -38.2%
195	9.27 <sup>+14.9%</sup> <sub>-13.2%</sub> <sup>+7.7%</sup> <sub>-7.8%</sub> <sup>+28.2%</sup> <sub>-18.8%</sub>	+52.7% -38.2%	+47.6% -38.3%
200	8.04 <sup>+14.8%</sup> <sub>-13.2%</sub> <sup>+7.7%</sup> <sub>-7.8%</sub> <sup>+28.0%</sup> <sub>-18.7%</sub>	+52.7% -38.3%	+47.8% -38.3%
225	4.12 <sup>+14.7%</sup> <sub>-13.4%</sub> <sup>+7.8%</sup> <sub>-8.0%</sub> <sup>+28.3%</sup> <sub>-19.0%</sub>	+52.6% -38.8%	+47.6% -39.0%
250	2.24 <sup>+14.5%</sup> <sub>-13.6%</sub> <sup>+7.9%</sup> <sub>-8.2%</sub> <sup>+28.4%</sup> <sub>-19.2%</sub>	+52.8% -39.3%	+47.8% -39.6%
275	1.28 <sup>+14.4%</sup> <sub>-13.7%</sub> <sup>+8.0%</sup> <sub>-8.4%</sub> <sup>+28.7%</sup> <sub>-19.4%</sub>	+53.0% -39.8%	+48.3% -39.9%
300	0.76 <sup>+14.2%</sup> <sub>-13.8%</sub> <sup>+8.2%</sup> <sub>-8.6%</sub> <sup>+28.9%</sup> <sub>-19.5%</sub>	+53.2% -40.3%	+48.2% -40.6%
325	0.47 <sup>+14.2%</sup> <sub>-13.9%</sub> <sup>+8.4%</sup> <sub>-8.9%</sub> <sup>+29.0%</sup> <sub>-19.6%</sub>	+53.4% -40.7%	+48.5% -41.0%
350	0.30 <sup>+14.2%</sup> <sub>-14.0%</sub> <sup>+8.7%</sup> <sub>-9.2%</sub> <sup>+29.1%</sup> <sub>-19.8%</sub>	+53.8% -41.3%	+48.9% -41.7%
375	0.19 <sup>+14.1%</sup> <sub>-14.1%</sub> <sup>+9.0%</sup> <sub>-9.5%</sub> <sup>+29.4%</sup> <sub>-19.9%</sub>	+54.2% -41.8%	+49.5% -41.9%
400	0.13 <sup>+14.1%</sup> <sub>-14.2%</sub> <sup>+9.3%</sup> <sub>-9.8%</sub> <sup>+29.4%</sup> <sub>-20.0%</sub>	+54.5% -42.1%	+49.8% -42.4%
425	0.09 <sup>+14.1%</sup> <sub>-14.3%</sub> <sup>+9.6%</sup> <sub>-10.1%</sub> <sup>+29.7%</sup> <sub>-20.2%</sub>	+55.1% -42.6%	+50.5% -42.9%
450	0.06 <sup>+14.1%</sup> <sub>-14.4%</sub> <sup>+9.9%</sup> <sub>-10.4%</sub> <sup>+29.8%</sup> <sub>-20.3%</sub>	+55.4% -43.1%	+50.8% -43.5%
500	0.03 <sup>+14.2%</sup> <sub>-14.5%</sub> <sup>+10.6%</sup> <sub>-11.0%</sub> <sup>+30.0%</sup> <sub>-20.5%</sub>	+56.5% -44.0%	+51.9% -44.3%

**Table 8:** The Higgs production cross sections in the  $gg \rightarrow \Phi$  channel (for  $\tan \beta = 1$ ) as well as the individual uncertainties (first from scale, then from  $\text{PDF} + \Delta^{\text{exp} + \text{th}} \alpha_s$  at 90%CL and from the input mass  $\overline{m}_b$  at  $1\sigma$ ) and the total uncertainties for selected values of the Higgs mass. The last column displays the total uncertainty when including the combination with the total uncertainty on  $\Phi \rightarrow \tau^+ \tau^-$  branching ratio.

$M_\Phi$	$\sigma_{b\bar{b} \rightarrow \Phi}^{\pm\Delta_\mu \pm\Delta^{\text{PDF}} \pm\Delta^{m_b}}$	$\Delta^{\text{tot}}$	$\times\text{BR}$
90	487.83 <sup>+26.8%</sup> <sub>-21.1%</sub> <sup>+6.2%</sup> <sub>-8.0%</sub> <sup>+17.8%</sup> <sub>-10.7%</sub>	+49.8% -32.8%	+44.3% -32.5%
95	409.59 <sup>+25.4%</sup> <sub>-19.5%</sub> <sup>+7.1%</sup> <sub>-7.3%</sub> <sup>+17.7%</sup> <sub>-10.3%</sub>	+47.8% -31.5%	+42.4% -31.3%
100	346.50 <sup>+23.9%</sup> <sub>-18.4%</sub> <sup>+6.4%</sup> <sub>-7.8%</sub> <sup>+17.8%</sup> <sub>-9.9%</sub>	+46.9% -29.9%	+41.4% -29.8%
105	294.57 <sup>+22.2%</sup> <sub>-17.8%</sub> <sup>+6.3%</sup> <sub>-8.3%</sub> <sup>+18.1%</sup> <sub>-9.6%</sub>	+45.4% -29.5%	+40.0% -29.3%
110	252.03 <sup>+21.3%</sup> <sub>-16.7%</sub> <sup>+6.9%</sup> <sub>-7.7%</sub> <sup>+17.2%</sup> <sub>-10.1%</sub>	+43.8% -28.9%	+38.5% -28.8%
115	215.89 <sup>+20.3%</sup> <sub>-15.9%</sub> <sup>+6.8%</sup> <sub>-8.0%</sub> <sup>+17.5%</sup> <sub>-9.5%</sub>	+43.0% -27.5%	+37.7% -27.3%
120	186.56 <sup>+18.8%</sup> <sub>-15.4%</sub> <sup>+7.2%</sup> <sub>-7.7%</sub> <sup>+17.6%</sup> <sub>-9.3%</sub>	+41.7% -26.9%	+36.4% -27.0%
125	161.84 <sup>+17.4%</sup> <sub>-15.2%</sub> <sup>+7.7%</sup> <sub>-7.6%</sub> <sup>+17.1%</sup> <sub>-9.4%</sub>	+39.4% -26.9%	+34.1% -26.8%
130	140.97 <sup>+16.4%</sup> <sub>-14.9%</sub> <sup>+7.6%</sup> <sub>-7.8%</sub> <sup>+17.5%</sup> <sub>-9.5%</sub>	+38.8% -26.8%	+33.7% -26.7%
135	122.98 <sup>+15.5%</sup> <sub>-14.6%</sub> <sup>+7.3%</sup> <sub>-8.0%</sub> <sup>+17.2%</sup> <sub>-9.2%</sub>	+38.0% -26.6%	+32.8% -26.6%
140	108.08 <sup>+14.1%</sup> <sub>-14.7%</sub> <sup>+7.5%</sup> <sub>-8.0%</sub> <sup>+16.6%</sup> <sub>-9.5%</sub>	+35.6% -26.9%	+30.5% -26.8%
145	94.85 <sup>+13.7%</sup> <sub>-14.7%</sub> <sup>+7.7%</sup> <sub>-8.2%</sub> <sup>+17.1%</sup> <sub>-9.2%</sub>	+35.5% -26.9%	+30.2% -27.0%
150	83.83 <sup>+13.0%</sup> <sub>-14.3%</sub> <sup>+8.2%</sup> <sub>-8.0%</sub> <sup>+17.0%</sup> <sub>-9.1%</sub>	+35.0% -26.4%	+29.7% -26.5%
155	74.13 <sup>+12.0%</sup> <sub>-14.2%</sub> <sup>+8.2%</sup> <sub>-8.2%</sub> <sup>+17.1%</sup> <sub>-9.0%</sub>	+34.0% -26.2%	+28.9% -26.1%
160	65.84 <sup>+11.0%</sup> <sub>-14.1%</sub> <sup>+8.3%</sup> <sub>-8.2%</sub> <sup>+16.9%</sup> <sub>-9.1%</sub>	+32.7% -26.4%	+27.6% -26.5%
165	58.60 <sup>+10.4%</sup> <sub>-13.6%</sub> <sup>+8.2%</sup> <sub>-8.5%</sub> <sup>+16.9%</sup> <sub>-8.8%</sub>	+32.6% -25.4%	+27.5% -25.5%
170	52.28 <sup>+9.6%</sup> <sub>-13.6%</sub> <sup>+8.5%</sup> <sub>-8.3%</sub> <sup>+16.6%</sup> <sub>-9.2%</sub>	+31.7% -25.7%	+26.5% -25.7%
175	46.75 <sup>+9.1%</sup> <sub>-13.4%</sub> <sup>+8.4%</sup> <sub>-8.6%</sub> <sup>+16.7%</sup> <sub>-8.9%</sub>	+31.3% -25.8%	+26.2% -25.8%
180	41.97 <sup>+8.3%</sup> <sub>-13.8%</sub> <sup>+8.5%</sup> <sub>-8.7%</sub> <sup>+16.9%</sup> <sub>-8.7%</sub>	+30.4% -25.7%	+25.4% -25.7%
185	37.69 <sup>+7.5%</sup> <sub>-13.3%</sub> <sup>+9.2%</sup> <sub>-8.2%</sub> <sup>+16.8%</sup> <sub>-8.8%</sub>	+29.8% -25.6%	+24.6% -25.8%
190	33.87 <sup>+7.5%</sup> <sub>-12.8%</sub> <sup>+8.6%</sup> <sub>-9.2%</sub> <sup>+16.5%</sup> <sub>-8.9%</sub>	+29.6% -25.5%	+24.4% -25.6%
195	30.55 <sup>+7.0%</sup> <sub>-12.3%</sub> <sup>+8.9%</sup> <sub>-9.1%</sub> <sup>+16.4%</sup> <sub>-9.1%</sub>	+29.0% -25.4%	+23.9% -25.5%
200	27.61 <sup>+6.3%</sup> <sub>-12.5%</sub> <sup>+8.7%</sup> <sub>-9.6%</sub> <sup>+16.4%</sup> <sub>-8.8%</sub>	+28.6% -25.5%	+23.7% -25.6%
225	17.10 <sup>+5.1%</sup> <sub>-11.9%</sub> <sup>+9.6%</sup> <sub>-9.7%</sub> <sup>+16.4%</sup> <sub>-8.9%</sub>	+27.6% -24.8%	+22.6% -25.0%
250	10.97 <sup>+5.0%</sup> <sub>-11.5%</sub> <sup>+10.6%</sup> <sub>-10.0%</sub> <sup>+16.1%</sup> <sub>-8.8%</sub>	+27.5% -25.1%	+22.5% -25.4%
275	7.27 <sup>+5.0%</sup> <sub>-10.6%</sub> <sup>+10.9%</sup> <sub>-10.8%</sub> <sup>+16.3%</sup> <sub>-8.6%</sub>	+28.6% -24.5%	+23.9% -24.6%
300	4.94 <sup>+4.8%</sup> <sub>-10.5%</sub> <sup>+11.6%</sup> <sub>-11.4%</sub> <sup>+16.4%</sup> <sub>-8.4%</sub>	+29.3% -24.9%	+24.3% -25.3%
325	3.43 <sup>+4.8%</sup> <sub>-9.8%</sub> <sup>+12.4%</sup> <sub>-11.8%</sub> <sup>+15.9%</sup> <sub>-8.6%</sub>	+29.7% -24.9%	+24.9% -25.2%
350	2.43 <sup>+5.0%</sup> <sub>-9.4%</sub> <sup>+13.1%</sup> <sub>-12.3%</sub> <sup>+16.2%</sup> <sub>-8.4%</sub>	+30.8% -24.6%	+25.9% -25.0%
375	1.75 <sup>+4.9%</sup> <sub>-9.1%</sub> <sup>+14.1%</sup> <sub>-12.5%</sub> <sup>+16.0%</sup> <sub>-8.2%</sub>	+31.6% -24.3%	+26.9% -24.5%
400	1.28 <sup>+4.7%</sup> <sub>-8.9%</sub> <sup>+14.9%</sup> <sub>-13.1%</sub> <sup>+15.9%</sup> <sub>-8.2%</sub>	+31.6% -24.8%	+26.9% -25.1%
425	0.95 <sup>+4.7%</sup> <sub>-8.6%</sub> <sup>+15.5%</sup> <sub>-13.6%</sub> <sup>+16.0%</sup> <sub>-8.3%</sub>	+32.5% -25.0%	+27.8% -25.3%
450	0.71 <sup>+4.7%</sup> <sub>-8.2%</sub> <sup>+16.1%</sup> <sub>-14.2%</sub> <sup>+16.1%</sup> <sub>-8.2%</sub>	+33.4% -25.2%	+28.8% -25.6%
500	0.41 <sup>+4.7%</sup> <sub>-7.9%</sub> <sup>+17.8%</sup> <sub>-15.1%</sub> <sup>+15.8%</sup> <sub>-8.2%</sub>	+34.4% -26.1%	+29.8% -26.5%

**Table 9:** The same as in Table. 8 but for the  $b\bar{b} \rightarrow \Phi$  channel.

Thus, the theoretical uncertainties in the  $b\bar{b}, gg \rightarrow \Phi \rightarrow \tau^+\tau^-$  production and decay channels for the MSSM CP-odd and one of the CP-even Higgs particles are extremely large. This has important consequences on the MSSM  $[\tan\beta, M_A]$  parameter space that can be probed at the LHC. In particular, if no Higgs boson is observed and only exclusion limits on the parameter space can be imposed, these uncertainties which can lower the production cross sections by a factor of two will have a significant impact. For instance, as the cross sections grow as  $\tan^2\beta$ , the values of  $\tan\beta$  which can be ruled out for a given  $A$  boson mass should be multiplied by a factor  $\approx\sqrt{2}$  in view of these large uncertainties.

## 5. Conclusions

In the first part of this paper, we have performed a detailed analysis for Standard Model Higgs production at the LHC with  $\sqrt{s} = 7$  TeV in the dominant gluon-gluon fusion channel,  $gg \rightarrow H$ . We have first updated the production cross sections, including the relevant higher order corrections in perturbation theory and then, discussed the theoretical uncertainties that affect the predictions: the scale uncertainties that are usually viewed as an estimate of the unknown higher order corrections, the uncertainties due to the parton distribution functions and the strong coupling constant, and finally, the uncertainties in using an effective field theory approach in calculating the higher order corrections beyond next-to-leading perturbative order.

We find that the scale uncertainties, estimated by varying the renormalization and factorization scales in the interval  $\frac{1}{2}\mu_0 \leq \mu_R, \mu_F \leq 2\mu_0$  with  $\mu_0 = \frac{1}{2}M_H$  being the central scale, are moderate,  $\approx \pm 12\%$  in the low mass range  $M_H \approx 120$  GeV, and  $\approx +5\%, -8\%$  in the high mass range,  $M_H \approx 500$  GeV. For the PDF uncertainty, we have considered the four NNLO PDF sets that are available, MSTW, ABKM, JR and HERAPDF, and shown that there is a sizable spread in the predictions of the cross section. This spread could be partly accounted for by taking into account the uncertainties, both experimental and theoretical, on the value of  $\alpha_s$ . The evaluation in the MSTW scheme of the correlated PDF  $+\Delta^{\text{exp+th}}\alpha_s$  uncertainties in the  $gg \rightarrow H$  cross section leads to a  $\approx \pm 10\%$  uncertainty in the entire Higgs mass range that is relevant at the LHC,  $M_H \lesssim 500$  GeV. A third source of uncertainties is due to the use of the approximation of an infinite mass for the particles running in the  $gg \rightarrow H$  loop when calculating the amplitude beyond NLO, i.e. for the NNLO QCD and the mixed QCD-electroweak corrections; an additional uncertainty arises from the renormalization of the bottom quark mass. These uncertainties are quite small when taken individually, at most a few percent each, but they add up to a non-negligible amount, 3 to 7% depending on the Higgs mass range and should be thus included.

We have then addressed the issue of combining these three sources of uncertainties. Arguing that the PDF uncertainty should be viewed as a pure theoretical one, we have proposed three procedures for combining it with those due the scale and the EFT/scheme, the simplest one being a linear addition. All three procedures lead to approximately the same total uncertainty on the  $gg \rightarrow H$  cross section at the LHC,  $\approx -25\%, +30\%$  in the low mass range  $M_H \lesssim 200$  GeV and  $\approx \pm 20\%$  at higher Higgs masses. The overall uncertainty at the LHC is significantly smaller than the one affecting the cross section at Tevatron

energies. This is a mere consequence of the smaller scale uncertainty, as the QCD corrections are more moderate at LHC energies, and the fact that, at the Tevatron, one is probing the high Bjorken- $x$  regime for the gluon densities which is more uncertain.

We have extended our analysis to other possible energies:  $\sqrt{s} = 8\text{--}10$  TeV that are planned to be explored after the  $\sqrt{s} = 7$  TeV run and the LHC design energy of  $\sqrt{s} = 14$  TeV. We provided numerical results for the  $gg \rightarrow H$  cross section and in the case of the LHC, we also estimated the associated theoretical uncertainties. The latter turned out to be comparable to those obtained at 7 TeV and these uncertainties are, thus, expected to be also the same at the intermediate energies.

In a second part of the paper, we have addressed the issue of the Higgs decay branching ratios and the uncertainties that affect them, namely, the parametric ones due to the errors in the determination of the bottom and charm quark masses and the QCD coupling  $\alpha_s$ . We obtain uncertainties that are significant in the critical intermediate Higgs mass range  $120 \text{ GeV} \lesssim M_H \lesssim 150 \text{ GeV}$  where the main Higgs decay channels  $H \rightarrow b\bar{b}$  and  $H \rightarrow WW$  have comparable rates. These uncertainties can reach the level of  $\approx \pm 3\text{--}10\%$  in the channels  $H \rightarrow WW, ZZ, \gamma\gamma$  used to detect the Higgs particle at the LHC; this is also the case for the decays  $H \rightarrow b\bar{b}$  and  $\tau^+\tau^-$  which are also being considered in Tevatron searches. One should therefore also take into account these uncertainties which, up to now, have been overlooked by the experimental collaborations not only at the LHC but also at the Tevatron.

Finally, in a third part of the paper, we have extended our analysis of Higgs production at the LHC to consider the case of the MSSM neutral Higgs particles. We have investigated the production of the CP-odd like particles,  $\Phi = A$  as well as one of the CP-even  $H$  or  $h$  particles (depending on whether we are in the decoupling or anti-decoupling regimes) that are degenerate in mass with  $A$  and have the same couplings, in particular, enhanced couplings to bottom quarks for the high values of  $\tan\beta$  than can be probed at the LHC. The two main production processes  $gg \rightarrow \Phi$  and  $b\bar{b} \rightarrow \Phi$ , which could have cross sections that are order of magnitude larger than in the SM Higgs case, have been considered. Numerical results at energies  $\sqrt{s} = 7\text{--}14$  TeV have been given and the associated theoretical uncertainties have been evaluated. The latter are due not only to the scale and PDF+ $\alpha_s$  uncertainties which appear in the SM case, but there are also uncertainties associated to the  $b$ -quark which plays a major role in the MSSM. The error on the input  $b$ -quark mass, the scheme dependence in the renormalization of the mass of the  $b$ -quark in its contribution to the  $gg \rightarrow \Phi$  amplitude and the effect of  $m_b$  on the bottom quark densities in the process  $b\bar{b} \rightarrow \Phi$  will induce additional uncertainties. To these, one has to add the parametric uncertainties in the branching ratio of the Higgs decay in tau lepton pairs, which is the cleanest detection channel at hadron colliders, that is found to be at the level of 10%.

The overall theoretical uncertainty in these two processes turn out to be extremely large at LHC energies, of the order of 50%. This large uncertainty will have a significant impact on the MSSM parameter space that can be probed. This is particularly true in the case where no MSSM Higgs signal is observed and only exclusion bounds can be derived by comparing the experimental data with the predicted Higgs production cross sections. As the cross sections in both the  $gg \rightarrow \Phi$  and  $b\bar{b} \rightarrow \Phi$  processes increase with  $\tan^2\beta$ , the values of  $\tan\beta$  which could be excluded in the absence of a signal will be smaller by a

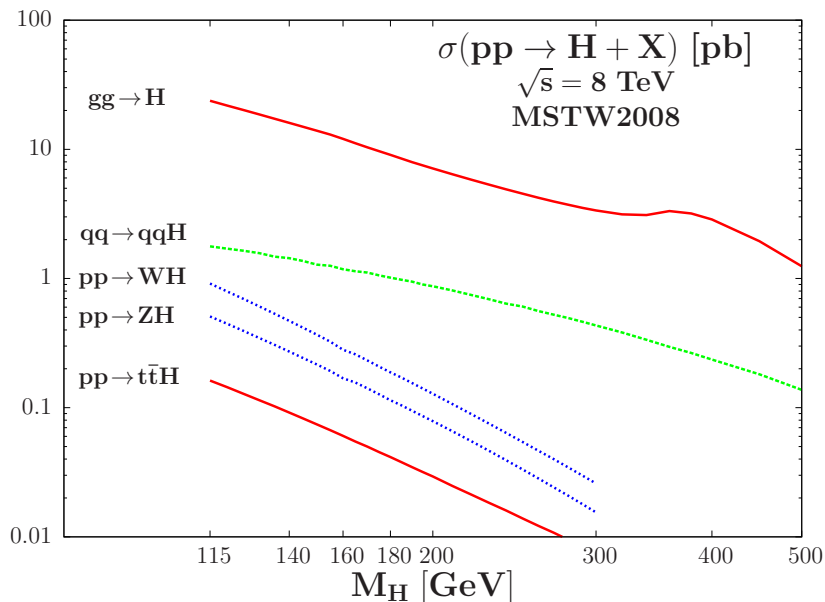


**Figure 20:** Same as in Fig. 1 for  $\sqrt{s} = 8$  TeV.

factor  $\approx \sqrt{2}$  if these theoretical uncertainties are taken into account<sup>27</sup>.

**Acknowledgments:** Illuminating discussions with Rohini Godbole on the PDFs and with Michael Spira on many aspects of this work are gratefully acknowledged. We would also like to thank the members of the LHC Higgs cross section Working Group, in particular C. Mariotti, M. Grazzini and G. Passarino, for discussions. This work is supported by the European Network HEPTOOLS.

#### A1. Addendum: SM cross sections and uncertainties at $\sqrt{s} = 8$ TeV

In this addendum, we summarize the Higgs production cross sections in the SM and in the case of  $gg \rightarrow H$  we detail the associated uncertainties, at a c.m. energy of  $\sqrt{s} = 8$  TeV, following exactly the discussion presented in section 2. In particular we update the numbers presented in Table 3 with more precision and a full account of the other main processes. The rates for the four production channels are displayed in Fig. 20 and Table 10. The scale, PDF (using either only the MSTW set or including also the other available NNLO PDF sets) and EFT as well as the total uncertainties are shown in Fig. 21 for the  $gg \rightarrow H$  process and the relevant numbers are given in Table 11.

<sup>27</sup>This is also the case for the exclusion bounds that have been obtained by the CDF and D0 collaborations from negative MSSM Higgs searches at the Tevatron [10]. See Ref. [79] for an analysis of this issue.

$M_H$	$\sigma_{gg \rightarrow H}^{\text{NNLO}}$	$\sigma_{qq \rightarrow Hqq}^{\text{NLO}}$	$\sigma_{q\bar{q} \rightarrow HW}^{\text{NNLO}}$	$\sigma_{q\bar{q} \rightarrow HZ}^{\text{NNLO}}$	$\sigma_{pp \rightarrow t\bar{t}H}^{\text{LO}}$
115	23757.4	1772.2	913.9	508.7	162.2
120	21832.4	1702.9	794.1	446.0	144.2
125	20126.9	1639.6	694.8	392.7	128.0
130	18608.7	1571.4	607.7	346.1	114.2
135	17252.0	1476.9	533.5	306.6	102.4
140	16032.9	1436.2	469.6	272.1	91.6
145	14933.7	1363.9	414.8	241.9	82.3
150	13934.8	1279.5	366.7	215.8	74.1
155	13009.0	1254.7	324.3	192.5	67.0
160	12063.1	1180.2	280.8	169.0	60.5
165	11143.1	1138.8	258.7	156.6	54.7
170	10360.9	1112.2	232.1	141.1	49.9
175	9688.5	1058.3	208.2	127.0	45.3
180	9065.7	1016.1	187.7	114.1	41.5
185	8483.1	977.8	171.0	104.2	37.9
190	7962.6	944.9	155.0	94.7	34.6
195	7509.0	900.0	141.0	86.2	31.8
200	7105.4	870.3	128.1	78.7	29.4
210	6408.1	807.9	106.6	65.7	24.8
220	5823.0	745.5	89.2	55.0	21.2
230	5326.7	690.4	75.3	46.3	18.3
240	4901.8	638.7	63.7	39.2	16.0
250	4536.1	607.0	54.3	33.3	13.9
260	4221.7	559.7	46.4	28.3	12.2
270	3951.5	525.4	40.0	24.2	10.8
280	3721.0	494.1	34.5	20.8	9.5
290	3524.8	462.8	29.8	17.9	8.5
300	3362.2	433.0	25.9	15.5	7.6

**Table 10:** Same as in Table 1 with  $\sqrt{s} = 8$  TeV.

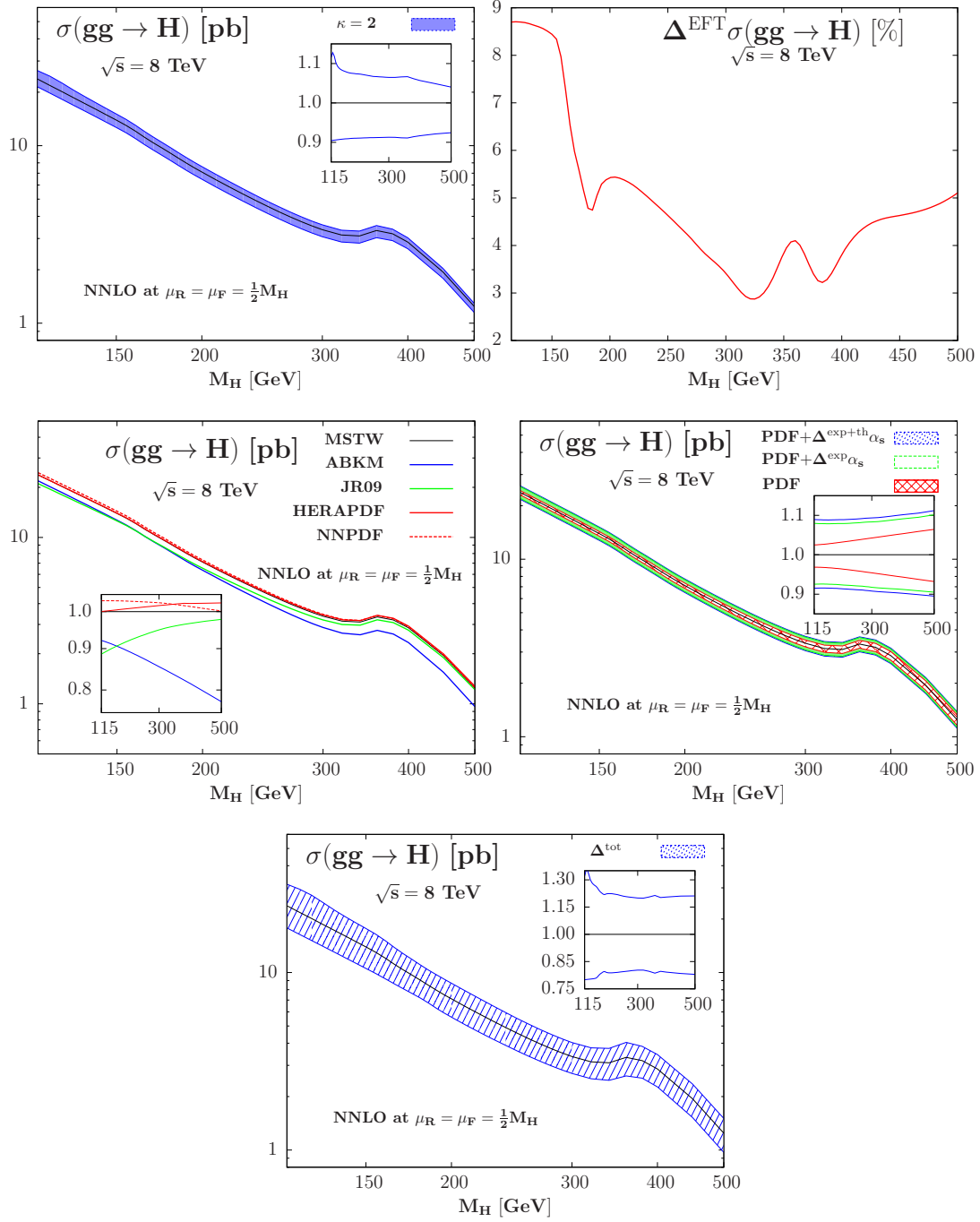


Figure 21: Same as in Figs. 9, 10, 11 for  $\sqrt{s} = 8$  TeV.



$M_H$	$\sigma$ [pb]	Scale [%]	PDF+ $\Delta_{\alpha_s}^{\text{exp+th}}$ [%]	EFT [%]	Total [%]
115	23.76	+11.6 -9.6	+8.9 -8.5	$\pm 8.7$	+32.3 -25.0
120	21.83	+12.8 -9.5	+8.9 -8.5	$\pm 8.7$	+35.0 -24.9
125	20.13	+11.9 -9.5	+8.9 -8.5	$\pm 8.7$	+35.3 -24.8
130	18.61	+10.3 -9.4	+8.9 -8.5	$\pm 8.7$	+32.7 -24.7
135	17.25	+9.4 -9.4	+8.9 -8.4	$\pm 8.6$	+30.0 -24.6
140	16.03	+8.9 -9.3	+8.9 -8.4	$\pm 8.6$	+28.5 -24.5
145	14.93	+8.5 -9.3	+8.9 -8.4	$\pm 8.5$	+27.6 -24.4
150	13.93	+8.3 -9.2	+8.8 -8.4	$\pm 8.4$	+27.0 -24.3
155	13.01	+8.1 -9.2	+8.8 -8.5	$\pm 8.3$	+26.4 -24.1
160	12.06	+8.0 -9.1	+8.8 -8.5	$\pm 7.6$	+25.5 -23.4
165	11.14	+7.8 -9.1	+8.8 -8.5	$\pm 6.6$	+24.3 -22.5
170	10.36	+7.7 -9.1	+8.8 -8.5	$\pm 5.9$	+23.3 -21.7
175	9.69	+7.6 -9.0	+8.9 -8.5	$\pm 5.4$	+22.7 -21.2
180	9.07	+7.5 -9.0	+8.9 -8.5	$\pm 4.9$	+22.0 -20.6
185	8.48	+7.5 -9.0	+8.9 -8.5	$\pm 4.7$	+21.9 -20.5
190	7.96	+7.5 -9.0	+8.9 -8.5	$\pm 5.1$	+22.2 -20.9
195	7.51	+7.4 -9.0	+8.9 -8.6	$\pm 5.3$	+22.4 -21.1
200	7.11	+7.4 -8.9	+8.9 -8.6	$\pm 5.4$	+22.4 -21.2
210	6.41	+7.3 -8.9	+8.9 -8.7	$\pm 5.4$	+22.4 -21.2
220	5.82	+7.2 -8.9	+8.9 -8.7	$\pm 5.3$	+22.1 -21.1
230	5.33	+7.0 -8.9	+9.0 -8.8	$\pm 5.1$	+21.8 -20.9
240	4.90	+6.9 -8.8	+9.0 -8.8	$\pm 4.9$	+21.4 -20.7
250	4.54	+6.7 -8.8	+9.1 -8.9	$\pm 4.6$	+21.0 -20.5
260	4.22	+6.7 -8.8	+9.1 -8.9	$\pm 4.4$	+20.7 -20.4
270	3.95	+6.6 -8.8	+9.2 -8.9	$\pm 4.1$	+20.5 -20.2
280	3.72	+6.6 -8.8	+9.3 -9.0	$\pm 3.9$	+20.3 -20.0
290	3.52	+6.5 -8.7	+9.3 -9.1	$\pm 3.7$	+20.1 -19.8
300	3.36	+6.5 -8.7	+9.3 -9.2	$\pm 3.4$	+20.0 -19.7
320	3.14	+6.5 -8.7	+9.4 -9.4	$\pm 2.9$	+19.9 -19.7
340	3.10	+6.6 -8.9	+9.6 -9.5	$\pm 3.3$	+20.5 -20.4
360	3.33	+6.7 -8.9	+9.8 -9.6	$\pm 4.1$	+21.4 -21.4
380	3.19	+6.1 -8.6	+10.0 -9.6	$\pm 3.2$	+20.2 -20.4
400	2.86	+5.7 -8.3	+10.2 -9.8	$\pm 3.8$	+20.5 -20.8
450	1.94	+4.9 -7.9	+10.6 -10.1	$\pm 4.6$	+21.1 -21.5
500	1.24	+4.0 -7.6	+11.2 -10.5	$\pm 5.1$	+21.1 -22.0

**Table 11:** Same as in Table 4 with  $\sqrt{s} = 8$  TeV, including only procedure A described in the text to calculate the total uncertainty.

## References

- [1] P. Higgs, Phys. Lett. 12 (1964) 132; F. Englert and R. Brout, Phys. Rev. Lett. 13 (1964) 321; G. Guralnik, C. Hagen and T. Kibble, Phys. Rev. Lett. 13 (1964) 585; P. Higgs, Phys. Rev. 145 (1966) 1156.
- [2] For a review, see: A. Djouadi, Phys. Rept. 457 (2008) 1 [hep-ph/0503172].
- [3] For a review see, M. Drees, R.M. Godbole and P. Roy, *Theory and Phenomenology of Sparticles*, World Scientific, Spring 2004.
- [4] J. Gunion, H. Haber, G. Kane and S. Dawson, *The Higgs Hunter's Guide*, Addison–Wesley, Reading 1990.
- [5] A. Djouadi, Phys. Rep. 459 (2008) 1 [hep-ph/0503173].
- [6] M. Spira, Fortschr. Phys. 46 (1998) 203.
- [7] S. Heinemeyer, W. Hollik and G. Weiglein, Phys. Rept. 425 (2006) 265; S. Heinemeyer, Int. J. Mod. Phys A21 (2006) 2659, B. Allanach et al., JHEP 0409 (2004) 044.
- [8] The LEP Collaborations, Phys. Lett. B565 (2003) 61.
- [9] The CDF and D0 coll., “Combination of Tevatron Searches for the Standard Model Higgs Boson in the  $W^+W^-$  Decay Mode”, Phys. Rev. Lett. 104 (2010) 061802; The CDF and D0 coll., “Combined CDF and D0 upper limits on Standard Model Higgs boson production with up to  $6.7 \text{ fb}^{-1}$  of Data”, arXiv:1007.4587 [hep-ex].
- [10] The TevNPHWG for the CDF/D0 Collaborations, arXiv:1003.3363 [hep-ex].
- [11] See for instance, R. Heuer, talk given at IWLC2010, CERN Geneva, October 2010.
- [12] ATLAS Collaboration, “ATLAS sensitivity prospects for Higgs boson production at the LHC running at 7,8 or 9 TeV”, ATLAS–PHYS–PUB–2010–015.
- [13] CMS Collaboration, “The CMS Physics reach for searches at 7 TeV”, CMS Note 2010/008.
- [14] LHC Higgs cross section Working Group, “Handbook of LHC Higgs Cross Sections”, in preparation; C. Mariotti, S. Dittmaier, G. Passarino and R. Tanaka (eds).
- [15] H. Georgi, S. Glashow, M. Machacek and D. Nanopoulos, Phys. Rev. Lett. 40 (1978) 692.
- [16] M. Dittmar and H. Dreiner, Phys. Rev. D55 (1997) 167.
- [17] S.L. Glashow, D.V. Nanopoulos and A. Yildiz, Phys. Rev. D18 (1978) 1724.
- [18] J. Baglio and A. Djouadi, JHEP 1010 (2010) 064.
- [19] A. Djouadi, M. Spira and P. Zerwas, Phys. Lett. B264 (1991) 440; S. Dawson, Nucl. Phys. B359 (1991) 283.
- [20] M. Spira, A. Djouadi, D. Graudenz and P.M. Zerwas, Nucl. Phys. B453 (1995) 17.
- [21] R.V. Harlander and W. Kilgore, Phys. Rev. Lett. 88 (2002) 201801; C. Anastasiou and K. Melnikov, Nucl. Phys. B646 (2002) 220; V. Ravindran, J. Smith and W.L. Van Neerven, Nucl. Phys. B665 (2003) 325.
- [22] S. Catani, D. de Florian, M. Grazzini and P. Nason, JHEP 0307 (2003) 028.
- [23] A. Djouadi, M. Spira and P.M. Zerwas, Z. Phys. C70 (1996) 427.
- [24] D. Dicus and S. Willenbrock, Phys. Rev. D39 (1989) 751.

- [25] J. Campbell, R. K. Ellis, F. Maltoni and S. Willenbrock, Phys. Rev. D67 (2003) 095002; F. Maltoni, Z. Sullivan and S. Willenbrock Phys. Rev. D67 (2003) 093005.
- [26] R. Harlander and W. Kilgore, Phys. Rev. D68 (2003) 013001.
- [27] C. Anastasiou, R. Boughezal and F. Petriello, JHEP 0904 (2009) 003.
- [28] D. de Florian and G. Grazzini, Phys. Lett. B674 (2009) 291.
- [29] S. Moch and A. Vogt, Phys. Lett. B631 (2005) 48; V. Ravindran, Nucl. Phys. B752 (2006) 173; V. Ahrens, T. Becher, M. Neubert and L.L. Yang, Eur. Phys. J. C62 (2009) 333.
- [30] See for instance, G. Corcella and L. Magnea, Phys. Rev. D72 (2005) 074017.
- [31] See for instance, V. Ravindran, J. Smith and W.L. van Neerven, Nucl. Phys. B634 (2002) 247; C. Anastasiou, K. Melnikov and F. Petriello, Nucl. Phys. B724 (2005) 197; S. Catani and M. Grazzini, Phys. Rev. Lett. 98 (2007) 222002; C. Anastasiou, S. Bucherer and Z. Kunszt, JHEP 0910 (2009) 068.
- [32] C. Anastasiou et al., JHEP 0908 (2009) 099.
- [33] C. Anastasiou, “Higgs production via gluon fusion”, talk given at Higgs Hunting Workshop, Orsay–France, 29–31 July 2010
- [34] S. Actis, G. Passarino, C. Sturm and S. Uccirati, Nucl. Phys. B811 (2009) 182.
- [35] For the electroweak corrections, see also: A. Djouadi and P. Gambino, Phys. Rev. Lett. 73 (1994) 2528; U. Aglietti, R. Bonciani, G. Degrassi and A. Vicini, Phys. Lett. B595 (2004) 432; G. Degrassi and F. Maltoni, Phys. Lett. B600 (2004) 255; S. Actis et al., Phys. Lett. B670 (2008) 12.
- [36] E. Berger, C. Qing-Hong, C. Jackson and G. Shaughnessy, Phys. Rev. D82 (2010) 053003; F. Demartin, S. Forte, E. Mariani, J. Rojo and A. Vicini, Phys. Rev. D82 (2010) 014002; V. Ahrens, T. Becher, M. Neubert and L.L. Yang, arXiv:1008.3162 [hep-ph]; S. Alekhin, J. Blumlein, P. Jimenez-Delgado, S. Moch and E. Reya, arXiv:1011.6259 [hep-ph].
- [37] The Fortran codes can be found in Michael Spira’s web page, <http://people.web.psi.ch/~mspira/>. For HIGLU, see hep-ph/9510347.
- [38] A.D. Martin, W. Stirling, R. Thorne and G. Watt, Eur. Phys. J. C63 (2009) 189.
- [39] G. Altarelli, R.K. Ellis and G. Martinelli, Nuc. Phys. B157 (1979) 461; J. Kubar–André and F. Paige, Phys. Rev. D19 (1979) 221; T. Han and S. Willenbrock, Phys. Lett. B273 (1991) 167; J. Ohnemus and W. J. Stirling, Phys. Rev. D47 (1993) 2722; A. Djouadi and M. Spira, Phys. Rev. D62 (2000) 014004.
- [40] R. Hamberg, W.L. van Neerven and T. Matsuura, Nucl. Phys. B359 (1991) 343 and (E) *ibid.* B644 (2002) 403; O. Brein, A. Djouadi and R. Harlander, Phys. Lett. B579 (2004) 149.
- [41] M. L. Ciccolini, S. Dittmaier and M. Krämer, Phys. Rev. D68 (2003) 073003.
- [42] T. Han, G. Valencia and S. Willenbrock, Phys. Rev. Lett. 69 (1992) 3274; T. Figy, C. Oleari and D. Zeppenfeld. Phys. Rev. D68 (2003) 073005.
- [43] P. Bolzoni, F. Maltoni, S. Moch and M. Zaro, Phys. Rev. Lett. 105 (2010) 011801 and arXiv:1006.2323 [hep-ph].
- [44] M. Ciccolini, A. Denner and S. Dittmaier, Phys. Rev. D77 (2008) 013002.

- [45] W. Beenakker et al., Phys. Rev. Lett. 87 (2001) 201805; Nucl. Phys. B653 (2003) 151; S. Dawson et al., Phys. Rev. Lett. 87 (2001) 201804 and Phys. Rev. D67 (2003) 071503.
- [46] We are grateful to Michael Spira for a discussion on this issue.
- [47] R. Harlander and K. Ozeren, arXiv:0909.3420; A. Pak, M. Rogal and M. Steinhauser, arXiv:0911.4662; R. Harlander, H. Mantler, S. Marzani, K. Ozeren, arXiv:0912.2104; S. Marzani et al. Nucl. Phys. B800 (2008) 127.
- [48] A.D. Martin, W. Stirling, R. Thorne and G. Watt, Eur. Phys. J. C64 (2009) 653.
- [49] P.M. Nadolsky et al. (CTEQ coll.), Phys. Rev. D78 (2008) 013004.
- [50] R.D. Ball et al., Nucl. Phys. B823 (2009) 195.
- [51] P. Jimenez-Delgado and E. Reya, Phys. Rev. D80 (2009) 114011.
- [52] S. Alekhin, J. Blumlein, S. Klein and S. Moch, arXiv:0908.2766.
- [53] The NNLO PDF sets can be found at: [www.desy.de/h1zeus/combined\\_results](http://www.desy.de/h1zeus/combined_results).
- [54] K. Nakamura et al., Particle Data Group, J. Phys. G37 (2010) 075021.
- [55] A.D. Martin, W.J. Stirling, R.S. Thorne and G. Watt, arXiv:1007.2624.
- [56] PDF4LHC recommendation can be found at:  
<http://www.hep.ucl.ac.uk/pdf4lhcrecom.pdf>.
- [57] M. Cacciari, S. Frixione, M.L. Mangano, P. Nason and G. Ridolfi, JHEP 0809 (2008) 127.
- [58] N. Gray, D.J. Broadhurst, W. Grafe and K. Schilcher, Z. Phys. C48 (1990) 673; K. Chetyrkin and M. Steinhauser, Nucl. Phys. B573 (2000) 617; K. Melnikov and T. van Ritbergen, Phys. Lett. B482 (2000) 99.
- [59] S. Gorishny, A. Kataev, S. Larin and L. Surguladze, Phys. Rev. D43 (1991) 1633; K. Chetyrkin, Phys. Lett. B404 (1997) 161; J. Vermaseren, S. Larin and T. van Ritbergen, Phys. Lett. B405 (1997) 327.
- [60] We thank Michael Spira for a discussion on this point.
- [61] K. Chetyrkin, B. Kniehl and M. Steinhauser, Phys. Rev. Lett. 79 (1997) 353; P. Baikolov and K. Chetyrkin, Phys. Rev. Lett. 97 (2006) 061803.
- [62] A. Bredenstein et al., Phys. Rev. D74 (2006) 013004 and JHEP 070 (2007) 080.
- [63] A. Ghinculov, Phys. Lett. B337 (1994) 137; L. Durand. K. Riesselman and B. Kniehl, Phys. Rev. Lett. 72 (1994) 2534; V. Borodulin and G. Jikia, Phys. Lett. B391 (1997) 434.
- [64] A. Djouadi, M. Spira, J. van de Bij and P.M. Zerwas, Phys. Lett. B257 (1991) 187; A. Djouadi, M. Spira and P.M. Zerwas, Phys. Lett. B311 (1993) 255.
- [65] K. Chetyrkin et al., Phys. Rev. D80 (2009) 074010.
- [66] A. Djouadi, J. Kalinowski and M. Spira, Comput. Phys. Commun. 108 (1998) 56.
- [67] A. Djouadi, N. Kauer and M. Kramer, in progress.
- [68] M. Carena, S. Heinemeyer, C. Wagner and G. Weiglein, Eur. J. Phys. C26 (2003) 601.
- [69] E. Boos et al., Phys. Rev. D66 (2002) 055004; E. Boos, A. Djouadi and A. Nikitenko, Phys. Lett. B578 (2004) 384.

- [70] D.M. Pierce, J.A. Bagger, K.T. Matchev and R.J. Zhang, Nucl. Phys. B491 (1997) 3.
- [71] See e.g., M. Carena, D. Garcia, U. Nierste and C.E. Wagner, Nucl. Phys. B577 (2000) 88.
- [72] D. Noth and M. Spira, Phys. Rev. Lett. 101 (2008) 181801.
- [73] S. Heinemeyer, W. Hollik and G. Weiglein, Comp. Phys. Commun. 124 (2000) 76.
- [74] A. Djouadi, J.L. Kneur and G. Moultaka, Comput. Phys. Commun. 176 (2007) 426.
- [75] S. Dawson, A. Djouadi and M. Spira, Phys. Rev. Lett. 77 (1996) 16; R. Harlander and M. Steinhauser, JHEP 0409 (2004) 066, *ibid.* Phys. Rev. D68 (2003) 111701; C. Anastasiou et al., JHEP 0701 (2007) 082; U. Aglietti et al., JHEP 0701 (2007) 021; R. Bonciani, G. Degrossi and A. Vicini, JHEP 0711 (2007) 095; M. Muhlleitner and M. Spira, Nucl. Phys. B790 (2008) 1; G. Degrossi and P. Slavich, Nucl. Phys. B805 (2008) 267; S. Dawson and C. Jackson, Phys. Rev. D77 (2008) 015019; C. Anastasiou, S. Beerli and A. Daleo, Phys. Rev. Lett. 100 (2008) 241806; M. Muhlleitner, H. Rzehak and M. Spira, arXiv:101.3214 [hep-ph].
- [76] S. Dittmaier, M. Kramer and M. Spira, Phys. Rev. D70 (2004) 074010; S. Dawson, C. Jackson, L. Reina and D. Wackerroth, Phys. Rev. D69 (2004) 074027.
- [77] We thank Robert Harlander for providing us with his code.
- [78] J. Campbell et al., hep-ph/0406152.
- [79] J. Baglio and A. Djouadi, *Revisiting the constraints on the Supersymmetric Higgs sector at the Tevatron*, arXiv:1012.2748.